Biomechanical properties of atherosclerotic plaques

Biomechanical properties of atherosclerotic plaques

Dipl.-Ing. (FH) Chen Ket Chai, MSc. VDI

Financial support by the Dutch Heart Foundation for the publication of this thesis is gratefully acknowledged.

A catalogue record is available from the Eindhoven University of Technology Library.

ISBN: 978-90-386-3770-9

This thesis was prepared with LYX 2.0.

Printed by Uitgeverij BOXPress, s'-Hertogenbosch

Cover design by Laura Cornet (www.lauracornet.nl)

This reseach was supported by the centre for Translational Molecular Medicine and the Dutch Heart Foundation (PARISk).

Biomechanical properties of atherosclerotic plaques

PROEFSCHRIFT

ter verkrijging van de graad van doctor aan de Technische Universiteit Eindhoven, op gezag van de rector magnificus prof.dr.ir. C.J. van Duijn, voor een commissie aangewezen door het College voor Promoties, in het openbaar te verdedigen op woensdag 28 januari 2015 om 16:00 uur

door

Chen Ket Chai

geboren te Schwerte, Duitsland

Dit proefschrift is goedgekeurd door de promotoren en de samenstelling van de promotiecommissie is als volgt:

voorzitter:	prof.dr. P.A.J. Hilbers
1e promotor:	prof.dr.ir. F.P.T. Baaijens
copromotor:	dr.ir. C.W.J. Oomens
leden:	prof.dr. A.F.W. van der Steen (Erasmus MC Rotterdam)
	prof.dr. M.J.A.P. Daemen (Universiteit van Amsterdam AMC)
	prof.dr.ir. F.N. van de Vosse
	dr.ir. G.J. Strijkers
adviseur:	dr. F.J.H. Gijsen (Erasmus MC Rotterdam)

Summary

Biomechanical properties

of atherosclerotic plaques

Atherosclerosis is a systemic disease of arteries, caused by an accumulation of inflammatory cells and lipids inside the arterial wall. This leads to thickening of the arterial wall and formation of atherosclerotic plaques. Plaques can become unstable and rupture-prone. Those so-called vulnerable plaques consist of a lipid-rich necrotic core, covered by a thin fibrous cap separating the lipid core from the blood stream. Rupture of the fibrous cap leads to thrombus formation and possibly to occlusion of an artery preventing blood supply to vital organs, which is the main cause of ischaemic strokes and heart attacks. Reliable cap rupture risk assessment is essential to prevent over-treatment of stable plaques and to guarantee all rupture-prone plaques are detected. Current methods to predict plaque rupture have a limited reliability because they focus on general morphological parameters, which are only indirectly connected to the actual cause of plaque rupture. From a mechanical point of view, plaque rupture occurs when strength of the plaque cap is exceeded by the stresses in the plaque cap. Investigating the cap strength as well as the stress distribution and identifying stress peaks may lead to a better understanding of plaque rupture.

Computer models of plaques may be a tool to improve plaque rupture risk assessment because it allows the visualisation of stress distributions and the detection of stress peaks. However, the accuracy of computer models depends on the input parameters used. This offers several challenges: 1.) Local mechanical testing is required to determine the heterogeneous mechanical properties. 2.) The method has to be capable of measuring anisotropic mechanical properties 3.) Knowledge of the plaque cap strength is crucial for plaque rupture prediction. The aim of the present thesis is to improve plaque rupture risk assessment by providing data on mechanical properties of human plaque tissues.

A literature review was conducted to investigate which method would be appropriate to characterise the mechanical properties of atherosclerotic plaques. The focus of the review was on micro- and nanoindentation tests, because of the ability to measure very local properties. It was concluded that micro-indentation is a suitable method.

Micro-indentation was used to analyse the local mechanical properties of human atherosclerotic carotid plaques. Inverse Finite Element Analysis was performed to infer the mechanical properties of different plaque components, namely the middle of the plaque cap, the shoulder of the plaque cap, lipid-rich necrotic core and remaining intima regions. It was shown that collagen-rich locations were much stiffer than collagen poor locations. However, a wide spread in data was found corresponding to the variability found in literature.

To analyse the anisotropic mechanical properties of plaque tissue, two different studies were conducted. One study focused on the mechanical properties of collagen fibres in atherosclerotic plaques. Micro-indentation tests were combined with confocal imaging to visualise the local fibre distribution and the deformation of collagen fibres in plaques during indentation. An inverse FE analysis was used to infer the stiffness of the collagen fibres.

Another study visualised the 3D global architecture of fibrous tissue in plaques. It is shown that, unlike in healthy arteries where fibres are oriented in helical direction, a lot of fibres in atherosclerotic plaques align in the longitudinal direction of the blood vessel. This reorganisation of fibres may be due to a change in stress and strain distribution during the progress of atherosclerosis in arteries.

Indentations in the radial direction were performed to investigate the failure properties of atherosclerotic plaque caps. The ultimate stress and strain values of the tissue were measured. The obtained ultimate stress showed a wide spread ranging from 5.2 MPa to 37.5 MPa (25th to 75th percentile). The ultimate strains had a much lower spread ranging from 0.3 to 1.0 (25th to 75th percentile), corresponding to the range found in literature. Because of this and the fact that stress data cannot be determined directly without exact knowledge of the mechanical properties of plaques, it is recommended that further research is focussed upon strain imaging.

The mechanical properties show a very wide variability. This indicates that plaque-specific mechanical properties are required for the reliable assessment of plaque rupture risk. The data provided allow the inclusion of anisotropic mechanical properties in computer modelling of atherosclerotic plaques thus increasing the accuracy of stress results considerably. On the other hand, the results found in literature and this disser-

tation suggest that because of the wide spread in mechanical properties and the lack of accurate imaging technology to determine the geometry of unstable plaques, reliable computer modelling of plaques still requires laborious investigations. Alternatives such as strain imaging may be a more promising approach to detect unstable plaques predicting plaque rupture, the main cause for cardiovascular events such as strokes and heart attacks.

Table of contents

Contents

Summary i

1 General introduction 1
- 1.1 Overview . . . 2
- 1.2 From arteries to atherosclerotic plaques . . . 2
- 1.3 Vulnerable plaques and plaque rupture prediction . . . 5
- 1.4 Computer modelling as possible predictor . . . 7
- 1.5 Aim and outline of the dissertation . . . 9

2 Compressive properties of plaques 13
- 2.1 Introduction . . . 14
- 2.2 Compressive properties of plaque tissue . . . 15
  - 2.2.1 Unconfined compression . . . 15
  - 2.2.2 Micro-indentation . . . 18
  - 2.2.3 Nano-indentation . . . 20
  - 2.2.4 Discussion of the compression techniques . . . 21
- 2.3 Local anisotropic behaviour of human carotid plaques . . . 26
  - 2.3.1 Sample preparation . . . 26
  - 2.3.2 Micro-indentation test . . . 27
  - 2.3.3 Inverse finite element analysis . . . 28
- 2.4 Discussion . . . 31
- 2.5 Main conclusions . . . 32

3 Local properties of carotid plaques 35
- 3.1 Introduction . . . 36
- 3.2 Methods . . . 36
  - 3.2.1 Preparing plaque tissue . . . 36
  - 3.2.2 Indentation test and imaging . . . 37
  - 3.2.3 Data analysis . . . 38

3.3 Results . . . 40
3.3.1 Representative plaque result . . . 40
3.3.2 Collagen structure . . . 43
3.3.3 Indentation locations . . . 43
3.3.4 Inter- and intra-plaque variability, comparison between longitudinal and transversal slices, and change of mechanical properties in longitudinal direction . . . 45
3.4 Discussions . . . 46

4 Anisotropic mechanical behaviour of plaques **51**
4.1 Introduction . . . 52
4.2 Methods . . . 53
4.2.1 Sample preparations . . . 53
4.2.2 Indentation test and imaging . . . 53
4.2.3 Inverse finite element (FE) analysis . . . 54
4.2.4 Parameter estimation . . . 55
4.2.5 Statistical analysis . . . 57
4.3 Results . . . 57
4.3.1 Parameter identification . . . 57
4.3.2 Material parameters . . . 58
4.3.3 Change of fibre stiffness in longitudinal direction, inter- and intra-plaque variability . . . 61
4.3.4 Collagen structure . . . 62
4.3.5 Comparing anisotropy, 2nd principal stretch and main fibre directions . . . 65
4.4 Discussion . . . 66
4.5 Limitations . . . 68
4.6 Conclusion . . . 69

5 3D fibrous structure of carotid plaques **71**
5.1 Introduction . . . 72
5.2 Methods . . . 72
5.2.1 Sample preparation . . . 72
5.2.2 Diffusion Tensor Imaging . . . 73
5.2.3 DTI analysis . . . 73
5.2.4 Histology . . . 73
5.3 Results . . . 74

5.3.1 DTI result of healthy porcine carotid artery . . . 74
5.3.2 DTI result of human carotid plaque . . . 74
5.3.3 Histology . . . 75
5.4 Discussion . . . 77
5.5 Limitations . . . 79
5.6 Conclusions . . . 80

6 Failure properties of plaques **81**
6.1 Introduction . . . 82
6.2 Materials and methods . . . 83
6.2.1 Sample preparation and cap thickness measurements . . . 83
6.2.2 Indentation test and loading protocol . . . 83
6.2.3 Inverse Finite Element Analysis . . . 85
6.3 Results . . . 87
6.3.1 Cap thickness . . . 87
6.3.2 Indentation results . . . 88
6.3.3 Parameter identification . . . 90
6.4 Discussion . . . 92

7 General discussion **99**
7.1 Overview . . . 100
7.2 Main findings . . . 100
7.2.1 Mechanical testing of local mechanical properties of atherosclerotic plaques . . . 100
7.2.2 Local mechanical properties of plaques . . . 101
7.2.3 Anisotropic mechanical properties . . . 102
7.2.4 Failure properties . . . 103
7.3 Discussion and future perspective . . . 103
7.3.1 Computer modelling of plaques . . . 103
7.3.2 Alternatives to computer modelling of plaques . . . 104
7.3.3 Plaque failure . . . 106
7.4 Final conclusions . . . 107

Bibliography **107**

Acknowledgement **128**

About the author **132**

List of publications 134

PhD portfolio 136

Chapter 1

General introduction

"There are relatively few data on the mechanical properties of arterial tissues, (...) and the materials-testing protocols have varied between the measurements that have been published. This is probably the most uncertain aspect in the whole body of study of plaque fracture." Richardson (2002) [1].

1.1 Overview

As stated by Richardson (2002) [1], knowledge of the biomechanical properties of atherosclerotic plaques is required to better understand when plaque rupture occurs. Since plaque rupture is the main cause of ischaemic strokes and heart attacks, it is important to improve the understanding of plaque failure, so that these potentially lethal cardiovascular events can be prevented. This introduction gives an overview of the anatomy and aetiology of atherosclerotic plaques.

1.2 From arteries to atherosclerotic plaques

The earliest document attempting to describe the human cardiovascular system was found in the Papyrus Ebers [2], an ancient Egyptian medical papyrus dating back to 16th century BC. It describes the heart as centre of the blood circulation, which is connected to all limbs through blood vessels. Today, blood vessels are distinguished into different types. The veins transport blood towards the heart and, except the pulmonary and umbilical veins; most veins carry deoxygenated blood, whereas most arteries, except the pulmonary and umbilical artery, transport oxygenated blood away from the heart [3].

The main function of a cardiovascular system is the constant supply of oxygen and nutrients to cells in the body as well as the removal of waste products. Moreover, the cardiovascular system is responsible for maintaining the pH and transporting proteins as well as immune cells. Thus, the cardiovascular system is essential for sustaining life.

Cardiovascular diseases, such as ischaemic heart disease and stroke, were the two leading causes of death in 2000 worldwide and the numbers of deaths associated to cardiovascular disease have increased since the last decade (Figure 1.1). The main

cause for cardiovascular events is connected to the development of atherosclerosis [4], an inflammatory disorder, leading to structural and morphological changes in the arterial wall. It starts in childhood and slowly advances throughout the life-span affecting major conduit arteries [5].

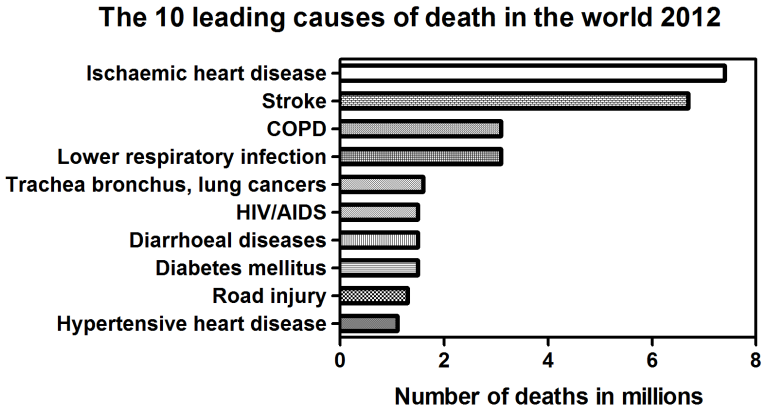

Figure 1.1: *Diagram showing the 10 leading causes of death worldwide in 2012. The cardiovascular diseases, ischaemic heart disease and stroke, are the two leading causes of death. They are mainly connected to the development of atherosclerosis and the rupture of an atherosclerotic plaque. COPD-Chronic obstructive pulmonary disease. Data obtained from [6].*

A healthy artery generally consists of three layers (Figure 1.2). The tunica adventitia is the outermost layer of an artery and comprises mainly collagen. Underneath the adventitia lies the external elastic lamina separating the adventitia from the tunica media, which is the thickest layer in arteries and consists of elastin and smooth muscle cells. The media covers the internal elastic lamina, which separates the media from the tunica intima. The intima comprises endothelial cells and has direct contact with the lumen and, thus, the blood flow [7]. The blood flow in arteries is regulated through vasodilatation (increase in lumen diameter) and vasoconstriction (narrowing of lumen diameter).

There are certain risk factors, such as smoking, obesity, hypertension, and diabetes, associated with the progress of atherosclerosis [7, 9]. However, the initial triggers for atherogenesis are believed to be low arterial wall shear stress, biochemical abnormal-

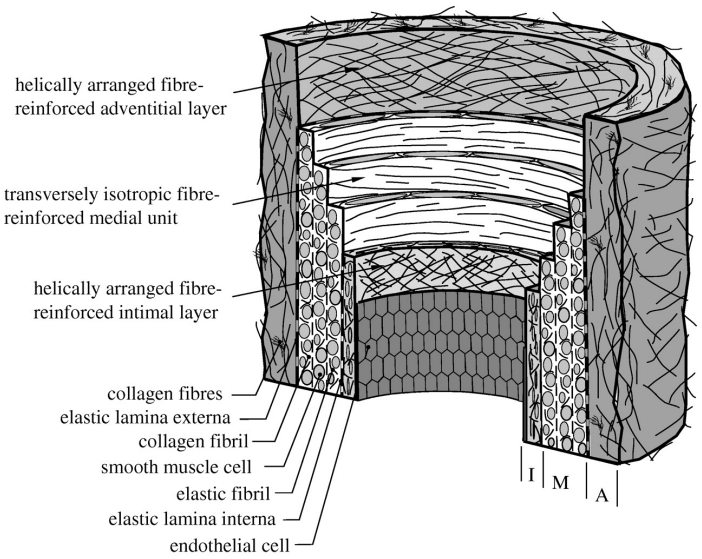

Figure 1.2: *Different layers in a healthy artery. It consists of three layers, the intima (I), media (M) and adventitia (A). During the progress of atherosclerosis the morphology and structure of the artery changes. Reprinted from Gasser et al. (2006) [8] with permission from Royal Society.*

ities, genetic alteration and immunological causes [10]. These factors might induce initial damage to the arterial intima causing endothelial dysfunction, leading to an increased permeability for macro-molecules, such as low-density lipids, cellular debris and calcium [11, 12]. Those macro-molecules accumulate in the sub-endothelial layer of the arterial wall stimulating the migration and proliferation of smooth muscles cells and inflammatory cells (Figure 1.3).

This causes initial thickening of the arterial wall (Figure 1.4, type I). Inflammatory cells engulf accumulated cellular debris and lipids forming so-called foam cells (Figure 1.4, type II). Foam cells can pool together to form extra-cellular lipid pools (Figure 1.4, type III), which can advance to a lipid-rich necrotic core (Figure 1.4, type IV). Until this point the arterial wall thickening caused mostly outwards remodelling of the wall. The diameter of the lumen is hardly affected, so that the patients are asymptomatic. At later stages, the atheroma can intrude into the lumen causing severe arterial stenosis. Further recruitment of smooth muscle cells from the media can synthesize connective tissue elements, such as collagen, entrapping lipids in the sub-intima. This can lead to the formation of a fibrous cap surrounding a lipid-rich necrotic core separating it

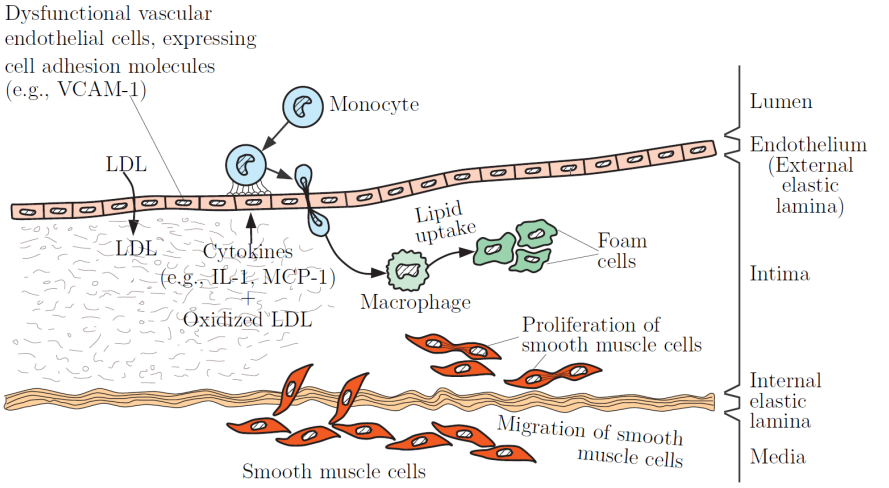

Figure 1.3: *Atherogenesis caused by dysfunctional vascular endothelial cells. Reprinted with permission from Sommer (2008) [13].*

from the blood flow (Figure 1.4, type V). Blood flow and blood pressure cause shear forces and stresses in the atherosclerotic plaque. Stress peaks can lead to fissuring of a fibrous cap leading to direct contact between the thrombogenetic lipid-rich necrotic core and the blood stream. This process can lead to atherosclerotic plaques with complicated lesions, which are in many cases clinically silent (Figure 1.4, type VI). Further advancement of atherosclerosis can lead to fibrotic plaques (plaque type VII) or calcified plaques (plaque type VIII) [5]. It has to be noted that atherosclerosis is a slowly developing disorder. During this slowly developing process the arterial wall initially forms fatty streaks, which can be found already in children, and over the years advance to atherosclerotic plaques intruding into the lumen causing arterial stenosis. Such advanced atherosclerotic plaques can become vulnerable and manifest clinically as strokes or myocardial infarctions.

1.3 Vulnerable plaques and plaque rupture prediction

Atherosclerotic plaques can be divided in stable and rupture-prone plaques. Rupture-prone plaques are commonly referred to as vulnerable plaques. Vulnerable plaques

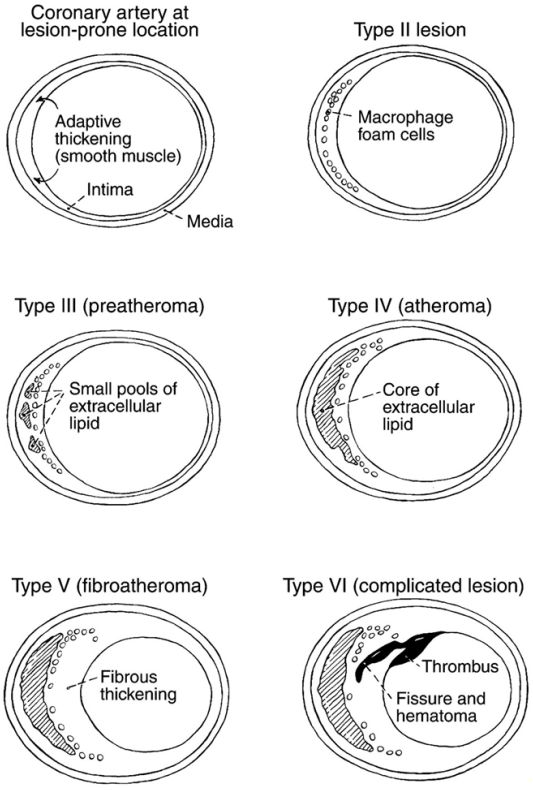

Figure 1.4: *Different types of atherosclerotic plaques. Reprinted from Stary et al. (1995) [14] with permission from Wolters Kluwer Health.*

comprise inflammatory cells, intra-plaque haemorrhages, and a lipid-rich necrotic core which is covered by a thin fibrous cap [15]. The cap is prone to rupture, which can lead to subsequent thrombus formation and distal embolism leading to cardiovascular events, such as stroke and myocardial infarction. In fact, more than 70% of all cardiovascular events are associated with plaque rupture [16]. Therefore, a reliable method to assess plaque rupture risk is widely considered as a good predictor for cardiovascular events [17, 18, 19, 20].

Current studies on plaque rupture risk focus on general morphological parameters, such as degree of stenosis [21], cap thickness [22], necrotic core size [23], and the presence of haemorrhage [24]. The results of these studies indicate that plaques with large necrotic cores and thin fibrous caps are more prone to rupture [25, 26, 27, 28]. However, it has been shown that not all plaques with large necrotic cores and thin fibrous

caps rupture. Also, not all ruptured plaques have large necrotic cores and thin caps. This indicates that these general morphological parameters are not always reliable. The sensitivity and specificity of methods to detect vulnerable plaques need to be increased.

Plaque rupture is the main cause of ischaemic strokes and myocardial infarction and it has been shown that the current rupture risk methods are unreliable. The aim of this thesis is to improve plaque rupture prediction. Plaques are often over-treated and patients undergo potentially inappropriate treatment, and on the other hand, unstable plaques are missed leading to preventable lethal cardiovascular events, such as ischaemic strokes and myocardial infarctions.

1.4 Computer modelling as possible predictor

From a mechanical point of view, plaque rupture occurs when the stresses in the plaque cap exceed the strength of the cap. Therefore, cap strength and plaque stresses are directly associated with plaque rupture and might offer a much better plaque rupture risk assessment in combination with the existing parameters or even as sole prediction parameter [29, 30].

Computer modelling, such as FE analysis, enables stress analysis in plaques (Figure 1.5), which may be a tool to assess the direct cause of plaque rupture. The accuracy of stress results obtained from FE models depends on the input parameters used. Most crucial parameters include geometric features, mechanical properties and boundary conditions [31, 32].

Geometric features can be obtained from histology, magnetic resonance imaging, ultrasound and optical coherence tomography. Most studies focus on the cap thickness and show that the peak stresses increase with thinner plaque caps [34, 35, 36]. On the other hand, Ohayon et al. (2008) [23] suggests that the necrotic core size also has a major influence on the peak stress.

Next to geometric properties it is necessary to determine the mechanical properties of atherosclerotic plaques. Different methods were applied to test the mechanical properties of plaques ranging from inflation tests [37] to tensile [38] and compression

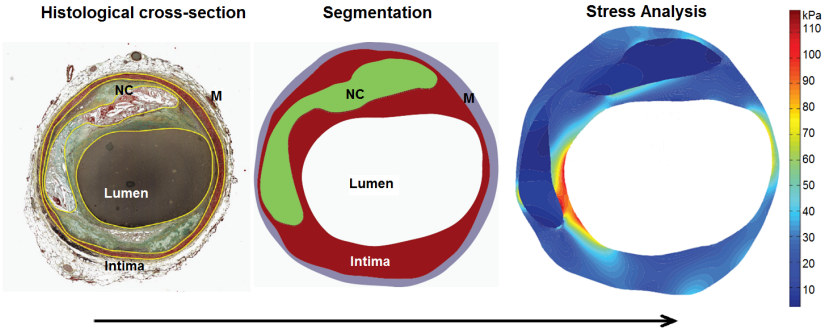

Figure 1.5: *Geometry and morphology can be obtained from imaging methods or histology. The different plaque components, such as lumen, intima, media (M), and necrotic core (NC), can be segmented. Stress analysis can be performed using FEM. Adapted from Speelman et al. (2011) [33] with permission from Elsevier.*

tests (see chapter 2). Most of the studies focus on measuring the mechanical plaque properties at small strain or physiological strain, not necessarily causing plaque failure. Data on plaque failure properties are scarce [39, 40, 41, 42, 43, 44, 45, 46, 47, 48] and most studies only focus on large arteries, such as the aorta and iliac artery. Therefore, further investigations on failure properties of plaque are required.

Another issue regarding characterisation of the mechanical properties of atherosclerotic plaque tissue is the heterogeneous morphology of the tissue. Almost all plaque types comprise a heterogeneous component distribution[49]. The plaque components behave mechanically very different. Ebenstein et al. (2009) [50] showed that the plaque components, such as hematoma can be more than 600-fold softer than calcifications in plaque tissue. Ebenstein et al. (2002) [51] used nano-indentation to perform very local measurements to capture the heterogeneous nature of plaque tissue.

It is well accepted that atherosclerotic plaque tissue behaves mechanically anisotropic. Several studies have shown that plaque tissue consists of fibrous tissue indicating anisotropic mechanical behaviour. Holzapfel et al. (2004) [45] performed uni-axial tensile tests in axial and circumferential directions of the atherosclerotic plaque obtained from iliac arteries. The results demonstrate the direction dependent behaviour of plaque tissue. The tested fibrous plaques exhibit much stiffer behaviour in axial direction than in circumferential direction [45]. Although it is well established that atherosclerotic plaque tissue behaves mechanically anisotropic, most studies work with

computer models assuming isotropic behaviour. This simplification has a negative influence on the accuracy of plaque modelling [52]. Therefore, for reliable plaque models anisotropic mechanical properties of plaque tissue need to be included.

In conclusion, FE modelling could be an important tool to improve plaque rupture risk assessment. However, the accuracy of stress analysis results obtained from FE models depends on the quality of the mechanical data of plaque tissue (heterogeneity, anisotropic mechanical behaviour, and plaque cap strength), which have not been extensively investigated. Addressing these requirements is the aim of this dissertation.

1.5 Aim and outline of the dissertation

The objective of this dissertation is to improve plaque rupture risk assessment by providing mechanical data of plaque tissue. Computer modelling of atherosclerotic plaques can help to improve plaque rupture risk assessment, because it enables analysis of the stress and strain distribution in plaque, including the fibrous cap. This analysis, however, depends strongly on the mechanical data and associated parameters used. The following requirements should be addressed:

1. Atherosclerotic plaques are heterogeneous structures comprising different plaque components. The morphologically different plaque components might also be mechanically very different. To address this issue, it is important to investigate the local mechanical properties of plaques.

2. It is commonly accepted that atherosclerotic plaque tissue behaves mechanically anisotropic. The assumption of isotropic behaviour might be a general oversimplification. Therefore, the anisotropic mechanical properties of plaques need to be characterised.

3. Computer models of plaque allow stress analysis and it is important to analyse the ultimate stress and/or strain, when plaque rupture occurs.

These requirements are addressed in the following chapters in this dissertation (Figure 1.6). Chapter 2 reviews the current methods to test the mechanical properties of atherosclerotic plaques locally. The literature review focuses on compression tests, which, unlike tensile tests, allow local measurement of mechanical properties. Different compression tests, ranging from unconfined compression tests through micro-

indentation to nano-indentation methods are evaluated. The advantages and disadvantages are discussed. Micro-indentation appeared to be a good compromise between local measurements and applying physiological strain. Therefore, it was decided to investigate the local mechanical properties of atherosclerotic plaques tissue using micro-indentation.

In chapter 3, the focus is on requirement 1, the local mechanical properties of plaques. Different plaque components are tested using micro-indentation. The indentations were performed in axial direction and inverse FE analysis was used to infer the local mechanical properties of shoulder cap, middle cap, lipid-rich necrotic core, and remaining intima regions. Furthermore, at each indentation location the collagen structures were examined using confocal imaging. Three different structures were distinguished, collagen-rich structured locations, collagen-rich unstructured locations, and collagen poor locations.

For requirement 2, the characterisation of the anisotropic mechanical behaviour of atherosclerotic plaques, two separate studies were conducted. The results of these two studies are presented in chapter 4 and chapter 5. In Chapter 4 the local mechanical properties of fibrous tissue in atherosclerotic plaques are described. Different fibrous plaque components were tested by means of micro-indentations. The deformations of the fibrous structure during indentation were visualised using confocal imaging. The deformations were quantified using digital image correlation. This was used as input parameter for inverse finite element analysis to determine the mechanical properties of the fibrous tissue.

For a full characterisation also the 3D global architecture of the fibrous tissue is required. Therefore, the aim in chapter 5 was the visualisation of the 3D structure of the fibrous tissue in plaques using diffusion tensor imaging.

Stress analysis using computer models allows visualising stress peaks in plaque caps. However, besides reliable stress analysis, also accurate knowledge about the plaque cap strength is essential for predicting plaque rupture (requirement 3). Therefore, chapter 6 focuses on the failure properties of plaque caps. The ultimate strength of atherosclerotic plaque caps are investigated by means of indentation. The last chapter 7 summarises the most important findings of the dissertation and provides a general discussion.

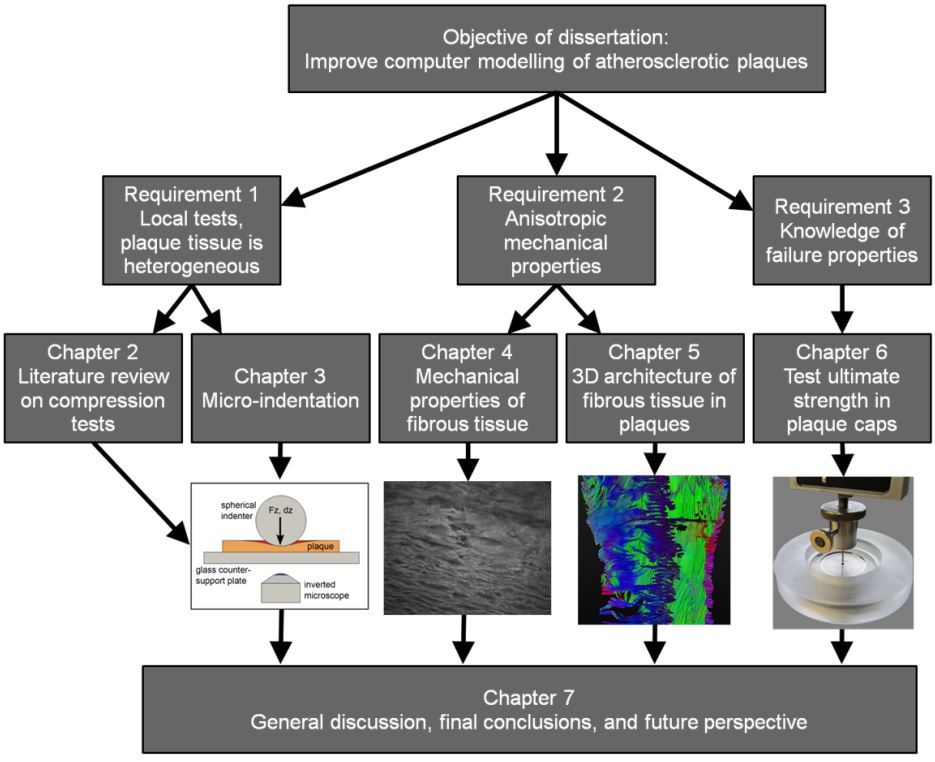

Figure 1.6: *Overview of the dissertation.*

Chapter 2

Compressive properties of plaques

The content of this chapter is based on C.-K. Chai*, L. Speelman*, C. W. J. Oomens and F. P. T. Baaijens. Compressive mechanical properties of atherosclerotic plaques-indentation test to characterise the local anisotropic behaviour. Journal of Biomechanics 47 (4), 784-792, 2014, *these authors contributed equally to this work (reprinted with permission from Elsevier).

2.1 Introduction

Atherosclerosis is a disorder of the arterial wall. The vessel wall is invaded by lipids and inflammatory cells that can eventually lead to formation of an atherosclerotic plaque. Some of these plaques develop into plaques that are vulnerable for plaque rupture. Such a vulnerable plaque consists of inflammatory cells, a lipid-rich necrotic core, intra-plaque haemorrhage, and a thin fibrous cap separating the thrombogenic lipid core from the bloodstream [16, 53]. In case of rupture of the thin fibrous cap, the lipid core comes into contact with the blood, causing luminal thrombus formation. This thrombus may cause a blockage in the vessels distal to the plaque. This is the major cause of ischaemic stroke and myocardial infarction [54].

Current methods to assess plaque rupture risk are mostly based on general risk factors (age, hypertension, and familial arterial diseases), and on geometrical plaque features (stenosis degree, intima-media thickness, and irregular, ulcerated plaque morphology) [55]. It has been shown that these risk factors are insufficient for predicting future plaque rupture events. A reliable computational model to predict cap rupture may, therefore, add to the diagnosis and treatment of atherosclerotic plaques. Since fibrous cap rupture occurs when the stresses in the cap exceed the strength of the cap, biomechanical plaque modelling has the potential to improve risk assessment of plaque rupture [56, 57]. Biomechanical plaque studies have revealed that patient-specific plaque models can accurately predict local stress peaks and rupture locations [33, 35, 49, 52, 58, 59, 60, 61, 62]. However, the stress results from these biomechanical models strongly depend on the material models and the parameters used [60, 63]. Determining the mechanical behaviour of the different plaque components is, therefore, a necessity.

Mechanical characterisation of plaque tissue is frequently done using (uni-)axial tensile tests [42, 44], which is discussed by Walsh et al. (2014) [38] in this special issue. Although plaque tissue *in vivo* experiences circumferential stretching during blood pressure pulsation, the tissue is also radially compressed during this pulsation. Therefore, also compression tests are physiologically relevant to determine the mechanical behaviour of plaque tissue.

The aim of this review paper is to give an overview of the methods used in literature to measure mechanical properties of atherosclerotic plaque tissue using compression experiments. In literature, studies were identified in which the compressive proper-

ties of human, porcine or murine plaques were tested, harvested from the aorta, iliac, femoral, or carotid arteries. Plaque tissue was tested using unconfined compression, micro-indentation, or nano-indentation. The results from the different studies and testing techniques will be compared. The advantages and disadvantages of each technique will be discussed. In case the stiffness data was presented non-conventionally, representative figures from the papers were digitised and used to fit a neo-Hookean material model and to extract tangential stiffness values.

After a summary of the literature on compressive plaque properties, an in-house developed micro-indentation test will be presented for the characterisation of anisotropic properties of plaque tissue. The relevance and limitations of this method will be discussed.

2.2 Compressive properties of plaque tissue

2.2.1 Unconfined compression

Unconfined compression tests are one of the most popular methods to determine mechanical behaviour of materials. The samples are mounted between two metal plates, of which the top plate is stationary and attached to a load measuring device. Generally, during unconfined compression, the tested tissue is smaller in size than the compression plates. The bottom plate can be raised and lowered with a pre-set speed to pre-set positions. Both displacement and force can be used as loading conditions. With unconfined compression tests, compressive mechanical plaque properties can be determined at large, physiologically relevant strain. It is a relatively straightforward test that allows both static and dynamic loading conditions. Using static loading conditions, material stiffness can be determined, while frequency-dependent dynamic characteristics can be identified using cyclic unconfined compression loading conditions at different frequencies.

Human aortic plaques

Lee et al. (1991) [64] evaluated radial compressive plaque properties, by compressing 27 fibrous caps from 14 abdominal aorta plaques using a 7 mm diameter cylindrical steel plate. Caps were classified as cellular (n=7), hypo-cellular (n=9), or calcified (n=11)

based on histological examination. The tests were conducted at room temperature within 16 hours of patient death. The dynamic stiffness of the test samples (thickness 1.1 $\pm$0.2 mm) was evaluated by applying a static compressive stress of 9.3 kPa in the radial direction first and, after a resting period to reach static equilibrium, a dynamic stress with an amplitude of 0.5 kPa at different frequencies afterwards. Stiffness values increased with increasing frequency; however, the change was less than 10% between 0.5 and 2 Hz. As the stiffness was determined at a fixed load, the samples were subjected to different compression levels (17 $\pm$6% for cellular, 7 $\pm$1% for hypo-cellular, and 1.2 $\pm$0.2% for calcified samples). The dynamic stiffness was 510 $\pm$220 kPa for cellular, 900 $\pm$220 kPa for hypo-cellular and 2.2 $\pm$1.0 MPa for calcified samples.

The same group studied the relation between compressive mechanical properties and intravascular ultrasound classification of aortic plaques, with a static measurement protocol, using the same set-up [65]. An initial compressive stress of 4.0 kPa was applied until a static equilibrium was reached. Thereafter, the compressive stress was increased up to 12 kPa. Strain and creep-times were recorded for this step and a stiffness modulus was determined. The compression strain was 24 $\pm$11% for non-fibrous caps, 11 $\pm$5% for fibrous caps and 3 $\pm$2% for calcified caps. Creep times varied from 20 minutes for calcified samples, 50 minutes for fibrous samples, and 80 minutes for non-fibrous samples. Non-fibrous samples had a stiffness modulus of 41 $\pm$18 kPa. The stiffness modulus for fibrous and calcified caps was 82 $\pm$33 kPa and 355 $\pm$245 kPa, respectively.

Although the static loading stress was not equal in both studies (9.3 kPa versus 8 kPa), the strain levels were comparable for the plaque samples. However, the reported static stiffness values were about one order lower compared to the reported dynamic stiffness values. Lee et al. (1992) [65] suggested that these differences may be attributed to the non-elastic mechanical behaviour of the tissue, as a different loading stress was applied in both studies (9.3 $\pm$0.5 kPa versus 8 kPa). Additionally, visco-elastic behaviour of the cap may play a role in the dynamic stiffness results. This is supported by the relative long creep-times, which were reported by Lee et al. (1992) [65].

Walraevens et al. (2008) [66] used unconfined compression to test the compressive mechanical properties of atherosclerotic calcified human aortas (n=19), obtained from aneurysm repair surgeries. The aortas were cut into 10 mm x 10 mm strips, with an average thickness of 1.84 $\pm$0.28 mm. The aortas were tested at room temperature using an impermeable pounder with a diameter of 6 mm. The E-moduli obtained at

10% strain were 321 ±258 kPa for calcified human plaques, which was similar to the calcified samples from Lee et al. (1992) [65], although the amount of compression was different (10% versus 3 ±2%).

Human iliac and femoral plaques

Topoleski et al. (1997) [67] investigated radial compressive behaviour of aortoiliac plaques by quasi-static compressing samples at 37°C using parallel flat acrylic fixtures (6.35 mm in radius) [67, 68]. Non-ulcerated lesions (n=24) were obtained from 6 autopsies and stripped from the remaining vessel wall. The samples (5 mm x 5 mm, 2.4 ±0.7 mm thickness) underwent two 15-cycle loading phases up to 350 kPa with a 10-15 minutes unloaded rest period in between. Three types of plaques were identified based on histological features, which all showed a distinct mechanical behaviour in terms of repeatability and recoverability. The maximum compressive strain at 350 kPa loading stress was 70 ±11% for atheromatous samples, 54 ±9% for fibrous samples, and 14 ±9% for calcified samples. Tangential stiffness values were extracted from the representative curves. Atheromatous samples showed the most compliant response (stiffness <10 kPa for compression values up to 25%). Fibrous samples were stiffer; however, much softer than calcified samples (<10 kPa versus 830 kPa at 5% compression and 85 kPa versus 13 MPa at 20% compression).

Using the same approach, Salunke et al. (2001) [69] investigated the compressive stress-relaxation behaviour of aortoiliac plaques in radial direction. Atherosclerotic plaques (5 calcified, 7 fibrous, and 6 atheromatous samples) were obtained post-mortem. After two 15-cycle preconditioning phases, the samples (5 mm x 5 mm, 1.5 ±0.7 mm thickness) were subjected to three stress-relaxation phases, with 25% compression within 1 second between 16 mm diameter parallel plates. Stiffness values were determined from representative curves. Fibrous plaques and calcified plaques showed similar stiffness values (100 kPa versus 70 kPa at 5% compression and 900 versus 1000 kPa at 20% compression), while atheromatous tissue had a lower average stiffness (25 kPa at 5% compression and 100 kPa at 20% compression). Compared to Topoleski et al. (1997) [67], the dynamic stiffness of fibrous and atheromatous plaque tissue was higher than the static stiffness, while calcified tissue had a lower dynamic stiffness. The non-elastic behaviour of the plaque tissue may have caused differences between quasi-static and dynamic experiments. This is supported by the differences found in relaxation behaviour for the various plaques types. Although none of the

plaques were completely recovered after 10 minutes, atheromatous plaques clearly showed a different response compared to fibrous and calcified samples.

Human carotid plaques

Maher et al. (2009) [42] performed unconfined compression tests in radial direction on carotid artery plaque sections (4 mm in diameter). Plaque samples (n=44 from 11 patients) were classified as calcified (n=16), echolucent (n=5), and mixed (n=23) based on ultrasound imaging and were loaded up to 60% compression with a rate of 1% per second. Significant variation was found in the compressive behaviour between and within patients. Calcified samples showed the stiffest response with an average tangential stiffness of 140 kPa at 5% compression and 2300 kPa at 20% compression. The echolucent and mixed samples showed softer average stiffness with 20 and 20 kPa at 5% compression and 100 and 330 kPa at 20% compression, respectively.

The same group evaluated the inelastic behaviour of carotid plaques using dynamic cyclic compressive tests at room temperature [43]. Tests were conducted using 21 samples from 8 patients. Also here ultrasound was used to classify the samples as calcified (n=8), echolucent (n=5), and mixed (n=8). The samples were loaded and unloaded at a rate of 5% per second, with 5 consecutive loading cycles at levels of 10, 20, 30, 40, and 50% strain. Corresponding to Maher et al. (2009) [42], the calcified plaques were on average the stiffest plaque type (2.7 MPa at 50% compression) while the echolucent plaques were the softest (1.4 MPa at 50% compression). The mixed samples showed an intermediate stiffness (2.1 MPa at 50% compression). For all plaque samples, permanent deformation was observed, which increased with the applied strain level. The magnitude of the permanent deformations occurring during unloading of the plaque was similar for all plaque types.

2.2.2 Micro-indentation

Micro-indentation tests can be used for measuring more local material stiffness of relatively small and inhomogeneous material. The indenters used in micro-indentation testing systems are relatively small compared to the tested tissue. Due to the shape of the indenter and variation in tissue thickness, tissue stiffness cannot be directly derived from the force-depth curves. Numerical simulations are necessary to extract

the mechanical properties from the force-depth curves using an inverse approach. The experimental curves are fitted to the curves of the numerical simulation of the indentation to determine the tissue stiffness.

Human carotid plaques

Barrett et al. (2009) [70] measured mechanical properties of carotid atherosclerotic plaque caps using a micro-indentation device. A spherical indenter with a diameter of 1 mm was used to study the quasi-static radial compressive properties of fibrous caps (thickness 0.25-0.75 mm) dissected from carotid artery plaques, within 3 hours after surgery. Indentations were carried out until either a force of 0.2 N was reached, or when an indentation depth of 0.5 mm was exceeded. Tangential stiffness values were determined with an inverse finite element model and ranged from 21 to 300 kPa (median of 33 kPa at 5-20% compression).

In a recent study, the local mechanical properties of carotid atherosclerotic plaque tissue were characterised in the axial direction [71]. Micro-indentations were performed with a 2 mm diameter spherical indenter on 8 human carotid plaques on 200 µm thick axial cross-sections. The plaques were snap-frozen directly after carotid endarterectomy and stored at -80°C until further processing. In total, 214 locations were tested in the middle of the fibrous cap (n=43), shoulder of the cap (n=61), intima (n=90), or lipid-rich necrotic core (n=20). Using an inverted confocal microscope, local collagen architecture was determined for all locations. The obtained force-response of up to 30% indentation was fitted to simulated data generated from a computational finite element model. Isotropic neo-Hookean behaviour and homogeneity of the tested plaque tissue were assumed. The obtained Young's moduli ranged from 6 kPa to 891 kPa (median of 30 kPa) at 30% compression, which was similar to the data obtained by Barrett et al. (2009) [70]. Due to considerable variation per location, no significant differences could be identified between the middle of the fibrous cap, the shoulder cap regions, and the intima locations. Also, no significant differences were found between the Young's moduli of structured and unstructured collagen architectures. This suggests that for the entire diseased intima the axial compressive mechanical properties might be considered as homogenous, although the large variation indicates that measurement uncertainties need to be taken into account in further analyses.

2.2.3 Nano-indentation

Even within the different plaque components the tissue is highly heterogeneous, which means that even micro-indentation might be insufficient to detect local difference in mechanical properties. To address this issue, nano-indentation can be applied. One possible method to apply nano-indentation is the use of an atomic force microscope (AFM). It is a very high resolution type of scanning probe microscope that can be used to measure how much force is required to push the micrometer indenter into the tissue. AFM is generally used to scan a tissue surface to produce images that reflect the forces that are experienced by the indenter. Additionally, it can be used to perform very local force-indentation measurements, to obtain the mechanical characteristics of the tissue. Generally, only very small displacements can be applied using this technique.

Human carotid plaques

Ebenstein et al. (2009) [50] tested fresh (n=5) and frozen (n=5) human carotid plaques using nano-indentation. The tissue was classified based on Fourier transform infrared (FTIR) spectroscopy to distinguish different plaque components. The plaque components were indented using a conospherical diamond probe tip with a diameter of 200 µm. The applied peak loads were between 10 to 600 µN, with a maximum indentation depth of 5 µm. In total 377 indentations were performed, 34 at hematoma, 172 at fibrous, 72 at partially calcified, and 99 at calcified locations. The resulting Young's moduli for the samples were 230 $\pm$210 kPa for hematoma, 270 $\pm$150 kPa for fibrous tissue, 2.1 $\pm$5.4 MPa for partially calcified fibrous tissue, and 0.7 $\pm$2.3 GPa for calcified tissue. Due to the limited indentation depth only properties at the low strain region were obtained, without capturing the non-linear material behavior at higher strains. There was no significant difference between frozen and fresh plaques, suggesting that freezing the tissue at -20°C does not change the mechanical properties.

Besides human atherosclerotic tissue, also murine aortic plaques were tested using an AFM to characterise mechanical plaque properties [72, 73]. Tracqui et al. (2011) [73] differentiated between cellular fibrotic (mean Young's modulus of 10 $\pm$6 kPa), hypocellular fibrous cap (mean Young's modulus of 59 $\pm$47 kPa), and lipid-rich regions (mean Young's modulus of 6 $\pm$4 kPa), based on histology. The results from Tracqui et al. (2011) [73] and Hayenga et al. (2011) [72] were very similar; however, it is unclear how stiffness results of murine plaques translate to stiffness data of human plaques. However, nano-indentation may prove to be a useful tool for mechanical characterisa-

tion of thin caps of human atherosclerotic plaques.

2.2.4 Discussion of the compression techniques

Different techniques to measure the compressive mechanical properties of plaque tissue have been reviewed. Advantages and disadvantages of each technique were discussed in this paper. Depending on the application of the obtained results, one should use the appropriate technique.

Unconfined compression is a widely available method, which can be used for static and dynamic testing, providing global stiffness and relaxation data. As plaque tissue is generally highly heterogeneous, the use of large indenter plates does not allow a very accurate classification of the tested tissue. Therefore, only global tissue classifications (non-fibrous, fibrous, or calcified) are possible, resulting in a large variation in reported mechanical properties within each classification group. As pointed out by Ebenstein et al. (2009) [50], even for the single classification 'calcified plaque', there are different gradations of calcification, depending on the degree of mineralisation of the tissue. This might explain why overlap is often found in the mechanical properties of fibrous and calcified testing locations. Micro-indentation techniques combine physiologically relevant strains with indenters with an appropriate size to perform local measurements and, therefore, seem to be a good candidate for determining local mechanical properties of atherosclerotic plaque tissue. Besides dedicated hardware, this method requires an inverse finite element analysis to reconstruct stiffness data from the measured force-indentation depth data. To achieve the most reproducible and accurate results with micro-indentation, the tested material under the indenter should be homogeneous. In Chai et al. (2013) [71], the plaque tissue was cut into 200 µm thin slices to obtain sections as homogeneous as possible in thickness [71]. However, since cutting the plaque tissue disrupts the local collagen fibres, which play an important role as load-bearing structure of the tissue, the resulting mechanical properties may be affected by this approach. Since plaque tissue is very heterogeneous, local measurements are relevant and testing locations away from tissue edges or damaged locations might have only a minimal influence. Barrett et al. (2009) [70] isolated atherosclerotic plaque caps from the underlying tissue, which is a difficult and laborious procedure and likely produces a bias towards thicker fibrous caps. The caps tested by Barrett et al. (2009) [70] were between 250 and 750 µm thick. Kolodgie et al. (2001) [25] concluded that unstable plaques show fibrous cap thicknesses of <65 µm. Besides the fact that handling of

these thin caps may be very challenging, the spherical micro-indenters with diameters of 1 mm or 2 mm are likely to be too large for these caps.

Nano-indentation enables stiffness characterisation of individual collagen fibres and cells, but generally at small strains. Reconstructing the measured data from nano-indentation into mechanical stiffness data is quite complex, as advanced contact algorithms are required due to the small size of the indenter. Extrapolating nano-indentation results to a more macroscopic plaque component material behaviour for biomechanical modelling is not trivial, as also volume fractions and interactions between components need to be known. Nevertheless, nano-indentation may provide valuable data for multi-scale biomechanical modelling. Moreover, nano-indentation might be more appropriate for very thin caps, since it can be applied on tissue as thin as 16 µm, as shown by Tracqui et al. (2011) [73]. However, nano-indentation can only be performed at limited indentation depths, and may, therefore, not be able to measure at physiological strains, depending on the thickness of the tested tissue. If the measurements are only performed at low strain, the non-linear mechanical behaviour of the plaque tissue may not be captured. Measuring at small strains might lead to underestimation of the stiffness of the tissue, as the collagenous fibrous plaque tissue often displays significant strain-stiffening. This can be clearly seen in the stiffness results from the unconfined compression studies indicated in Table 2.1 [42, 43, 67, 69]. In all cases, the samples are stiffer at higher strain values. On the other hand, micro-indentation experiments of Chai et al. (2013) [71] and Barrett et al. (2009) [70] did not show a clear non-linear behaviour, while in these studies also physiological strains were applied.

In all the studies evaluated here, a lot of variation in testing protocol can be observed (Table 2.2). Although the mechanical tests are preferably performed on fresh tissue, at body temperature (37°C), with an appropriate preconditioning protocol, not all studies are performed under these conditions. Additionally, differences in loading protocol are apparent. Most of the studies found in literature performed static or quasi-static measurements [42, 50, 65, 66, 67, 70, 71], avoiding dynamic effects caused by inelasticity. Measuring at slow testing rates might allow tissue components to fully adjust to the applied loads. In other studies, dynamic loading conditions were applied to obtain inelastic and recoverability parameters [43, 64, 69]. High testing rates and cyclic tests with high frequencies does not allow the tissue to fully respond, possibly causing less deformation and consequently higher stiffness results. This might explain the results

Table 2.1: *Results of the studies treating human atherosclerotic tissue*

Authors (year)	Artery	Testing Method	Sample type	Compression	Stiffness
Lee et al. (1991) [64]	Aorta	Unconfined Compression (dynamic)	Cellular	17±6%	510±220 kPa
			Hypocellular	7±1%	900±200 kPa
			Calcified	1.2±0.2%	2.2±1.0 MPa
Lee et al. (1992) [65]	Aorta	Unconfined Compression (static)	Non-fibrous	24±11%	41±18 kPa
			Fibrous	11±5%	82±33 kPa
			Calcified	3±2%	355±245 kPa
Walraevens et al. (2008) [66]	Aorta	Unconfined Compression (static)	Calcified	10%	321±258 kPa
Topoleski et al. (1997) [67]	Aortoiliac	Unconfined Compression (static)	Atheromatous	70±11%	< 10 kPa
			Fibrous	54±9%	<10 kPa (5%); 85 kPa (20%)
			Calcified	14±9%	830 kPa (5%); 13 MPa (20%)
Salunke et al. (2001) [69]	Aortoiliac	Unconfined Compression (dynamic)	Atheromatous	25%	25 kPa (5%); 100 kPa (20%)
			Fibrous	25%	100 kPa (5%); 900 kPa (20%)
			Calcified	25%	70 kPa (5%); 1.0 MPa (20%)
Maher et al. (2009) [42]	Carotid	Unconfined Compression (static)	Echolucent	60%	20 kPa (5%); 100 kPa (20%)
			Mixed	60%	20 kPa (5%); 330 kPa (20%)
			Calcified	60%	140 kPa (5%); 2.3 MPa (20%)
Maher et al. (2011) [43]	Carotid	Unconfined Compression (dynamic)	Echolucent	10-50%	189 kPa (20%); 1.4 MPa (50%)
			Mixed	10-50%	105 kPa (20%); 2.7 MPa (50%)
			Calcified	10-50%	147 kPa (20%); 2.1 MPa (50%)
Barrett et al. (2009) [70]	Carotid	Micro-Indentation	Fibrous cap	5-20%	33 (21-300) kPa
Chai et al. (2013) [71]	Carotid	Micro-Indentation	Intima	30%	30 (6-891) kPa
Ebenstein et al. (2009) [50]	Carotid	Nano-indentation	Hematoma	<5µm	230±210 kPa
			Fibrous	<5µm	270±150 kPa
			Calcified/fibrous	<5µm	2.1±5.4 MPa
			Calcified	<5µm	0.7±2.3 GPa

found by Lee et al. (1991) [64] where the dynamic stiffness was found to be higher than the static stiffness. In general, the stiffness values between static and dynamic mechanical studies were very different. This might be, as mentioned by Lee et al. (1991) [64], attributed to visco-elastic and poro-elastic behaviour of the tissue, which may be different for different plaque components. Topoleski et al. (1997) [67] applied quasi-static unconfined compression and obtained stiffness data ranging from 10 kPa (atheromatous plaques) to 13 MPa (calcified plaques). The same group [69] used the same set-up and obtained dynamic stiffness results ranging between 100 kPa and 1000 kPa (20% compression). For atheromatous and fibrous tissue, the dynamic stiffness was higher than the static stiffness, although for calcified tissue the static results were stiffer than the dynamic results. It should be noted that the data from all studies showed a large variability. This is partly caused by the different techniques, but also by the high natural variability in mechanical behaviour of the tested samples. An accurate classification of the tissue could be beneficial for the interpretation of the results from different studies and might reduce the variability within the studies. A better classification method might for example be based on Fourier transform infrared spectroscopy, as previously used by Ebenstein et al. (2009) [50]. Investigating the dynamic mechanical behaviour of plaque tissue is certainly relevant since the cardiovascular system is a dynamic system which also applies hemodynamic loads on atherosclerotic plaques and causes dynamic responses of the tissue.

Due to the large variation of the stiffness results in all studies, it is impossible to draw definite conclusions on the differences in mechanical behaviour of plaques from different vascular locations. Even for plaques originating from the same vascular territory, but tested with different compression protocols, results cannot be compared directly. On average, micro-indentation results of carotid plaques [70, 71] showed much lower stiffness values than results from unconfined compression of plaques from the same territory [42], although overlap exists in the testing results. If unconfined compression tests are dominated by relative stiff inclusions in the tested tissue, this may explain why the local micro-indentation tests results in lower stiffness values on average, with values closer to the unconfined compression stiffness values for calcified inclusions. Since differences in testing approach also leads to differences in mechanical stiffness results, it is important to put the results from these studies in the correct perspective. The application (multi-scale modelling, macroscopic plaque modelling, and stiffness comparison for different plaque types or location) should determine which type of testing

Table 2.2: *Details of the studies treating human atherosclerotic tissue*

Authors (year)	Artery	Testing Method	Testng direction	Numbers of Patients	Number of samples and description in the study	Sample size	Testing temperature	Testing time	Preconditioning
Lee et al. (1991) [64]	Aorta	Unconfined Compression (dynamic)	Radial	14	27 fibrous caps (7 cellular, 9 hypocellular, 11 calcified)	≥4.5 mm in radius	room temperature	Within 16 hours after death	Allowed to creep for 30 min
Lee et al. (1992) [65]	Aorta	Unconfined Compression (static)	Radial	22	43 atheroma caps (18 fibrous, 14 nonfibrous, 11 calcified)	≥4.5 mm in radius	room temperature	NF	Allowed to creep and creep times were reported
Walraevens et al. (2008) [66]	Aorta	Unconfined Compression (static)	Radial	19	19 samples	10 mm x 10 mm cylindrical pounder 6 mm diameter	room temperature	Within 5 hours after aortic repair surgery	no
Topoleski et al. (1997) [67]	Aortoiliac	Unconfined Compression (static)	Radial	6	24 samples from non-ulcerated lesions	5 mm x 5 mm fixtures with 6.35 mm radius	37°C	Within 12-48 hours after death	Repeatability and recoverability experiments
Salunke et al. (2001) [69]	Aortoiliac	Unconfined Compression (dynamic)	Radial	NF	18 samples from non-ulcerated lesions (5 calcified, 7 fibrous, 6 atheromatous)	5 mm x 5 mm plates with 16 mm diameter	37°C	Within 12-48 hours after death	Repeatability and recoverability experiments
Maher et al. (2009) [42]	Carotid	Unconfined Compression (static)	Radial	11	44 plaque samples (16 calcified, 5 echolucent, 23 mixed)	4 mm in diameter	NF	Within 2 hours after endarterectomy	10 times up to 10% strain
Maher et al. (2011) [43]	Carotid	Unconfined Compression (dynamic)	Radial	8	21 plaque samples (8 calcified, 5 echolucent, 8 mixed)	4 mm in diameter	room temperature	Within 2 hours after endarterectomy	Repeatability and recoverability experiments
Barrett et al. (2009) [70]	Carotid	Micro-Indentation	Radial	8	8 plaques	Indenter radius 0.5 mm	NF	Within 3 hours after endarterectomy	NF
Chai et al. (2013) [71]	Carotid	Micro-Indentation	Axial	8	6-13 slices per plaque, 214 locations in total (43 fibrous cap, 61 plaque shoulder, 90 intima, 20 necrotic core)	Indenter radius 1 mm	room temperature	Snapfrozen directly after endarterectomy, storage time unknown	2 pre-conditioning cycles
Ebenstein et al. (2009) [50]	Carotid	Nano-indentation	Radial	10	377 locations (34 hematoma, 172 fibrous, 72 partially calcified, 99 calcified locations)	Conospherical indenter diameter 200 μm	room temperature	5 samples stored at -20ºC, 5 samples fresh <24h	NF

NF: not found

system and protocol is most applicable. In the reviewed experimental studies, the most occurring compression direction is radial, except for Chai et al. (2013) [71], where the compression direction was axial. Indentation in the radial direction is a more physiologically relevant loading condition, as plaque tissue is mostly compressed in this direction and stretched circumferentially. The expected anisotropy of the tissue suggests that testing the stiffness of plaque tissue in different directions will lead to different results [45]. However, in Chai et al. (2013) [71] a small set of longitudinal samples was also tested and the circumferential compressive stiffness results were comparable to the axial results.

A major limitation of the three presented measurements techniques is the fact that only isotropic behaviour can be determined from the measurement data. Given the high collagen fibre content and alignment in the plaque, the assumption of isotropic behaviour is likely not valid. In the next section, a method based on micro-indentation is presented that can be applied to determine anisotropic material behaviour of atherosclerotic plaque tissue.

2.3 Local anisotropic behaviour of human carotid plaques

In this section, an in-house developed micro-indentation test setup [74] is introduced that can be used to perform mechanical testing on soft tissue and allows the analysis of the anisotropic mechanical behaviour [75]. With this set-up, anisotropic material properties were previously derived of tissue-engineered constructs, tissue engineered heart valves, and bio-artificial muscle tissue [75, 76, 77] The testing method will be illustrated with data from a single atherosclerotic carotid plaque sample, which was obtained during carotid endarterectomy.

2.3.1 Sample preparation

After carotid endarterectomy, the sample was snap-frozen in liquid nitrogen and stored at a temperature of -80°C. In a later stage, the frozen sample was axially sliced using a cryotome at -20°C, to obtain 200 µm thick sections at 1 mm intervals (Figure 2.1). Prior to the indentation tests, the sections were thawed and a fluorescent collagen

staining (CNA-35; [78]) was applied overnight at 4°C. Approval was given by the local institutional review board and informed consent was obtained from the patient. A more detailed description of the sample preparation can be found in Chai et al. (2013) [71].

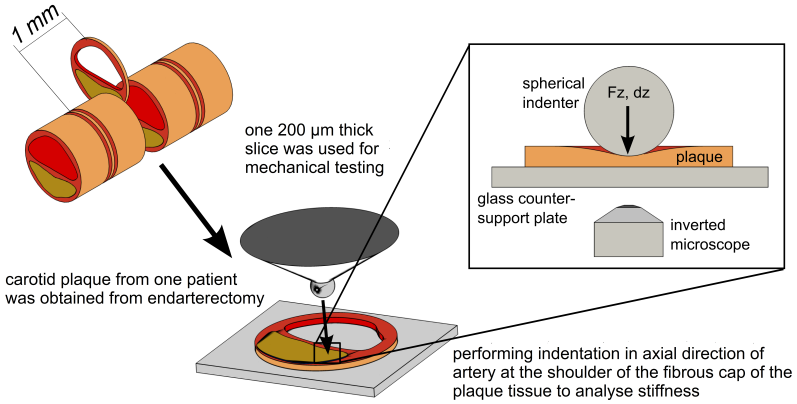

Figure 2.1: *Sectioning of plaque tissue with a cryotome to create a 200 µm thick slice for mechanical testing.*

2.3.2 Micro-indentation test

For the mechanical testing, the section of the plaque was placed under the micro-indentation setup. The micro-indentation was performed in the axial direction of the vessel using a sapphire spherical indenter with a diameter of 2 mm. The indenter was placed above an inverted confocal microscope to visualise the collagen deformation during indentation in the bottom plane of the section. During the indentation experiment, the force-response, indentation depth and collagen deformation were recorded. Digital image correlation (DIC) was applied on the collagen deformation images using commercially available software (ARAMIS, GmbH, Germany), the local displacement field during indentation. From the displacement field, the local deformations and principal strain directions were determined. The displacements, local first (ε_x) and second (ε_y) principal strain magnitude and direction of the collagen fibres were quantified as function of the indentation depth (Figure 2.2). The fibre displacement versus the global stress clearly illustrates the anisotropic behaviour of the plaque (Figure 2.3). The tissue offers much more resistance in the direction of the fibre alignment whereas

perpendicular to the fibre direction much higher strain occurred during indentation. More details on the testing protocol can be found in Chai et al. (2013) [71].

The force-response, the indentation depth, and the quantified collagen deformation were used as input for an inverse finite element analysis to determine the in-plane anisotropic behaviour of the tested tissue.

2.3.3 Inverse finite element analysis

To represent the indentation test setup for the inverse finite element analysis (FEA), a three-dimensional computational model was generated (Figure 2.2). An anisotropic material model, proposed by Driessen et al. (2008) [79], was applied for the atherosclerotic tissue:

$$\tau = \tau_m + \tau_f = G_m(F \cdot F^T - I) + \sum_{i=1}^{N_f} \phi_f^i [\psi_f^i - \vec{e}_f^i \cdot \tau_m \cdot \vec{e}_f^i] \vec{e}_f^i \vec{e}_f^i \qquad (2.1)$$

Here, the local collagen structure of the atherosclerotic plaque is described by splitting the extra stress tensor $\boldsymbol{\tau}$ into an isotropic matrix part τ_m and an anisotropic fibre part τ_f. The extracellular matrix is characterised by τ_m and modelled as an incompressible neo-Hookean material, with matrix shear modulus G_m. $\boldsymbol{F}$ is the deformation tensor and $\boldsymbol{I}$ the unity tensor. The anisotropic part τ_f represents the collagen fibres in the tissue with $\vec{e}_f^i$ the current fibre direction, ψ_f^i the fibre stress, and N_f the discrete number of fibres. The volume fraction of fibres ϕ_f^i is modelled with a periodic Gaussian distribution, as shown below:

$$\phi_f^i(\gamma_i) = Aexp(\frac{\cos[2(\gamma_i - \alpha)] + 1}{\beta}) \qquad (2.2)$$

Here, γ_i is the fibre angle and A the scaling factor to make sure that $\phi_{tot} = 1$. The main fibre direction is α, and β is the fibre distribution, both parameters α and β are derived from the confocal images (Figure 2.2). In our test sample, the main fibre direction α was 101°, which is close to a circumferential orientation. The fibre distribution β was 0.7 indicating a rather anisotropic distribution, which matches with the image in Figure 2.2.

The fibre stress ψ_f was modelled based on Holzapfel et al. (2000) [80], where ψ_f was described as a function of the fibre stretch λ_f, the fibre stiffness k_1 and the non-linearity factor k_2.

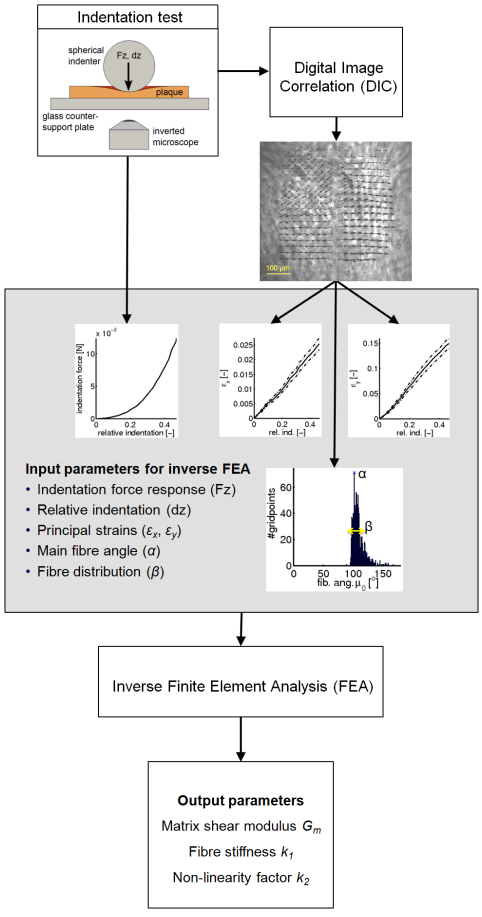

Figure 2.2: *Flowchart depicting the input and output parameters of the inverse Finite Element Analysis. From the indentation experiment the force-depth curves were obtained. Confocal imaging of the collagen structure of atherosclerotic plaque tissue during indentation allows digital image correlation (black arrows indicate the deformation) to derive the principal strains. From the confocal images also the fibre main angle and fibre dispersion were obtained. This data was used as input for the inverse FEA to infer matrix shear modulus G_m, fibre stiffness k_1, and non-linearity factor k_2.*

$$\psi_f^i = 2k_1\lambda_f^2(\lambda_f^2 - 1)exp(k_2(\lambda_f^2 - 1)^2) \tag{2.3}$$

The fibre stretch λ_f is derived from the digital image correlation (DIC), while k_1 and k_2 are output parameters from the inverse FEA, together with the matrix shear modulus G_m. For the inverse FEA, an iterative mixed experimental-computational approach based on the method by Cox et al. (2006) [76] and Meuwissen et al. (1998) [81] was applied. The difference between experimental measurements and the simulated data

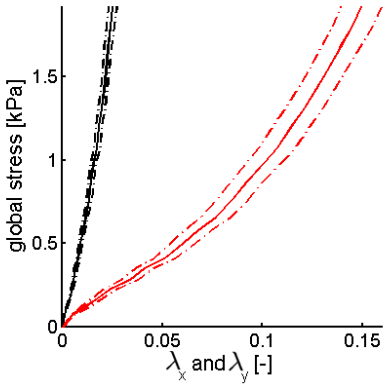

Figure 2.3: *The diagram shows the global stress against the collagen fibre displacement. - λ_x fibre stretch, - λ_y displacement perpendicular to fibre alignment. It shows again highly anisotropic behaviour of the tissue. The resistance in the direction of the fibres is much higher, whereas much higher strain appears perpendicular to the fibre direction.*

obtained from the FEA was minimised by applying a Gaussian-Newton minimisation algorithm. For our test sample, the matrix stiffness G_m reached the lower limit of 1.0 kPa, while the fibre stiffness k_1 was determined as 16.3 kPa. The non-linearity factor k_2 was 0.8. The tested sample showed a very anisotropic material (Figure 2.3) with a non-linear behaviour and a relative low fibre stiffness, compared to reported values (Table 2.1). Future anisotropic characterisation of plaque tissue will provide insight in the values and variation of the mechanical properties of human atherosclerotic tissue. For more information on the DIC and inverse finite element analysis, see Cox et al. (2006, 2008) [75, 76].

Figure 2.4 shows the experimental and simulated data for our test sample with the optimal material parameters. The simulated data corresponded very well to the experimental data, indicating that the proposed material model accurately describes the mechanical behaviour of the tested tissue. Future studies will show if this material model also appropriately characterises atherosclerotic plaque tissue in general.

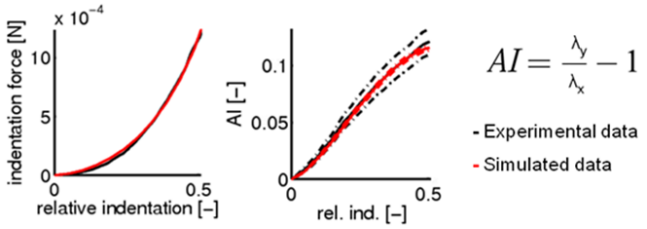

Figure 2.4: *For the parameter estimation the indentation force, indentation depth, and the collagen fibre displacement depicted as AI were used as input. These measurements were fitted to the simulated data from the FE simulations.*

2.4 Discussion

The combination of an indentation test with a confocal microscope does not only enable the measurement of indentation force and depth, but also the visualisation of collagen fibre deformation, perpendicular to the indentation direction. From this, anisotropic mechanical data can be extracted that is representative for the extensional properties in the plane perpendicular to the indentation direction at finite strains. Information on anisotropic material parameters may improve the accuracy and reliability of biomechanical plaque models and, additionally, the risk assessment of plaque rupture.

In this paper, material parameters of a single atherosclerotic carotid plaque sample were presented, revealing highly anisotropic mechanical behaviour of the plaque. Confocal microscopy confirmed a high alignment of collagen fibres. The global stress-strain behaviour showed that the highest strain occurred perpendicular to the main fibre direction and that tissue stretch in the fibre direction was much smaller. More atherosclerotic plaque samples need to be tested to fully evaluate the anisotropic mechanical behaviour of carotid plaque tissue.

In the *in vivo* situation, the blood vessel experiences global blood pressure in the radial direction, with circumferential (and axial) stretching and radial compression of the vessel wall. The used indentation technique applies a local compressive force in axial direction, resulting in local circumferential and radial stretching of the tissue. Computer simulations have shown that the level of circumferential stretch in this study corresponds to the level of stretch in the physiological situation. As the collagen fibres are the major load-bearing structures in the wall, mainly oriented in the circumferential direction, the indentation technique evaluates the mechanical properties of the collagen fibres in the most relevant direction. Additionally, by testing relatively thin slices in

axial direction it was strived to test a slice of homogeneous material over the thickness. Also, these thin slices enable the assumption of a uniform fibre distribution throughout the slice thickness, required for the inverse finite element analysis. On the other hand, the slicing may also disrupt the coherence in the collagen fibre architecture. Since the collagen fibres are the load-bearing structure of the blood vessel, this might have an impact on the mechanical properties.

Another factor that can affect the collagen structure is the axial *in vivo* pre-stretch. On average, arteries are under 30% pre-stretch [82, 83, 84], likely resulting in a more axial collagen distribution than the stretch free samples tested with the indentation test. This altered collagen distribution may have an effect on the macroscopic stiffness results as determined with the inverse finite element analysis. Accounting for the axial pre-stretch in the inverse finite element analysis may give more insight in the effect of this pre-stretch on the mechanical behaviour of the tissue.

The studied plaque tissue was frozen and stored due to logistical reasons. The collagen fibres might be damaged due to the freezing process. However, ice-crystal formation was minimised by snap-freezing the tissue in liquid nitrogen after endarterectomy. The confocal images, histological images, and light microscopy evaluation did not show any tissue damage due to ice-crystal formation. Additionally, Ebenstein et al. (2009) [50] concluded that there were no differences in mechanical behaviour between fresh and frozen plaque samples.

2.5 Main conclusions

Mechanical testing of atherosclerotic plaque tissue involves several difficulties. Depending on the required information, more global or local measurements can be applied. Global mechanical properties of plaque tissue have been characterised using unconfined compression, tensile, or inflation tests. These tests rely on (intact) blood vessels with a significant size. However, atherosclerotic plaque tissue is often only available in small samples, insufficient for a proper handling and testing. Testing small-sized plaques with compression, inflation, bi-axial, or uni-axial tensile tests is rather difficult. Additionally, since plaque tissue is heterogeneous, consisting of different components, it can be assumed that its mechanical properties are also heterogeneous. Tests using a smaller sized indenter allow a more local measurement, therefore, avoiding the tissue

size problem. Nano-indentation tests allow very local measurements. However, the found studies applying small micro-meter indenter tips could only test plaque tissue at small strains. To characterise the mechanical properties of plaque tissue, it is crucial that mechanical testing is done at physiological strain. Using micro-indentation, local force-indentation measurements can be performed on relative homogeneous tissue at physiological relevant strain values. As shown in this review, micro-indentation may also be used to identify anisotropic material behaviour of plaque tissue. In conclusion, compressive mechanical properties of atherosclerotic plaques can be determined using unconfined compression (global and dynamic properties), micro-indentation (local properties) or nano-indentation (micro level properties). Depending on the desired information, one of these techniques can be used and the advantages and disadvantages can be found in this review.

Chapter 3

Local properties of carotid plaques

The content of this chapter is based on C.-K. Chai, A. C. Akyildiz, L. Speelman, F. J. H. Gijsen, C. W. J. Oomens, M. R. H. M. van Sambeek, A. van der Lugt, and F. P. T. Baaijens. Local axial compressive mechanical properties of human carotid atherosclerotic plaques-characterisation by indentation test and inverse finite element analysis. Journal of Biomechanics, 46 (10), 1759-1766, 2013 (reprinted with permission from Elsevier).

3.1 Introduction

Atherosclerotic plaque rupture is the main cause of ischemic stroke and myocardial infarction. Plaque rupture can lead to thrombus formation on the disrupted plaque surface and subsequent embolisation of thrombus into the distal vessels or to acute vessel occlusion. Rupture-prone plaques are characterised by the presence of inflammatory cells, intraplaque haemorrhage and a lipid-rich necrotic core (LRNC) covered by a thin fibrous cap. A reliable prediction model of cap rupture has a big impact on the diagnosis and treatment of atherosclerosis and atherosclerosis-related diseases [21]. Currently, the used methods to estimate plaque rupture is merely based on geometrical parameters, whereas biomechanical models have shown to provide a better risk assessment [36, 60, 72, 73, 85]. However, the results of these models strongly depend on material properties of individual plaque components. Therefore, these models will benefit from specific knowledge of material properties of individual plaque components.

Experimental data on the mechanical properties of atherosclerotic tissue are scarce and show large variability, ranging from very soft (30-40 kPa, [65, 70]) to very stiff (of order 1 MPa, [41, 45, 51, 64]). Moreover, most of the data represent only the average global stiffness of the plaque tissue tested and do not distinguish between different components within a plaque.

Recently, an experimental technique was developed by [75, 76], combining micro-indentation tests on soft biological materials with confocal laser scanning microscope imaging. We apply this technique to investigate the compressive Young's moduli of different plaque components in the axial direction.

3.2 Methods

3.2.1 Preparing plaque tissue

Eight carotid artery endarterectomy specimens were obtained from eight symptomatic patients (2 female, 6 male, age 59 to 87 years). All plaques had $\geq$ 70% stenosis and low calcium content on preoperative CT angiography. Approval was given by the Institutional Review Board of the Erasmus MC, and informed consent was obtained. The plaques were snap-frozen, using liquid nitrogen and stored at -80°C. In a later stage, the plaques were sectioned, using a Leica cryotome at 20°C. Slices of 200 µm thick-

nesses were obtained with 1 mm spacing in between for the indentation experiments (Figure 3.1).

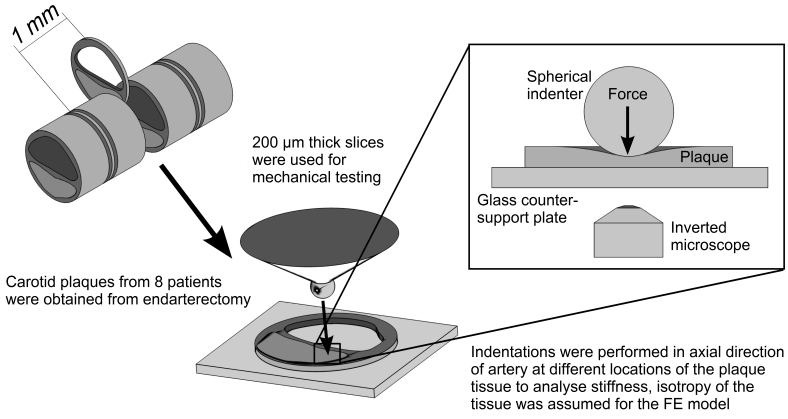

Figure 3.1: Sectioning of plaque tissues with a cryotome to create 200 mm thick slices for mechanical testing. Depending on the axial length of the plaque, 6-13 slices were obtained. Adjacent slices are used for histology.

Distal and proximal to each test section, slices of 5 µm thickness were cut for histology. A Gomori trichrome staining was applied on these slices. This stains collagen green/blue, muscle cells red, and nuclei black/blue. The histological images were used to determine indentation locations by visual registration before the experiments.

Prior to the mechanical testing, the 200 µm thick sections were thawed to room temperature and stained overnight using a fluorescent CNA35-OG488 probe [78]. This fluorescent staining was applied to visualise the collagen architecture of the plaque tissue.

3.2.2 Indentation test and imaging

To analyse the local mechanical properties of a plaque tissue, an existing indentation test set-up [75] was adapted, using a surface force apparatus developed by Vaenkatesan et al. (2006) [74]. At each testing location at least three consecutive indentations were performed using a spherical indenter with a diameter of 2 mm. During indentation the force response and the indentation depth were recorded. As described in Cox et al.

(2010) [77], the first indentation was considered as preconditioning and these results were not included. The measurements at the same indentation location were averaged. An inverted confocal laser scanning microscope (magnification 10x, excitation 488 nm, emission 500 nm high-pass), located underneath the set-up, was used to visualise the collagen structure, which were fluorescently stained (Figure 3.1, Figure 3.2, [78, 86]). More detailed information regarding the indentation set-up can be found in Cox et al. (2005) [87].

3.2.3 Data analysis

A 3D finite element model was created to simulate the indentation experiments, as previously described by Cox et al. (2008) [75]. The behaviour of the tissue was described with an isotropic incompressible Neo-Hookean model. The local shear modulus G at the test location was estimated by fitting the model to the experimental force-indentation-depth curve. The force response of up to 30% indentation of the tissue thickness was used for the parameter identification (Figure 3.3). Simulations confirmed that the circumferential strain at 30% indentation of tissue thickness was about 20%, which corresponds to the upper limit of physiological strain range. The contact radius between indenter and tissue was about 0.4 mm². To fit the experimental data with the simulated data, the least-square method was used. To compare the results obtained in this study with the results in literature the Young's modulus E was calculated from the shear modulus G with

$$E = 3G \tag{3.1}$$

Measurement positions were classified by their indentation location and collagen structure. Based on the collagen structure, three different types of collagen architectures were distinguished using the confocal microscope (Figure 3.2). Following the approach of Timmins et al. (2010) [88] and Ng et al. (2006) [89], a customised MATLAB script was generated to estimate the alignment index (AI) of the collagen fibres. The AI was given by

$$AI = \frac{\delta/(\Delta+\delta)}{\delta_{IR}/(\Delta+\delta)_{IR}} = \frac{\delta/(\Delta+\delta)}{40/180} \tag{3.2}$$

where δ described the sum of frequencies of fibres within ± 20° of the preferred fibre alignment (PFA) and Δ was the sum of frequencies of the remaining fibres outside of this range. The sums of frequencies δ_{IR} and Δ_{IR} described the corresponding sum of

frequencies for an ideal random (IR) distribution, where the fibre dispersion is isotropic. These sum of frequencies were per definition δ_{IR}=40 and Δ_{IR}=140.

To decide if the collagen distribution was structured or unstructured an arbitrary threshold of AI=1.4 was chosen. Therefore, locations which showed a high amount of collagen fibres with a clear alignment (AI>1.4) of the fibres were classified as dense structured collagen areas (SC). Positions with high amounts of collagen, but no clear alignment of the fibres (AI<1.4), were characterised as loose unstructured collagen locations (UC). Collagen poor areas, primarily in the lipid-rich necrotic core (LRNC) region, were classified as CP.

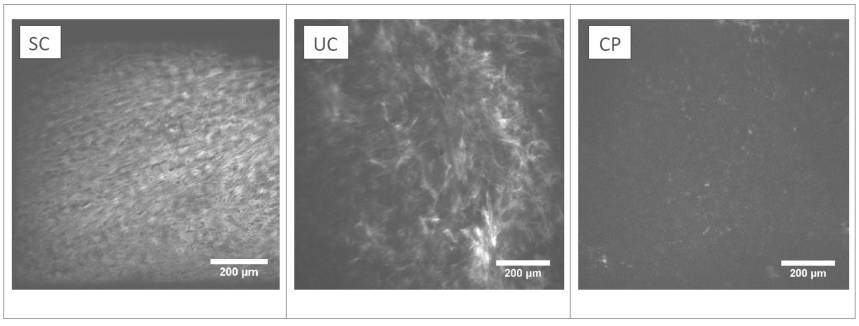

Figure 3.2: *Examples of a dense structured collagen location (SC), a loose unstructured collagen location (UC) and a collagen poor location (CP).*

Each slice was indented at one to eight different locations. The locations were classified as middle of the fibrous cap, shoulder region of the fibrous cap, lipid-rich necrotic core (LRNC) region and intima (remaining arterial wall regions, Figure 3.4).

After the measurements the homogeneity at the tissue testing locations were examined based on the confocal images. Two observers (CKC and ACA), who were blinded to the stiffness results, conducted this evaluation. The following criteria led to the exclusion of the results from further analysis:

- Presence of debris or other foreign material, which were not identified as collagen fibres.
- Ruptured collagen fibres.

- Gap in the tissue which did not correspond to the structure of the surrounding tissue.
- Folded tissue, which can lead to slipping of the tissue influencing the stiffness results.

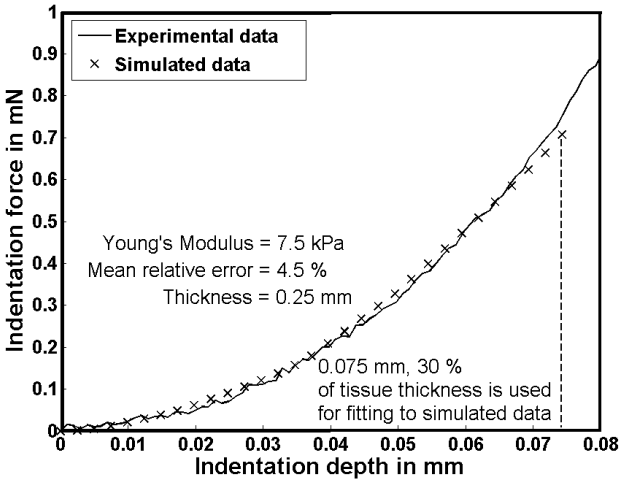

Figure 3.3: *A least-square method was used to fit a neo-Hookean material model to the experimental force-indentation data, 30% of the tissue thickness is indented and used for fitting to simulated data (here:0.075 mm).*

Statistical analysis was conducted to compare stiffness between indentation locations and between collagen types. The stiffness results showed a non-Gaussian distribution. The Kruskal-Wallis test (Dunn procedure) was applied using GraphPad Prism version 5.04 for Windows. A p-value < 0.05 was considered as significant result.

3.3 Results

3.3.1 Representative plaque result

In total, eight human carotid plaques were tested. Depending on the length of the plaque, 6 to 13 slices were obtained per plaque. At 284 locations, 574 measurements were performed. After examining the confocal images for homogeneity of test locations,

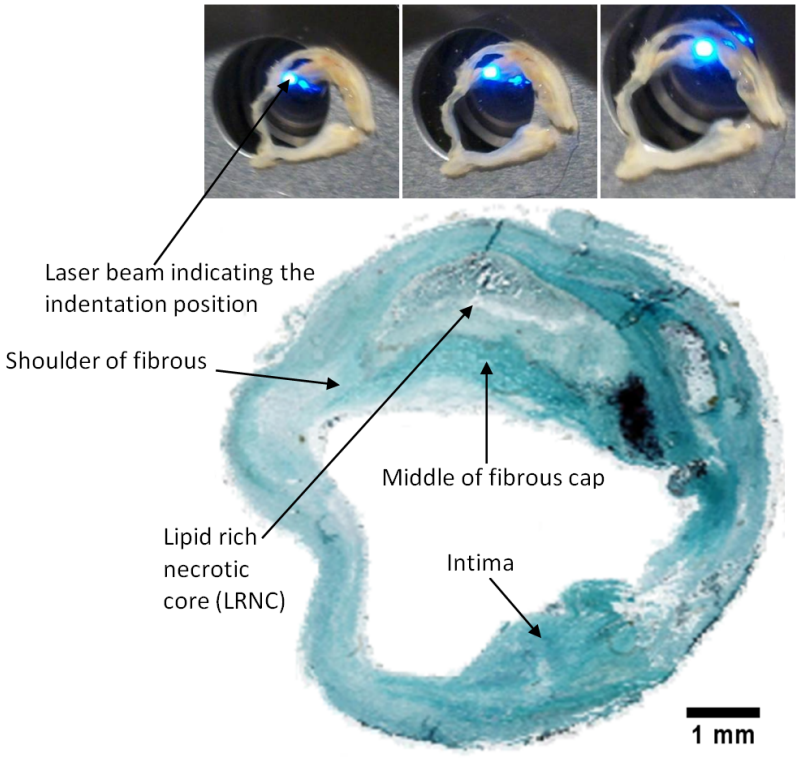

Figure 3.4: *Histological slice (bottom). The top figures show the indentation positions indicated by the laser beam.*

214 locations were used for further analysis. The average thickness of the tested plaque sections was 240 µm (±80 µm).

Representative results of one plaque are shown in Figure 3.5. On the left-hand side of Figure 3.5, a schematic representation of the plaque is shown where the common carotid artery bifurcates into internal (ICA) and external carotid artery (ECA). Among 9 slices obtained from the plaque, the most 3 proximal slices (slice 7 to 9 in Figure 3.5) contained both the internal and the external artery. The other slices only included the internal carotid artery. Above the illustration of the bifurcation, a schematic image of a slice is shown, where the different coloured areas represent the indentation locations. On the right-hand side of Figure 3.5, a table shows the Young's moduli in kPa. Corresponding to the schematic image of the slice, the different coloured columns represent the indentation locations. The collagen-rich fibrous cap and intima locations, where

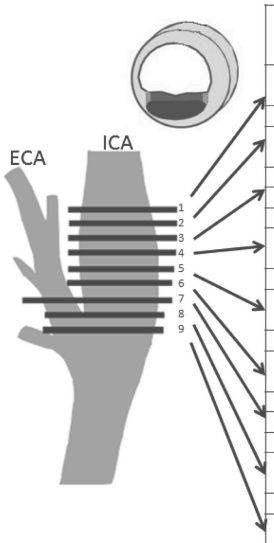

Slice	Middle cap SC	Middle cap UC	Shoulder cap SC	Shoulder cap UC	Intima SC	Intima UC	LRNC CP	Average (SD) of fibrous cap in kPa
1	52		43 37					
2	15			36		94 114		34 (11)
3	34		23					
4	45		29 51		7			
5	53 42		30		57			40 (9)
6	44		34 31					
7			104			33		
8				65 37	51		18	69 (27)
9					20 64			
Average (SD) in kPa	41 (12)		42 (23)	46 (13)	40 (22)	80 (34)	18 (0)	

Figure 3.5: *Left: Schema of a carotid plaque at the bifurcation of common carotid into internal (ICA) and external carotid artery (ECA), Right: Young's moduli in kPa for this plaque, SC (dense structured collagen), UC (loose unstructured collagen) and CP (collagen poor), LRNC (lipid-rich necrotic core).*

further divided into dense structured collagen (SC) and loose unstructured collagen (UC). LRNC locations were collagen poor (CP). At slice 1 to 4 and at slice 6 a single location in the middle of the cap was measured. Slice 5 had a fibrous cap large enough to perform indentation tests at two different middle cap locations. Each value in the table represents the average of at least two consecutive measurements at the same location. For the middle of the cap all values were in the range from 15 to 53 kPa with an average of 41 kPa and standard deviation (SD) of 12 kPa. Moreover, based on the collagen dispersion, only SC regions were found in the middle of the cap. Most of the indentation locations at the shoulder of the cap were also found to be SC regions. Only at slice 2 and 8 UC regions were present. The Young's modulus of the shoulder regions ranged from 23 to 104 kPa. For this location the average value was 42 kPa, similar to the middle of the cap. At the intima regions, five SC and three UC locations were found. The Young's moduli varied from 7 to 114 kPa with an average of 40 kPa for SC and 80 kPa for UC. For this plaque only one CP location with a Young's modulus of 18 kPa was available for testing. To investigate the difference of mechanical properties in the longitudinal direction of a vessel, plaques were divided into three parts each con-

sisting of three slices representing proximal, middle and distal regions of the plaque. This last column of the table shows the average values and the standard deviation of these three regions. For this particular plaque the proximal region is stiffer than the distal region.

3.3.2 Collagen structure

There were 119 positions classified as SC, 75 positions as UC, and 20 positions as CP areas. No significant differences could be found between the collagen-rich location SC and UC (Figure 3.6). The collagen-rich locations showed a high variation of stiffness results, ranging from 6 to 891 kPa. However, CP areas had a smaller range (9 to 143 kPa), and the results were significantly lower (median 16 kPa) compared to the collagen-rich locations SC (median 31 kPa) and UC (median 33 kPa) (Figure 3.6).

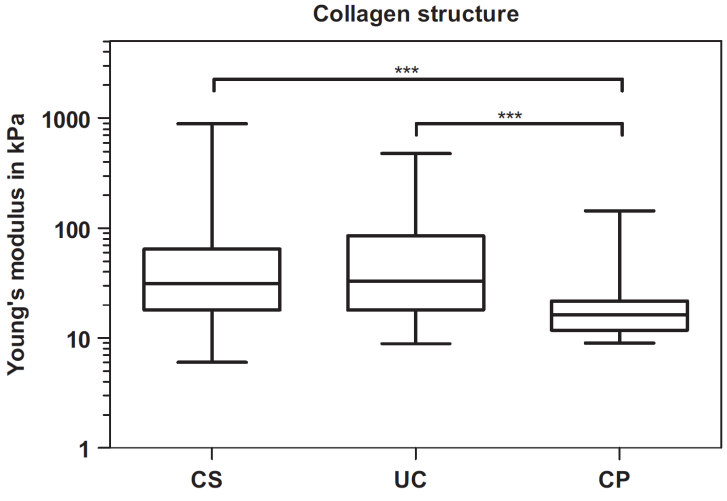

Figure 3.6: *Box and whisker plots (minimum–maximum) of the Young's moduli, structured (SC), unstructured (UC) and collagen poor areas (CP), ***p-value < 0.001.*

3.3.3 Indentation locations

Based on the histology images, indentation locations were chosen before performing the experiments. There were 43 indentation locations identified as middle of the fi-

brous cap, 61 as shoulder regions of the cap, 90 indentation locations as intima, and 20 as LRNC.

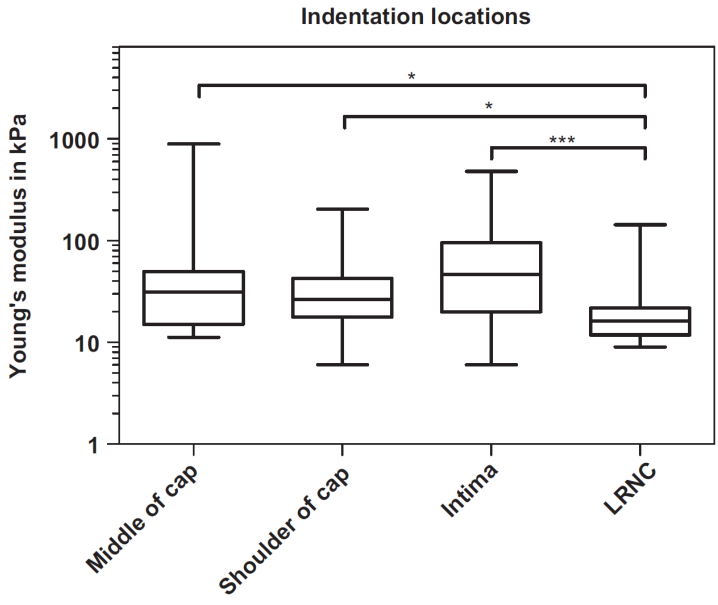

Figure 3.7: *Box and whisker plots (minimum-maximum) of the Young's moduli of the different indentation locations and the significance of the values compared to each other, *p-value <0.05, ***p-value <0.001.*

Table 3.1 summarises the results of all plaques tested. In Figure 3.7, the logarithmic scaled y-axis displays the Young's modulus in kPa, the x-axis shows the indentation location, middle of cap (median=31 kPa), shoulder of cap (median=27 kPa), intima (median=46 kPa), and LRNC locations (median=16 kPa). It was found that the fibrous cap and intima regions are significantly stiffer than the LRNC regions. No differences were observed between the middle and shoulder of cap, and the intima locations.

Table 3.1: *Summary of indentation test results, Mid-Middle of fibrous cap, Sh-Shoulder of cap.*

	SC/Mid	SC/Sh	SC/Intima	UC/Mid	UC/Sh	UC/Intima	CP/LRNC
No. of test locations	29	36	54	14	25	36	20
Minimum in kPa	12	6	6	11	9	11	9
25% Percentile in kPa	18	18	17	14	15	30	12
Median in kPa	36	26	35	28	27	58	16
75% Percentile in kPa	54	43	95	34	46	109	22
Maximum in kPa	891	182	305	166	203	475	143

3.3.4 Inter- and intra-plaque variability, comparison between longitudinal and transversal slices, and change of mechanical properties in longitudinal direction

The axial compressive Young's modulus of each plaque, excluding the collagen poor locations, are summarised in Figure 3.8. The results show that there is a large variation in Young's moduli within each plaque, especially for plaque 6 (11 to 891 kPa). Due to this variation, no significant differences between plaques were observed.

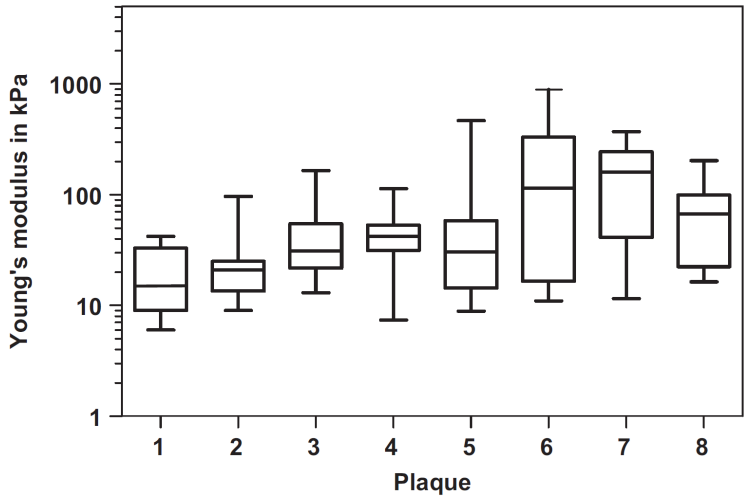

Figure 3.8: *Box and whisker plots (minimum–maximum) of theYoung's moduli of 8 human carotid atherosclerotic plaques, excluding collagen poor locations.*

The indentation tests were performed in axial direction of the artery on transversal slices. For one plaque, part of the tissue was sliced in the longitudinal direction and

these longitudinal slices were used for testing. The resulting Young's moduli show no significant differences between the transversal and longitudinal slices (data not shown).

From proximal to distal, the results indicated no significant differences in Young's modulus. In three atherosclerotic plaques the fibrous cap at the proximal region showed higher stiffness than the distal region. However, in two cases the proximal site was softer than the distal side. For the remaining three plaques, numbers of indentation locations at the fibrous cap were not sufficient to make a comparison between proximal and distal regions.

3.4 Discussions

In this study we used an indentation test and inverse FE analysis to estimate the compressive Young's moduli of carotid atherosclerotic plaque tissue in axial direction. Assuming isotropic neo-Hookean behaviour, the Young's moduli were found in the range from 6 kPa to 891 kPa (median of 30 kPa) corresponding to values found in the literature. Collagen poor regions were softer than collagen-rich locations. However, no significant differences were observed between the Young's moduli of structured and unstructured collagen architectures. Moreover, no significant differences were found between the middle of the fibrous cap, the shoulder regions, and remaining intima locations. Therefore, the results indicate that the macroscopic behaviour of carotid atherosclerotic fibrous plaque tissue can be approximated by a single material model. However, it should be noted that the sample size (8 endarterectomy specimens) may not be sufficiently large to detect a statistical difference between the middle and shoulder regions of the fibrous cap, particularly since other patient-specific variables (age, gender, etc.) had not been controlled for.

A literature review revealed that there is a high variability of stiffness values of plaque tissue [41, 45, 59, 64, 65, 70, 90, 91, 92]. Our results are in the lower region of the range reported in literature and are consistent with the values obtained by Lee et al. (1992) [65] and Barrett et al. (2009) [70] (Table 3.2). However, our results differ from the values obtained by other groups [41, 45, 59, 64, 90, 91, 92]. Possible explanations for this might be the different methods used to measure the mechanical properties of atherosclerotic plaque tissue which lead to the measurement of different

Table 3.2: *Measured Young's moduli (in kPa) for atherosclerotic plaque tissue.*

Specimen type		Test method	Classification		
			Cellular		Hypocellular
Lee et al. [64]	Abdominal aorta	Radial compression, dynamic, values at 1 Hz	510±220 (n=7)		900±220(n=9)
Loree et al. [41]	Abdominal/thoratic aorta	Circumferential tension, static creep type test	927±468 (n=12)		2312±2180 (n=9)
			Non-fibrous		Fibrous
Lee et al. [65]	Abdominal aorta	Radial compression, static creep type test and ultrasound	41±19 (n=14)		82±33 (n=18)
Beattie et al. [90]	Aorta	Bi-linear isotropic	4, strain <18%		483, strain <8.2%
			39, strain >18%		1820, strain >8.2%
de Korte et al. [91]	Femoral/coronary arteries	Incremental pressure-strain	222 (n=13)		493 (n=62)
Ebenstein et al. [51]	Carotid artery	Radial nano-indentation and FTIR	620 (60-4900)		1500 (100-21500)
Kanai et al. [92]	Iliac artery	Circumferential incrementalwith transcutaneous ultrasound	81±40 (n=9)		1000±630 (n=9)
Holzapfel et al. [45]	Iliac artery	Axial and circumferential tension	-		Axial, 1200 Circum, 840 (n=107)
Barrett et al. [70]	Carotid artery	Radial indentation and inverse FE analysis	-		33 (21-300, n=8)
			Collagen poor		Collagen-rich
Current study	Carotid artery	Axial indentation and inverse FE analysis	16 (9-143)		32 (6-891)
			Middle Cap	Shoulder Cap	Intima
			31 (11-891)	27 (6-203)	46 (6-475)

Young's moduli (Table 3.2). In addition, the direction of measured stiffness also plays a role. The anisotropy of the tissue suggests that testing the stiffness of plaque tissue in different directions will lead to different results, although our values obtained from testing a small set of longitudinal slices were comparable to the results we obtained for transversal slices. Furthermore, different values might be the result of the measurements of different specimen types. Since the geometry of arteries at different locations varies and arteries from various locations experience different stresses and strains, it is suggested that the biomechanical properties of arteries from different location also vary. Differences between the values we obtained and the results of the other research groups might be also caused by the various methods used to classify the tissue. In our study we distinguish between collagen structure and between different plaque locations.

Measurements at same indentation positions led to a mean difference of 12% ($\pm$14%) showing that the indentation test method itself is reproducible. Taking the 25% and 75% percentile as range, the variability is similar to the range obtained by Barrett et al. (2009) [70] and Lee et al. (1992) [65]. It is smaller than the variability obtained by other research groups [41, 51, 90]. Since the range of values we found is similar for each plaque we tested and this is also observed by most research groups, the obtained range must reflect the variable nature of the mechanical properties of biological tissue.

It is suggested that, due to the different shear stress between the proximal and distal regions, different plaque morphology and therefore different stiffness results in those regions of the plaque can be expected [93, 94, 95]. Gijsen et al. (2008) [95] showed on human coronary arteries that the shear stress upstream is significantly higher than downstream. Dirksen et al. (1998) [93] found a significant difference between the cell compositions of proximal and distal parts of carotid plaques. Therefore, the results from literature suggest that also the stiffness of the fibrous cap proximal and distal of a plaque could be different. Using plaque tissue from carotid endarterectomy patients, it was possible to analyse the changes of stiffness from proximal to distal locations in five samples. No significant differences could be observed.

To analyse the influence of the collagen structure on the mechanical properties a confocal microscope was used to identify the collagen structure of the tested tissue location. The results show a wide spread of mechanical properties between plaques. Stiffness values of collagen poor locations, which are mostly found in the LRNC, have less variation than collagen-rich regions. A statistical analysis using a non-parametric

approach indicated that the collagen-rich locations (structured and unstructured) are significantly stiffer than collagen poor locations. For collagen-rich positions, no significant differences are found between the different collagen structures, suggesting that the architecture of collagen has no obvious effect on the Young's modulus. It is surprising that our results show no influence of the collagen structure on the stiffness results. Reasons for this might be the use of an isotropic model assuming homogeneity of the sample which might not reflect the actual mechanical behaviour of the tissue. In addition, it has to be noted that not only the collagen structure but also the amount of collagen influences the stiffness of the plaque tissue. The quantity of collagen was not measured during this study. Burleigh et al. (1992) [40] showed that plaque caps seem to require more quantities of collagen than neighbouring intima to maintain the same mechanical strength indicating that the collagen structure in the cap is less efficiently organised than in adjunct intima. The result of Burleigh et al. (1992) [40] suggests that for the stiffness of plaque caps the amount of collagen play a bigger role rather than the collagen structure. Therefore, the last point is probably the main reason why we could not observe a significant difference between structured and unstructured collagen fibres.

For different indentation locations of single slices, it is observed that the fibrous cap tissue and intima tissue are significantly stiffer than the collagen poor regions which could be expected. However, no differences were found between the middle parts of the cap tissue, shoulder regions of the cap, and intima positions suggesting that one material model can be used to approximate the diseased intima and fibrous cap. On the other hand, considering the high variability of results, it is clear that finding a significant tendency is difficult.

A limitation of the study is the fact that the samples were frozen for logistical reasons. According to Schaar et al. (2002) [96], the influence of freezing on the mechanical properties of coronary arteries plays only a limited role. The freezing protocol applied in this study included dipping the sample in liquid nitrogen for snap-freezing. This procedure is widely used to avoid ice-crystal formation. Hemmasizadeh et al. (2012) [97] used nano-indentation to show that snap-freezing and storage at -80°C had no significant influence on the mechanical properties of porcine aortas. Therefore, the probability of damage of thecollagen fibres due to ice-crystal formation was minimised. Furthermore, the indentation tests were performed at least twice at the same indentation location and the results were reproducible indicating that no damage to the tissue

architecture occurred. The measurements were controlled by confocal microscopic visualisation and also no damage to the tissue was observed. Moreover, the histological data was examined and indicated that no damage due to ice-crystallisation was present.

In literature the mechanical properties of atherosclerotic plaques are usually given only as Young's moduli. Furthermore, it is not always clear whether or not this is aYoung's modulus determined at small strains, or a secant modulus of the slope of a curve at a certain strain level. Considering these reservations, the obtained values from this study were compared to the results in literature using $E = 3G$, which is only valid at small strains.

The values of the lipid core regions appear to be higher than previously reported data [29]. A possible explanation might be that the mechanical tests were performed at room temperature. Testing at this temperature might affect the values for lipid core regions. The physiological mechanical properties of the lipid-rich necrotic core at body temperature might be very different from their mechanical properties at room temperature. Therefore, these results should be dealt with caution when including them in simulations, since this may have a strong impact on the biomechanical stress analysis of plaques [62].

In conclusion, the system proved to be suitable to measure the local mechanical properties of plaque tissue. The compressive mechanical properties of human plaques in axial direction are lower than previously reported. Mechanical testing of fibrous cap tissue and surrounding intima tissue showed similar mechanical properties between these locations. They are significantly stiffer than collagen poor regions.

Chapter 4

Anisotropic mechanical behaviour of plaques

The content of this chapter is based on C.-K. Chai, A. C. Akyildiz, L. Speelman, F. J. H. Gijsen, C. W. J. Oomens M. R. H. M. van Sambeek, A. van der Lugt and F. P. T. Baaijens. Local anisotropic mechanical behaviour of human carotid atherosclerotic plaques - characterisation by indentation test and inverse finite element analysis (*accepted*).

4.1 Introduction

Atherosclerosis is a disorder of the arterial wall, characterised as wall thickening due to invasion of cholesterol, macrophages, and smooth muscle cells. Eventually, this process can result in a rupture-prone atherosclerotic plaque. When an atherosclerotic plaque is at high risk for rupture, it is called a vulnerable plaque. Such a vulnerable plaque may consist of haemorrhage, macrophages, and a lipid-rich necrotic core which is covered by a thin fibrous cap. This thin fibrous cap separates the thrombogenic lipid core from the blood stream and is prone to rupture. Plaque rupture can lead to thrombus formation and acute vessel occlusion or embolisation of plaque debris and/or thrombus in the distal vessel bed. If this happens in the carotid artery, it may lead to an transient ischaemic attack or an ischaemic stroke. In fact, carotid plaque rupture is a major cause of ischaemic strokes [98].

Reliable diagnostic methods for plaque rupture are desired. Current methods are based on morphological plaque parameters, for example the degree of stenosis. However, studies showed that this is insufficient and that better risk assessment methods for plaque rupture are required [99]. From a mechanical point of view plaque rupture occurs when mechanical stresses exceed the strength of the thin fibrous cap of the plaque [36, 60, 72, 73, 85]. Biomechanical models are able to compute stresses and strains inside an atherosclerotic plaque allowing a prediction of local stress peaks and failure locations of the plaque [85]. However, the reliability of these computer models depends strongly on the applied material models. Currently, the used models mostly comprise isotropic material behaviour of the plaque tissue, although it is generally accepted that atherosclerotic plaque tissue behave highly anisotropic [45]. This is especially the case for plaque components with high collagen content, such as the fibrous cap. Therefore, including anisotropic model parameters will improve biomechanical models and may improve the risk assessment of rupture of atherosclerotic plaques.

The aim of the present study was to measure the local anisotropic mechanical behaviour of collagenous rich plaque components at large strains. An in-house developed unique indentation test setup was used to perform mechanical testing. During the indentation, the deformation of the collagen fibres of the plaque tissue perpendicular to the indentation direction was visualised via confocal microscopy. Using digital image correlation, the displacements of the collagen fibres were quantified. By means of inverse finite element analysis, the anisotropic behaviour of collagenous atherosclerotic plaque tissue was characterised.

4.2 Methods

4.2.1 Sample preparations

The sample preparation and mechanical tests have been extensively described in Chai et al. (2013, 2014) [71, 100]. Atherosclerotic plaques from 5 symptomatic patients (2 female, 3 male, age 65 to 87 years) were obtained by carotid endarterectomy, after written consent was given. Before the mechanical tests the samples were snap-frozen and stored at -80°C. In a later stage, the obtained plaques were sliced using a cryotome to create transversal cross-sections. These cross-sections were thawed and a fluorescent staining was applied to visualise the collagen fibre type I and III [78] in the atherosclerotic plaques so that the deformation of the fibres can be quantified during mechanical testing. For the mechanical testing an in-house developed indentation device was used. The spherical indenter of the device with a diameter of 2 mm allowed local measurement at room temperature. Phosphate buffer saline solution was used to prevent dehydration of the plaque tissue.

4.2.2 Indentation test and imaging

For a detailed description of the indentation test, one is referred to chapter 2. Plaque cross-sections were placed underneath the indentation test device [71]. A sphere head with a diameter of 2 mm indented the tissue along the axial direction of the vessel at a quasi-static rate of 0.01 mm/s. The small sphere allowed a local measurement. The first indentation to half of the tissue thickness was applied as preconditioning. Afterwards, another indentation to half of the tissue thickness was applied while recording the force-response. The resolution of the force measurement was 15 µN, whereas the indentation measurement was performed at a resolution of 15 nm. For a detailed description of the indentation test, see Cox et al. (2005) [87] and Vaekatesan et al. (2006) [74]. The indentation test device was placed above an inverted confocal microscope, which allowed the visualisation of collagen fibres in the plaque. The main collagen fibre direction and collagen fibre dispersion were determined using Fourier component analysis of ImageJ 1.47n plug-in 'Directionality'. The confocal imaging also enabled the visualisation of the collagen fibre displacement perpendicular to the indentation direction. Using digital image correlation [75], it was possible to quantify

the collagen deformation during indentation (Figure 2.2, see chapter 2). Therefore, the experimental setup allowed the measurement of indentation force-response, collagen fibre displacement perpendicular to fibre alignment, and collagen fibre stretch (Figure 2.2). These parameters were used as input for the inverse finite element (FE) analysis to determine anisotropic mechanical properties.

4.2.3 Inverse finite element (FE) analysis

For the inverse FE analysis, the material model based on Driessen et al. (2008) [79] was applied. Advanced atherosclerotic plaques consist of different plaque components. Therefores, it is important to address this issue by applying local measurements. As depicted in Figure 4.1 indentations were performed in the middle of the fibrous cap (shown in green, n=7), at the shoulder region of the cap (shown in red, n=10), and at the remaining diseased intima regions (shown in blue, n=11).

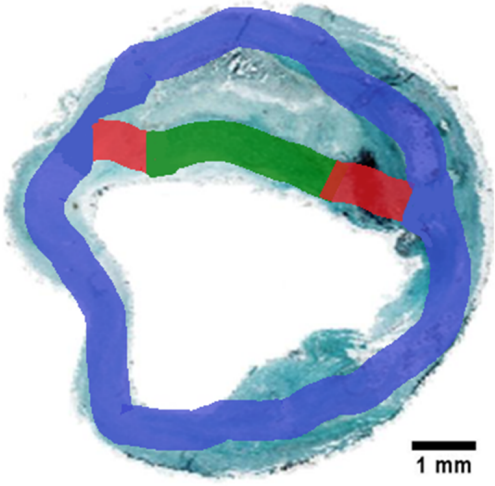

Figure 4.1: *Different indentation locations were tested. In blue the remaining intima tissue surrounding the shoulder cap regions in red and the middle of the fibrous cap in green.*

Indentations were conducted at different plaque components which were pre-selected based on histology images and which were visually inspected using the confocal microscope to find locally homogenous structure in the proximity of the testing locations.

For the FE model, the material was considered homogeneous in the region of interest. Furthermore, the contact between indenter and tissue as well as between tissue and glass counter plate was assumed to be frictionless. Assuming incompressibility, the Cauchy stress $\boldsymbol{\sigma}$ consists of a hydrostatic pressure p and the extra stress $\boldsymbol{\tau}$, as described in equation (4.1).

$$\boldsymbol{\sigma} = -p\mathbf{I} + \boldsymbol{\tau} \tag{4.1}$$

$$\boldsymbol{\tau} = \boldsymbol{\tau}_m + \boldsymbol{\tau}_f = G_m(\mathbf{F}\cdot\mathbf{F}^T - \mathbf{I}) + \sum_{i=1}^{N_f} \phi_f^i[\psi_f^i - \vec{e}_f^i\cdot\boldsymbol{\tau}_m\cdot\vec{e}_f^i]\vec{e}_f^i\vec{e}_f^i \tag{4.2}$$

As shown in equation (4.2) the local collagen structure of the atherosclerotic plaque was described by splitting the extra stress $\boldsymbol{\tau}$ into an isotropic matrix part $\boldsymbol{\tau}_m$ and an anisotropic fibre part $\boldsymbol{\tau}_f$. The isotropic part $\boldsymbol{\tau}_m$ represents the extracellular matrix and is described by the matrix shear modulus G_m. The anisotropic part $\boldsymbol{\tau}_f$ depicted the collagen fibres of the tissue where N_f is the number of fibres in the direction of $\vec{e}_f$. The fibre fraction ϕ_f^i in direction of $\vec{e}_f$ follows a periodic Gaussian distribution [79, 101], as shown in equation (4.3) where γ_i is the fibre angle, A a scaling factor, so that the total fibre volume fraction equalled ϕ_{tot}, α the main fibre direction and β the fibre distribution.

$$\phi_f^i(\gamma_i) = Aexp\frac{cos[2(\gamma_i-\alpha)]+1}{\beta} \tag{4.3}$$

The fibre stress ψ_f was modelled with an exponential function according to Holzapfel et al. (2000) [80].

$$\psi_f = 2k_1\lambda_f^2(\lambda_f^2-1)exp(k_2(\lambda_f^2-1)^2) \tag{4.4}$$

4.2.4 Parameter estimation

To infer the anisotropic mechanical parameters of the plaque tissue an iterative mixed experimental-numerical approach based on the method by Meuwissen et al. (1998) [81] and Cox et al (2008). [76] was applied. The difference between experimental measurements $\underset{\sim}{m}$ and the predicted data $\underset{\sim}{h}$, obtained from the finite element simulations, were minimised by applying a Gaussian-Newton minimisation algorithm. Experimental data $\underset{\sim}{m}$ and simulated data $\underset{\sim}{h}$ consisted of indentation force F and the anisotropic index $AI = \frac{\lambda_y}{\lambda_x} - 1$, where λ_y and λ_x were the two in-plane principal stretches of the tissue determined from the confocal images using digital image correlation. For each experiment, a 3D FE model was generated, where for each measurement point

m_i a prediction h_i was simulated. These simulated data $\underset{\sim}{h}$ depended on the boundary conditions $\underset{\sim}{u}$ as input and on the material parameters $\underset{\sim}{\vartheta} = [\vartheta_1, ..., \vartheta_P]^T$, where P is the number of parameters. The results obtained from the indentation experiments $\underset{\sim}{m}$ related to the material parameters $\underset{\sim}{\vartheta}$, as described in equation (4.5), where the measurement and modelling error were depicted by $\underset{\sim}{\xi}$.

$$\underset{\sim}{m} = \underset{\sim}{h}(\underset{\sim}{u}, \underset{\sim}{\vartheta}) + \underset{\sim}{\xi} \tag{4.5}$$

There were three material parameters $\underset{\sim}{\vartheta}$, the non-linearity factor k_2, the fibre stiffness k_1, and the matrix shear modulus G_m. For 14 cases the matrix shear modulus G_m was very low compared to the value of k_1. The value for G_m went towards almost zero causing numerical issues. To avoid these, the matrix shear modulus was fixed at a lower limit of G_m = 1 kPa, so that for these cases only two material parameters needed adjustment for minimisation, namely the fibre stiffness k_1 and the non-linearity factor k_2. Initially, the starting parameters for the iteration process were set to k_1= 1 kPa and k_2=1. If no convergence was reached, the starting parameters were varied. Since a value for k_2< 0 suggests strain-softening, which is not expected for biological tissue, a lower limit of k_2 = 0 was enforced. A quadratic objective function $J(\underset{\sim}{\vartheta})$ was used to describe the quality of the fit between the experimental results obtained from the indentation tests and the simulated data obtained from the FE simulations.

$$J(\underset{\sim}{\vartheta}) = [\underset{\sim}{m} - \underset{\sim}{h}(\underset{\sim}{u}, \underset{\sim}{\vartheta})]^T \underline{V} [\underset{\sim}{m} - \underset{\sim}{h}(\underset{\sim}{u}, \underset{\sim}{\vartheta})] \tag{4.6}$$

To ensure that all data points contributed equally, the objective function $J(\underset{\sim}{\vartheta})$ included a weighting matrix $\underline{V}$, which is shown in equation (4.7).

$$V(i,i) = \frac{1}{m(i)^2},\ i = 1,\ ...,\ N. \tag{4.7}$$

The stop-criterion for the minimisation algorithm was reached when the sum of changes of all material parameter was < 1% between iterations. The quality of the fit between the experimental and simulated data was quantified as Mean Relative Error (MRE) of indentation force and anisotropic index AI (Figure 4.3).

The Mean Relative Error (MRE) for the indentation force-depth curves MRE_{Force} and the anisotropic index AI-relative indentation curves MRE_{AI} were defined as

$$MRE_{Force} = \frac{100\%}{n} \cdot \sum_{i=1}^{n} \frac{|F_{exp}(i) - F_{sim}(i)|}{\overline{F}_{exp}(i)} \tag{4.8}$$

$$MRE_{AI} = \frac{100\%}{n} \cdot \sum_{i=1}^{n} \frac{|AI_{exp}(i) - AI_{sim}(i)|}{\overline{AI}_{exp}(i)} \tag{4.9}$$

where F_{exp} is the measured force-response, F_{sim} represents the simulated force-response, AI_{exp} is the anisotropic index AI as define and AI_{sim} is the anisotropic index resulting

from the FE simulations. All parameters were obtained at different indentation depths in 20 steps. The inverse FE analysis was performed until a maximum indentation of 20% of the tissue thickness.

4.2.5 Statistical analysis

Plaque tissue consists of a heterogeneous morphology as it is a multi-component structure. Local measurements with the described micro-indentation setup allowed comparison between the results obtained at different collagenous sites on a plaque. To compare the data obtained from the different indentation locations, statistical analysis was conducted using Graph-Pad Prism version 5.04 for Windows. The obtained data showed a non-Gaussian distribution. Therefore, a non-parametric approach (Kruskal-Wallis, Dunn procedure) was chosen to analyse if significant differences between the material parameters at different indentation locations could be found.

4.3 Results

4.3.1 Parameter identification

A representative example of a confocal image with results from the digital image correlation (DIC) is shown in Figure 4.2. The indenter was placed in the centre of the image and was moving towards the observer, compressing the tissue. This compression led to extension of the collagen fibres in the 2D-bottom plane perpendicular to the indentation direction. From this 2D-displacement fields the local deformation gradient and local strain fields were inferred using the algorithm described in Geers et al. (1996) [102]. From this the first and second principal stretches were obtained, indicated by the black arrows in Figure 4.2. The fibre deformation patterns were often heterogeneously distributed. Averaged fibre tensile curves were fitted to averaged tensile properties $\overline{k_1}$ and $\overline{k_2}$ according to equation (4.4). A typical indentation force-depth-curve and the two principal stretches, summarised as anisotropic index AI, are shown in Figure 4.3. It is shown that the final numerical data from the FE simulations correspond very well to the average experimental data.

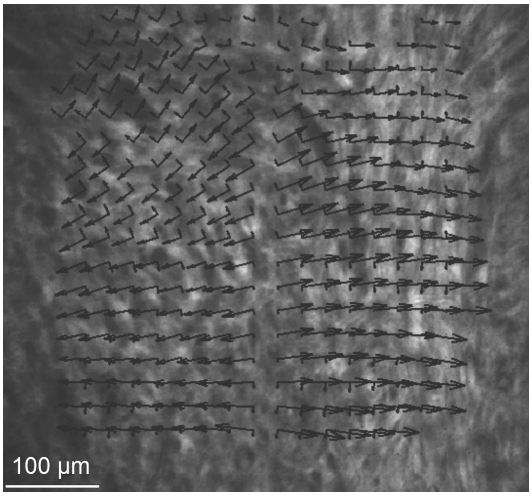

Figure 4.2: *Digital Image Correlation (DIC) result of one measurement. Arrows indicate the directions of first and second principal stretches. The arrow length show the strain-magnitude.*

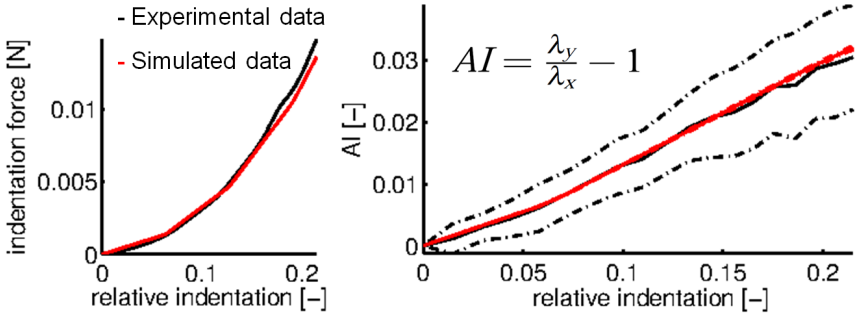

Figure 4.3: *For the parameter estimation the indentation force, indentation depth, and the collagen fibre displacement depicted as AI were used as input $\underset{\sim}{m}$. These measurements were fitted to the simulated data $\underset{\sim}{h}$ from the FE simulations. Here one representative fitting for one indentation location is shown (patient I, intima location). For the AI the averaged value at each indentation depth is shown. The dash-dotted lines show the standard deviation for the experimental results. The MRE was 11% indicating a very good fit.*

4.3.2 Material parameters

The material parameters obtained from the inverse finite element analysis are summarised in Table 4.1 and Table 4.2. The columns show the indentation locations, the patient, and the used shear moduli of the non-fibrous matrix G_m. Further material parameters include the fibre stiffness k_1, the non-linearity factor k_2 and the fibre dispersion

β. The last column shows the averaged mean relative error $MRE = \frac{MRE_{Force}+MRE_{AI}}{2}$. After each indentation location the median values, 25th percentile and 75th percentiles are presented. The last rows of Table 4.2 summarise the total median values, 25th percentile and 75th percentiles of all material parameters.

It should be noted that generally the matrix stiffness G_m was much softer than the collagen fibre stiffness k_1. In fact, the matrix shear modulus G_m sometimes was almost zero causing numerical problems. If this was the case, G_m was fixed to a lower limit of G_m= 1 kPa to overcome this problem. The fibre stiffness k_1 had a median value of 80.6 kPa (25th percentile and 75th percentile was 17.7-157.0 kPa). The 25th percentile and 75th percentile for the non-linearity factor k_2 was from 1.0 to 10.7 with a median value of 3.4. The fibre dispersion β was found to be 0.6 (0.4-0.9).

The 25th percentile and 75th percentiles for the fibre stiffness k_1 at the remaining intima regions was from 24.5 kPa (25th percentile) to 892.8 kPa (75th percentile) with median value of 99.2 kPa (Figure 4.4). The fibre stiffness k_1 at the middle of the fibrous cap was stiffer than at the shoulder cap regions, median 73.7 kPa (11.4-260.3 kPa) versus 27.5 kPa (6.4-131.7 kPa). However, due to a wide spread, no significant statistical differences in fibre stiffness k_1 were found between different testing locations.

The non-linearity factor k_2 determines the stiffness of the tissue at high strain. The median (25th-75th percentile) value for k_2 at intima regions was 11.5 (7.0-21.5). For the middle of the fibrous cap the median value was obtained at 3.4 (1.9-8.7). The shoulder cap regions showed a strong linear behaviour with a median k_2 value of 1.0 (0.4-1.6). The difference in k_2 for the intima region compared to the shoulder region was statistically significant. No significant differences were found between the middle of the cap and the remaining testing locations (Figure 4.5).

The fibre dispersions β is a measure for the anisotropy of the plaque tissue. A more isotropic behaviour is given by high values for β. For the plaque tissue, the tested locations suggest rather anisotropic mechanical behaviour. The median (25th-75th percentile) value for intima regions was 0.6 (0.4-0.7), comparable to the middle of the

Table 4.1: *Summary of the final output parameters (Intima and Middle of the fibrous cap data) obtained from the parameter estimation. If the mean relative error (MRE) for the final material parameters was higher than 35%, the data was considered as a bad fit and omitted.*

Indentation location	Patient	Matrix stiffness G_m[kPa]	Fibre stiffness k_1[kPa]	Non-linearity factor k_2[-]	Fibre dispersion β [-]	Mean Relative Error [%]
Intima	I	4.3	1539.4	11.5	0.4	4.5
(n=11)	I	17.0	80.6	23.7	0.1	15.7
	I	75.0	2029.7	25.2	1.0	11.0
	II	1.0	120.6	0.0	0.6	26.3
	II	15.2	99.2	23.1	0.5	18.4
	II	12.4	892.8	10.6	0.3	15.5
	III	2.7	422.7	9.1	0.8	3.2
	III	5.1	24.5	14.1	0.6	8.4
	IV	1.0	40.5	4.8	0.5	17.8
	IV	1.0	19.2	0.6	0.9	25.0
	V	11.8	16.2	19.8	0.6	15.1
25th percentile			24.5	7.0	0.4	10.3
Median			99.2	11.5	0.6	15.5
75th percentile			892.8	21.5	0.7	20.1
Middle of fibrous cap	I	4.7	12.7	6.6	0.3	17.9
(n=7)	III	1.0	365.2	2.7	0.7	13.2
	III	21.7	73.7	27.4	0.3	20.7
	IV	1.0	11.4	3.4	0.4	29.1
	IV	1.0	6.8	1.0	8.1	29.9
	IV	1.0	119.5	1.0	1.1	20.2
	V	14.7	260.3	10.9	0.4	21.6
25th percentile			11.4	1.9	0.4	19.1
Median			73.7	3.4	0.4	20.7
75th percentile			260.3	8.7	0.9	25.4

fibrous cap with a median value of 0.4 (0.4-0.9) and the shoulder cap regions with a median of 0.8 (0.5-1.3). No significant differences were found between the three indentation location classifications (Figure 4.6).

Table 4.2: *Summary of the final output parameters (Shoulder of the fibrous cap and total median, 25th percentile, 75th percentile, including the data in table 4.1) obtained from the parameter estimation.*

Indentation location	Patient	Matrix stiffness G_m[kPa]	Fibre stiffness k_1[kPa]	Non-linearity factor k_2[-]	Fibre dispersion β [-]	Mean Relative Error [%]
Shoulder of fibrous cap	I	5.1	5.6	2.9	0.0	10.2
(n=10)	IV	1.0	16.3	0.8	0.7	21.1
	IV	1.0	6.2	0.0	1.3	31.6
	IV	1.0	27.0	1.3	0.6	13.6
	IV	1.0	27.9	1.0	0.8	18.9
	IV	1.0	6.4	1.0	1.0	12.4
	IV	1.0	173.0	6.8	1.3	14.1
	IV	8.5	152.8	1.9	5.0	8.9
	V	1.0	110.5	0.1	5.8	16.8
	V	10.9	161.1	0.0	0.0	17.7
25th percentile			6.4	0.4	0.5	13.3
Median			27.5	1.0	0.8	17.2
75th percentile			131.7	1.6	1.3	23.7
Total 25th percentile			17.7	1.0	0.4	13.2
Total Median			80.6	3.4	0.6	17.2
Total 75th percentile			157.0	10.7	0.9	21.6

4.3.3 Change of fibre stiffness in longitudinal direction, inter- and intra-plaque variability

The fibre stiffness k_1 was compared for indentation locations proximal to distal of the plaque stenosis. Statistical analysis showed that the collagen fibre stiffness was significantly higher in the proximal locations, upstream of the plaque, compared to the location with the maximum plaque stenosis (Figure 4.7). It has to be noted that only a limited number of measurements (n=3) were performed at distal locations.

The wide spread of data might be caused by the fact that different patients with different biological factors were included in this study. Therefore, the fibre stress at 20% strain were compared for the different patients (Figure 4.8). A wide spread can be observed even within a plaque obtained from one single patient.

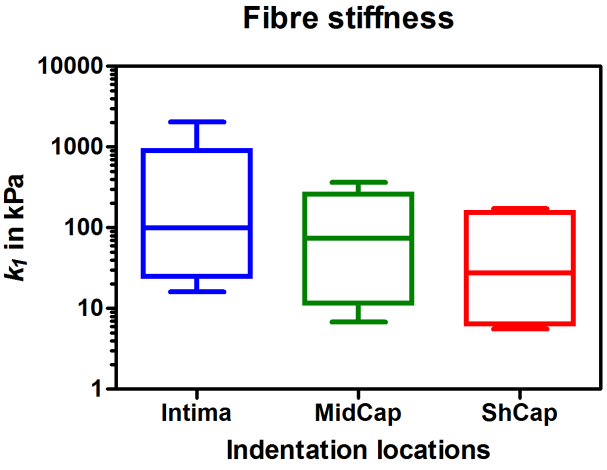

Figure 4.4: *Box and whisker plots (minimum-maximum) of the fibre stiffness k_1 in kPa for the different indentation locations. No significant differences were found between the indentation locations of the plaque tissue (MidCap- Middle of the fibrous cap, ShCap- Shoulder region of the fibrous cap).*

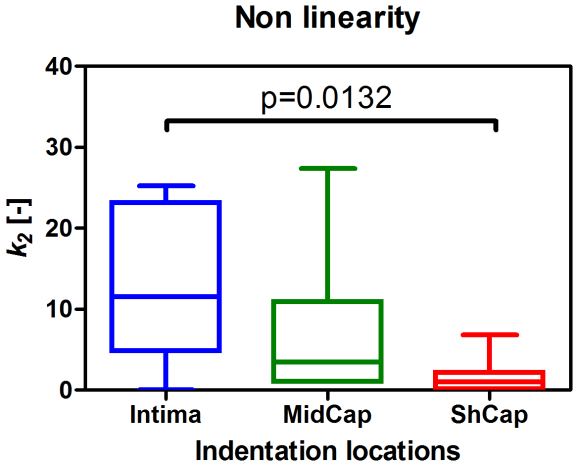

Figure 4.5: *Box and whisker plots (minimum-maximum) of the dimensionless non-linearity factor k_2 for the different indentation locations. A significant difference was found between intima and shoulder cap regions of the plaque tissue (MidCap- Middle of the fibrous cap, ShCap- Shoulder region of the fibrous cap).*

4.3.4 Collagen structure

Similar to the method used in Chai et al. (2013) [71], the confocal images were used to identify the collagen structure at the indentation location, based on the approach

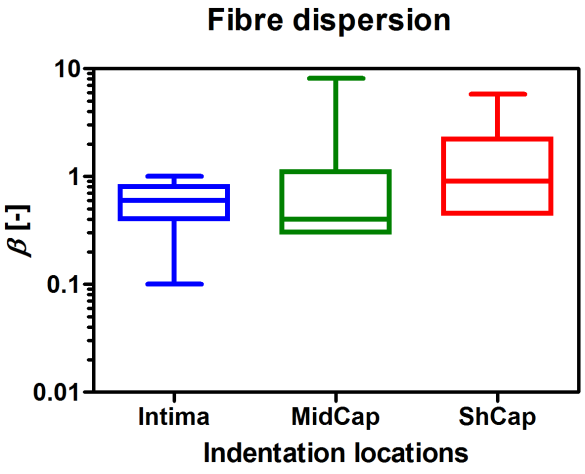

Figure 4.6: *Box and whisker plots (minimum-maximum) of the dimensionless fibre disperion β for the different indentation locations. No significant differences were found between the different indentation locations (MidCap- Middle of the fibrous cap, ShCap- Shoulder region of the fibrous cap).*

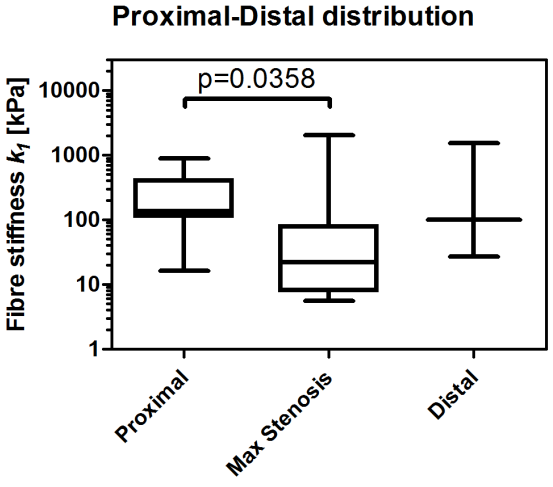

Figure 4.7: *Collagen fibre stiffness from proximal to distal testing locations. Different stresses between up- and downstream of plaques might cause different mechanical properties at those cap locations. Here it is shown that collagen fibres are significantly stiffer proximal to the plaque stenosis than at the maximum stenosis locations.*

of Timmins et al. (2010) [88] and Ng et al. (2006) [89]. From the 28 indentations, 12 were performed at highly anisotropic (structured) regions. For all these regions, the results show that the collagen fibres are aligned in circumferential direction around the

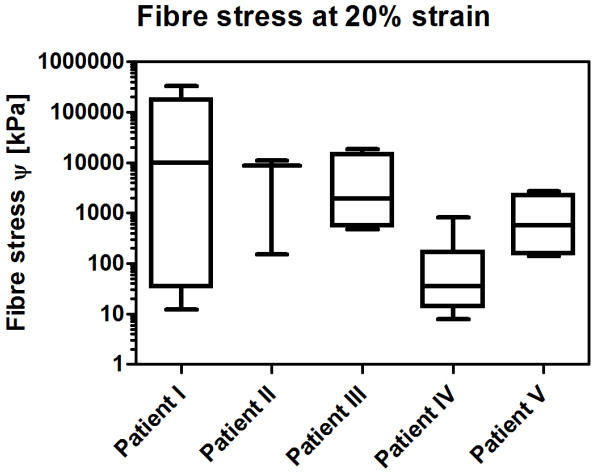

Figure 4.8: *Fibre stress at 20% strain for the different patients. A wide spread is already apparent for each patient, which complicates comparisons of the results.*

lumen of the atherosclerotic plaque tissue (Figure 4.9).

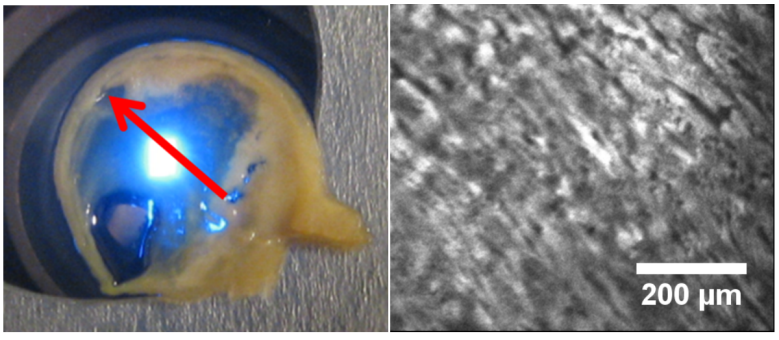

Figure 4.9: *Picture of the tested plaque cross-section (left), the laser indicates the indentation location. The red arrow depicts the direction of the main fibre direction. Confocal image of the indentation location shows highly anisotropic collagen structure (right). The fibres are aligned in circumferential direction around the lumen of the carotid plaque.*

4.3.5 Comparing anisotropy, 2nd principal stretch and main fibre directions

To verify if the computer model represented the anisotropic mechanical behaviour appropriately, the difference between 2nd principal stretch directions and main fibre directions was checked (Figure 4.10). In this experimental set-up, a homogeneous anisotropic material would show that the 2nd principle stretch direction (least amount of stretch) coincides with the main fibre direction. Because we work with averaged properties in a heterogeneous material, this might not be the case and this can cause large differences in properties.

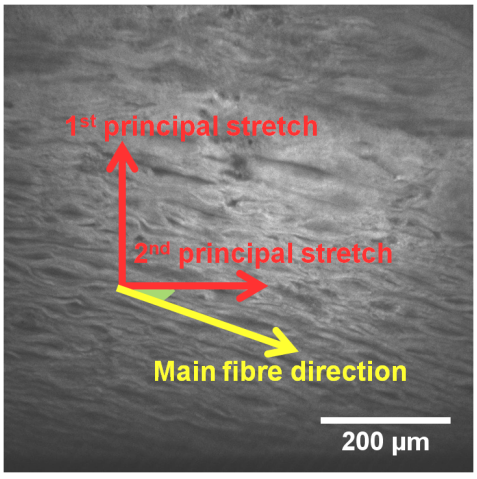

Figure 4.10: *The 1st principal stretch describes the main stretch which occurs perpendicular to the main fibre direction. The 2nd principal stretch direction lies perpendicular to the 1st principal stretch and represents the fibre stretch (in red) and should coincide with the main fibre direction (in yellow).*

The anisotropic mechanical behaviour summarised as AI was plotted against the difference between 2nd principal stretch directions and main fibre directions (Figure 4.11). The results show that the differences between main fibre direction and second principal stretch direction are relatively low with a mean difference of 14.4° (±14.6°). High differences of more than 25° showed a low AI indicating a rather isotropic mechanical behaviour of the plaque tissue at those locations. Interestingly, the highest differences were at the intima locations, which also showed a low AI.

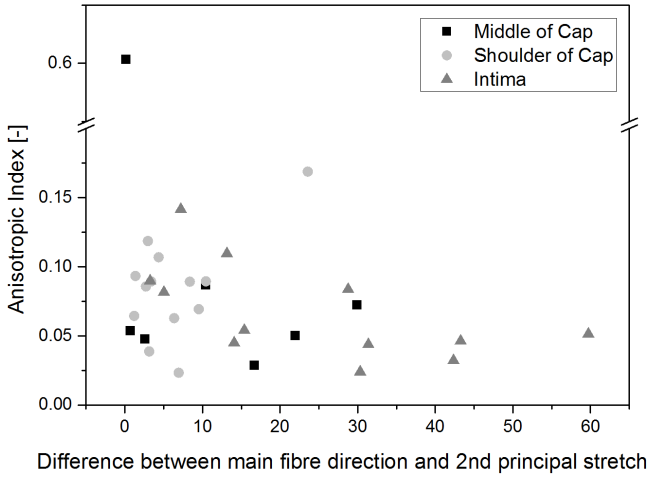

Figure 4.11: *The anisotropic index, defined as ratio between 1st and 2nd principal stretch minus 1, was plotted against the difference between main fibre directions and the direction of the 2nd principal stretch.*

4.4 Discussion

Most of the current biomechanical computer models assume isotropic mechanical behaviour, although studies have shown that atherosclerotic plaque tissue is highly anisotropic [45, 52]. This study shows that atherosclerotic plaque tissue mostly consists of anisotropic components with some regions behaving isotropic. The aim of the study was to characterise the anisotropic behaviour of plaques by measuring the local collagen fibre stiffness and distribution. The fibre distribution was determined using confocal imaging. The fibre stiffness was inferred from the indentation force and displacement distribution by applying inverse FE analysis. The FE model described the experiment well, which is shown by low mean relative errors. The results show that the extra-cellular matrix component in the plaque tissue was much softer compared to the collagen fibres, which shows that collagen fibres are the most load-bearing structure in atherosclerotic plaque tissue. It appeared that the fibre stiffness at proximal shoulder regions of plaques is significantly higher than at distal regions. Lateral shoulder regions of the plaque show no significant differences in fibre stiffness compared to middle cap and surrounding intima regions. A significant difference between the level of non-linearity has been observed for intima regions and shoulder regions of plaque caps.

The level of non-linearity is more pronounced in the shoulder regions. We speculate that at higher stress larger strain might occur at shoulder regions than at intima regions, potentially making the shoulder region more vulnerable to rupture at high blood pressure.

The fibre stiffness at different longitudinal locations (proximal/upstream, maximum stenosis, distal/downstream) were compared to each other and it was found that the fibre stiffness in plaques are significantly stiffer at the proximal shoulder than at the region with maximum stenosis. Huang et al. [103] found that the stiffness of plaques of symptomatic patients upstream might be lower than downstream. Therefore, for those patients, the plaque cap at the proximal shoulder was more vulnerable for rupture than distal downstream locations. In fact, Huang et al. [103] reported that a possibly softer upstream cap was found for the patient group who suffered from cerebral events, whereas non-symptomatic patients had stiffer upstream caps.

Literature suggests that shoulder regions are more prone to rupture than middle regions of fibrous caps, possibly due to higher stress concentrations at shoulder locations [30, 95, 104, 105]. Our study shows that the shoulder cap regions behave significantly less non-linear than the surrounding intima tissue of the plaque (Figure 4.5). Therefore, at high stress, the shoulder cap experiences more strain than the neighbouring intima region. A highly strained shoulder cap region combined with accumulation of activated mast cells [106], infiltrating macrophage releasing matrix metalloproteinases (MMPs) [107], high shear stress [95, 108], micro-calcification, iron accumulation within the fibrous cap [109], and macrophage cell death [110], all contribute to an increased rupture risk at the shoulder region. However, it has also been shown that the majority of plaques that rupture at the shoulder regions occurs in patients at rest and that rupture at midcap regions occur predominantly in patients during exertion [54, 111]. One possible explanation is described in Abdelali et al. (2014) [112], who proposed that stress peaks might relocate from shoulder regions of fibrous caps to the middle of the fibrous cap due to buckling effects. Another explanation for failure at the middle of the fibrous cap is the development of micro-calcification as proposed by Vengrenyuk et al. (2006) [104, 109, 113, 114, 115, 116, 117], which can increase the stress inside the cap and increase the rupture risk.

A problem with regard to predictability of future mechanical models is the huge spread in the measured results. The fibre stiffness in the present study ranged from 18 to

157 kPa (25th percentile and 75th percentile). It is difficult to compare the values found in this study to other data found in literature, but the obtained range of mechanical properties does correspond to the range found by other research groups. The inter-patient variability was lower than the intra-patient variability.

To characterise the anisotropic mechanical behaviour of plaques, the local collagen fibre stiffness was measured. However, for a full characterisation, the fibre direction also needs to be determined. In the current study, the collagen fibre directions were visualised using confocal imaging. The images show that at highly anisotropic locations, the collagen fibres were mainly aligned in the circumferential direction around the lumen, similar to the healthy state of the artery. It has to be noted though that these collagen fibre directions were observed very locally. For a full characterisation the global 3D collagen architecture needs to be known.

4.5 Limitations

Since collagen fibres in the arterial wall are mainly oriented in the circumferential direction the indentation technique measured the mechanical properties of the collagen fibres in the most relevant direction. Relatively thin plaque slices in longitudinal direction were tested. This supported the assumption of a uniform fibre distribution throughout the slice thickness required for the inverse finite element analysis. However, the slicing of the tissue may have compromised the collagen fibre architecture, which will influence the mechanical behaviour.

Healthy arteries are under 30% pre-stretch [82, 83, 84], resulting in a more axial collagen distribution than the stress-free samples tested with the indentation test. This altered collagen distribution may have an impact on the determined stiffness results. It should be noted, however, that 30% pre-stretch occurs for healthy arteries. For atherosclerotic tissue the pre-stretch might be less pronounced. Dobrin et al. (1990) [118] and Cardamone et al. (2009) [119] have demonstrated that almost all axial pre-stretch is due to the presence of elastin. The group of Robert et al. (1998) [120] have shown that significant decrease of elastin content occurs during the progress of atherosclerosis. Therefore, the reduced elastin content of atherosclerotic plaques might induce a significant reduction of axial pre-stretch *in vivo* of the atherosclerotic plaque. Hence, this factor might only play a minor role. However, it should be noted

that Robert et al. [120] shows a decrease in elastin content in the lesion-free areas of atherosclerotic aortas, not within the lesions themselves.

Another limitation may be that the freezing and thawing process damaged the collagen structure due to ice-crystal formation. However, a snap-freezing protocol was applied minimising ice-crystal formation. Confocal images, histological images, and light microscopy did not suggest any tissue damage. Furthermore, Ebenstein et al. (2009) [50] have not found any differences between mechanical behaviour of fresh and frozen plaque samples. According to Schaar et al. (2002) [96], the influence of freezing on the mechanical properties of coronary arteries plays only a limited role.

4.6 Conclusion

In conclusion, a huge spread in plaque mechanical properties was found, much higher than in healthy tissue. Furthermore, most of the plaque regions were highly anisotropic. Proximal shoulder locations were significantly stiffer than at the maximum stenosis regions. It was observed that the intima tissue behaves mechanically more non-linear than shoulder caps of plaques, which would make the shoulder regions more prone for rupture at higher stress.

Chapter 5

3D fibrous structure of carotid plaques

5.1 Introduction

Current methods to assess plaque rupture risk require improvement. They are based on general morphological parameters, such as the degree of stenosis, which are only indirectly connected to the cause of plaque rupture. Plaque rupture occurs when the plaque cap strength is exceeded by the cap stresses. Computer modelling is a useful tool to improve plaque rupture risk assessment. They enable simulation of the occurring stresses in plaques and can be used to visualise stress peaks in plaque caps.

However, the accuracy of stress analyses from computer models strongly depend on the used material models and input parameters. Most of the current computer models assume isotropic behaviour although it is well accepted that plaque tissue behaves anisotropic [45, 100]. Thus, those computer models might be over-simplified and the inclusion of anisotropic mechanical behaviour will improve the accuracy of plaque modelling [52, 121].

Previous studies [100] focused on the mechanical properties of collagen fibres in plaque tissue. For a full characterisation of the anisotropic mechanical behaviour of plaque tissue also the 3D architecture of the fibrous structure of plaques are required.

Therefore, the aim of the present study is to visualise the 3D architecture of the fibrous tissue in human atherosclerotic plaques using Diffusion Tensor Imaging (DTI), a technique that has already been used for visualising the collagen structure in healthy porcine carotid arteries [122].

5.2 Methods

5.2.1 Sample preparation

The Medical Ethical Committee of the involved hospitals approved the study. Nine human carotid atherosclerotic plaques were obtained from endarterectomy patients. Six endarterectomy surgeries were performed at the Catharina Hospital in Eindhoven. Three plaques were obtained from the Erasmus Medical Centre in Rotterdam (in total 9 male, age 55-80 years). Furthermore, two healthy porcine carotid arteries were obtained from the local slaughterhouse. Initially, the samples were snap-frozen and stored at -80°C. At a later stage the samples were thawed, placed in a cryovial (Sigma, USA)

and embedded in 4% type VII agarose (Sigma, USA) similar to the protocol used in Ghazanfari et al. (2012) [122].

5.2.2 Diffusion Tensor Imaging

DTI scanning was performed with a 9.4 T horizontal-bore MRI scanner (Bruker, Ettlingen, Germany) using a 35-mm-diameter send-receive quadrature birdcage radiofrequency coil. Two carotids embedded in type VII agarose were placed in the RF coil and measured simultaneously. Diffusion imaging was done with a three-dimensional spin-echo sequence with uni-polar diffusion sensitizing pulsed field gradients placed symmetrically around the 180° radiofrequency pulse. Sequence parameters were: echo time TE=27 ms, repetition time TR=1000 ms, number of averages NA=1, field of view FOV=30 x 30 x 30-60 mm^3, acquisition matrix = 256x96x96, reconstruction matrix = 256x256x256, 10 diffusion directions with diffusion weighting b-value = 1500 s/mm^2, 1 image without diffusion weighting, total acquisition time ca. 28 h.

5.2.3 DTI analysis

Fibre tractography was performed by using the in-house developed software called vIST/e [123] (http://bmia.bmt.tue.nl/software/viste/). To further analyze the fibre orientation, fibre coordinates obtained from vIST/e were imported in Matlab (Mathwork, USA). First, the alignment of the arterial axis was set parallel to an arbitrary axis and the whole volume was translated to the centre of coordinates. Subsequently, the coordinates of fibres in the image reference system were converted to the cylindrical coordinate system. Finally, the fibres orientation was calculated with respect to the horizontal plane [122].

5.2.4 Histology

After the Diffusion Tensor Imaging, the agarose, in which the plaques were embedded, was removed and one plaque was sliced using a cryotome to obtain longitudinal cross-sections for histology. Picro-Sirius Red staining was applied to visualise the collagen fibres in the plaque tissue.

5.3 Results

5.3.1 DTI result of healthy porcine carotid artery

Diffusion Tensor Imaging results for one porcine carotid artery is shown in Figure 5.1, being representative for both porcine carotid arteries. On the left-hand side of Figure 5.1, the tracked fibres of one porcine carotid artery are visible. The different colours indicate the direction of the fibres. In red are all fibres aligned in the circumferential direction, whereas in green are fibres aligned in the longitudinal direction. From the DTI results it is apparent that almost all fibres of the porcine carotid arteries follow the circumferential direction (0° to 10°). The observations are quantified in the diagram on the right-hand side of Figure 5.1. The x-axis represents the fibre direction from -90° to 90°, where values close to 0° indicate a more circumferential alignment, whereas values close to $\pm 90°$ correspond to longitudinal alignment. The y-axis describes the amount of fibres found, while the z-axis indicates the arterial wall position. A position at 0.0 is at the luminal side, whereas a position at 1.0 is at the outer wall of the sample.

5.3.2 DTI result of human carotid plaque

On the left-hand side of Figure 5.2, the fibre tractography analysis of a plaque is shown, which is representative for 4 out of the 9 plaques. Fibres in green follow the longitudinal direction of the artery, whereas fibres in blue and red are aligned in circumferential direction. In these 4 plaques, an inner layer of fibres was found with clear fibre orientation in the longitudinal direction. The inner layer is partly surrounded by an outer layer of fibres, which are oriented in the circumferential direction. These observations are also clear from the quantification of the fibre directions, which is summarised in the diagram on the right-hand side of Figure 5.2. The z-axis shows the normalised wall position; where position 0.0 indicates fibres at the luminal side of the artery and 1.0 the outer wall position. At the outer wall positions the fibres are more oriented in the circumferential direction (10°), while the fibre further down towards the luminal side are oriented much more towards the longitudinal direction (50° to 90°).

Five plaques were found where the orientation was less clear, a disorganised and more heterogeneous structure appeared. A representative result of those plaques is shown

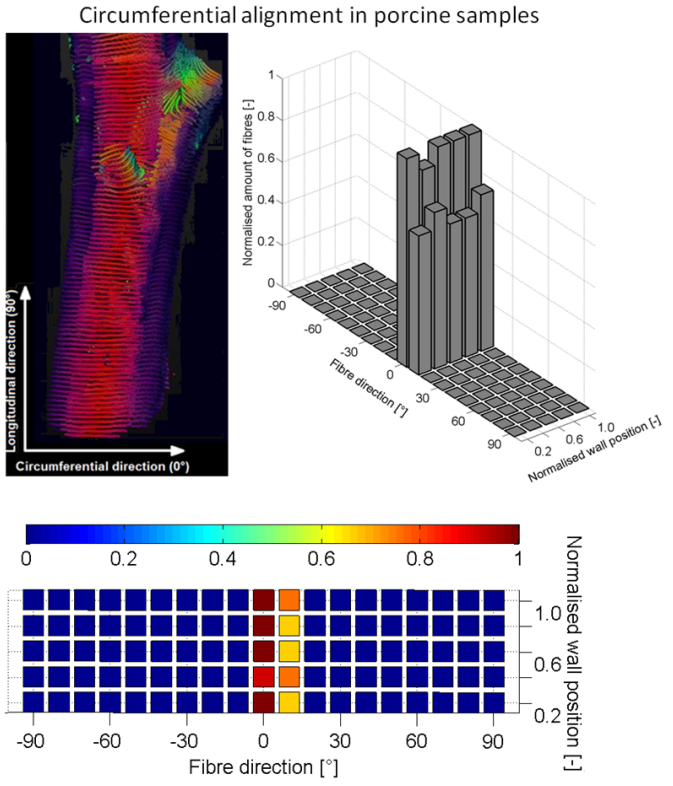

Figure 5.1: *DTI results of one healthy porcine carotid artery, where almost all tracked fibres are oriented in the circumferential direction (0º) of the plaque tissue. No fibres were aligned in the longitudinal direction (±90º).*

in Figure 5.3. On the left-hand side the tracked fibres are visualised. Those plaques display, contrary to the plaque shown in Figure 5.2, no clear layers. This is also apparent in the quantification summarised in the diagram shown in Figure 5.3. Although the fibre orientation is not as clear as shown in Figure 5.2, the plaques do display some fibres that are aligned in the longitudinal directions.

5.3.3 Histology

The histology results for one plaque are shown in Figure 5.4. The DTI results for this plaque showed clear fibre alignment in the longitudinal direction on the luminal side

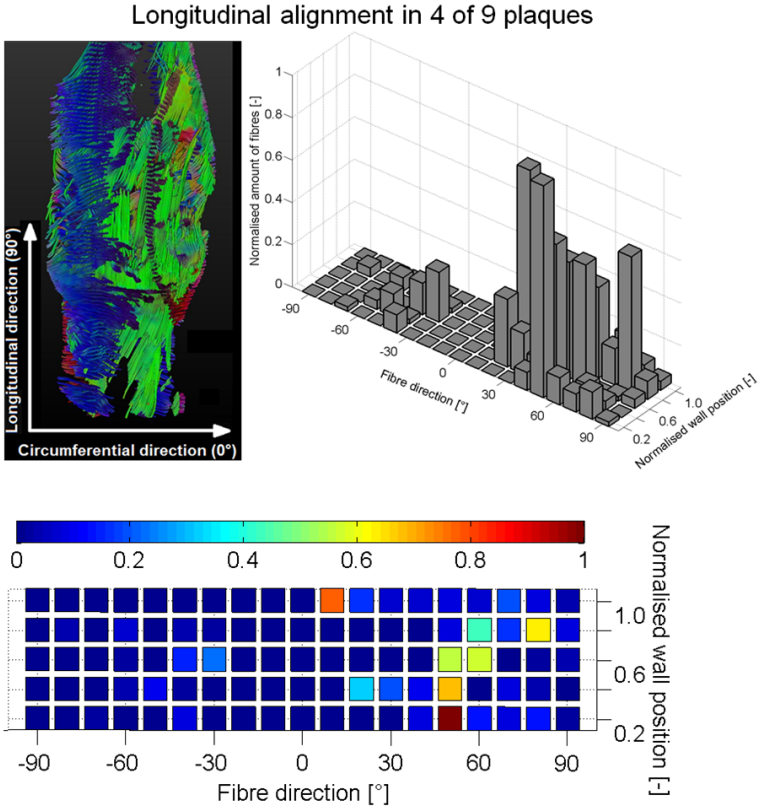

Figure 5.2: *Tracked collagen fibres of one sample representing the general fibre alignment (figure on the left-hand side), fibres in green are aligned in the more longitudinal direction (90°), whereas fibres in red and blue represent the circumferential direction (0°), the graph (on the right-hand side) shows the number of fibres against the fibre directions and the luminal wall position. Here the fibres at the luminal side are clearly oriented in the longitudinal direction (50° to 80°), further lateral the fibres are oriented towards the circumferential direction (10°). This figure is representative for 4 out of 9 cases.*

of the arterial wall (see Figure 5.2). Also, on the histology images the collagen fibres were clearly oriented in the longitudinal direction at the luminal side confirming the DTI results. Further away from the luminal side, towards the outer wall, the collagen fibres appeared more disrupted.

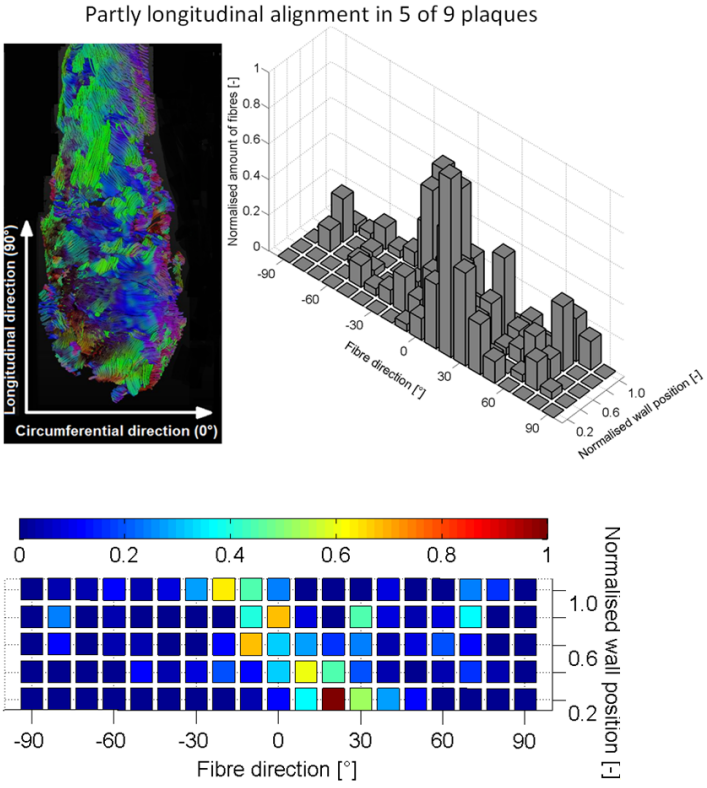

Figure 5.3: *DTI result for another sample representative for 5 out of 9 cases, where the collagen fibre alignments are not as clearly structured as in Figure 5.2, green fibres are showing fibres in the longitudinal direction, whereas fibres in the circumferential direction are in red and in blue, the diagram shows the amount of fibre against the fibre direction and normalised wall position. In this example the fibres were oriented in two directions, in circumferential (0°) and longitudinal (90°) direction throughout the arterial wall.*

5.4 Discussion

The aim of this study was to characterise the global 3D architecture of fibrous tissue in human carotid atherosclerotic plaque tissue using DTI. All tested plaques consisted of fibrous tissue indicating the presence of regions which behave mechanically anisotropic. For 4 out of 9 plaques the fibrous regions showed clear longitudinal alignment. The remaining plaques revealed partly longitudinal alignment of fibres. This was also apparent in the histology results for one plaque, supporting the DTI findings.

DTI is a well established method [124] to visualise fibrous tissue, also for arterial tissue

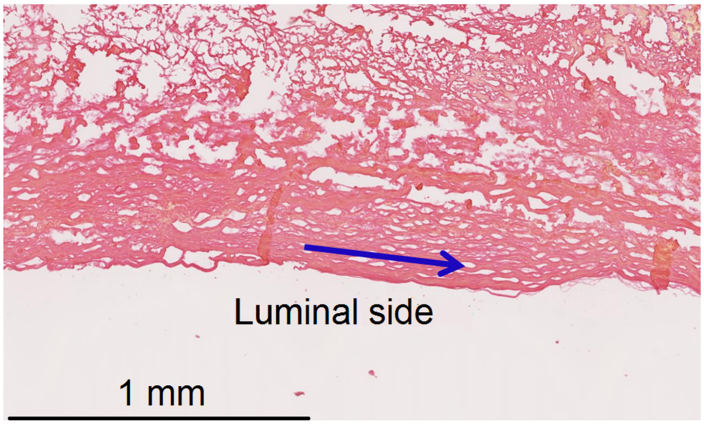

Figure 5.4: *PSR (Picro-Sirius Red)-staining for one human plaque confirms collagen fibres are oriented in longitudinal direction on the luminal side of the artery. Further away from the luminal side, the collagen fibres appear disrupted.*

[122]. The presence of aligned fibrous regions in all plaques indicate that atherosclerotic plaques behave anisotropic, which corresponds to published data on mechanical properties of atherosclerotic plaques [45, 100].

The fibrous regions for 4 out of 9 tested plaques showed a longitudinal alignment of fibres at the innermost layer of the plaque tissue. This inner layer was partly surrounded by an outer layer of fibrous tissue, where the fibres were aligned in the circumferential direction of the vessel. In 5 out of 9 cases the fibre structure showed not a clear continuous layer in longitudinal direction as mentioned above. Still in these cases many fibres were aligned in the longitudinal direction. This is a surprising result considering that in the healthy state, as shown with porcine carotid arteries, fibres were oriented in the circumferential direction of the artery.

A possible explanation for the longitudinal alignment of fibres may be a change of strain and stress distribution during the formation of the atherosclerotic plaque. In a healthy human artery the stresses due to blood pressure pulsation cause the artery to deform. The main strain occurs in the radial direction as compression and in the circumferential direction as tension. As a result, collagen fibres tend to align in a helical structure. In this study the tissue was embedded in agarose for DTI, without pre-stretching the artery. Without the axial pre-stretch the fibres, which *in vivo* appears as a helical structure, rotate to a circumferential direction.

Atherosclerosis causes a substantial thickening of the arterial wall. This thickening will cause a change in strain and stress distribution. The thickened wall presents much more resistance compared to a healthy wall, so it is possible that the main strain is no longer in the circumferential and radial direction, but in the longitudinal direction. This was observed by McCormick et al. (2012) [125]. Even for healthy arteries, it has been shown by Cinthio et al. (2006) [126] that some longitudinal movement and shear strain occurred. Assuming that collagen fibre orient in the direction of main strain [79, 127, 128, 129], this might explain why fibres in atherosclerotic plaques are aligned in longitudinal direction of the artery.

The partly alignment of fibres in longitudinal direction observed in 5 of the 9 plaques may be caused by very heterogeneous plaques containing substantial calcifications. McCormick et al. (2012) [125] suggested that the strain in longitudinal direction in atherosclerotic plaques might be influenced by its calcification content.

Furthermore, the alignment of collagen fibres might be connected to the amount of MMP-13 present. Deguchi et al. (2005) [130] have shown the fibre distribution is influenced by the presence of MMP-13.

5.5 Limitations

The imaging method cannot distinguish between different types of fibrous tissue. Therefore, the tracked fibres from DTI might show also other fibrous structures, such as elastin fibres. The histology results using collagen-specific PSR staining suggests that the visualised fibre structure is predominately collagen.

Healthy arteries *in vivo* experience an axial pre-stretch [82], while the samples, tested in this study, were stress-free. For atherosclerotic plaques the effect of axial pre-stretch might be less pronounced. Studies have shown that axial pre-stretch is mostly caused by the presence of elastin fibres in arteries [118, 119], but Robert et al. (1998) [120] demonstrated that the amount of elastin is decreased in plaques.

The freezing process prior to DTI may have caused ice-crystal formation which can damage the tissue integrity, disrupting collagen fibres. To minimise ice-crystal forma-

tion a snap-freezing protocol was applied. Moreover, Ebenstein et al. (2002) [51] and Schaar et al. (2002) [96] investigated the influence of freezing on mechanical properties of atherosclerotic plaques and it was suggested that the freezing process has no significant influence on the mechanical properties of plaque tissue.

It has to be also noted that the samples were obtained from carotid endarterectomy surgery, a procedure where the clinician removes the inner layers of a stenotic plaque. Thus, the samples only represent the luminal layer of the diseased artery and the outer layer of the plaque might contain disrupted structures, which were damaged during the surgery.

5.6 Conclusions

To the author's knowledge, this is the first study attempting to visualise the architecture of fibrous tissue in plaques using Diffusion Tensor Imaging. The results indicate that during the progress of atherosclerosis a major reorganisation of fibrous tissue occurs. The fibrous tissue in plaques appears to orient in the longitudinal direction. These new results showing the 3D fibre architecture of atherosclerotic plaques can in combination with previous studies improve the accuracy of biomechanical models of plaques. This will be another step towards reliable plaque rupture prediction and improve the prevention of atherosclerosis related cardiovascular events, such as strokes and heart attacks.

Chapter 6

Failure properties of plaques

The content of this chapter is based on C.-K. Chai, K. H. J. Groenen, L. Speelman, F. J. H. Gijsen, C. W. J. Oomens, M. R. H. M. van Sambeek, A. van der Lugt, and F. P. T. Baaijens. Mechanical failure properties of human atherosclerotic carotid plaque caps - characterisation using indentation test (*submitted*).

6.1 Introduction

Atherosclerosis is characterised by accumulation of lipids and macrophages inside the arterial wall, leading to a thickening of the wall and to the development of a plaque. A specific type of advanced atherosclerotic plaque is the so-called vulnerable plaque, which is prone to rupture. In general, vulnerable plaques consist of macrophages, intra-plaque haemorrhages, and a lipid-rich necrotic core, covered by a thin fibrous cap separating the thrombogenic core from the blood flow. The blood flow and blood pressure cause stresses inside the fibrous plaque cap. The cap ruptures if the ultimate stress in the cap is exceeded, leading to direct contact between blood and necrotic core. Subsequent thrombus formation may cause a local occlusion of the artery or distal embolisation of thrombus, both obstructing blood flow. This is the main cause for cardiovascular events, such as ischaemic strokes, transient ischaemic attacks, and myocardial infarctions [131].

Since plaque rupture can lead to potentially lethal cardiovascular events, it is desired to reliably assess the plaque stability. Currently, plaque stability assessment is based on general morphological parameters such as cap thickness or degree of stenosis. However, it has been suggested that this is not sufficient and rupture risk assessment needs to be improved to prevent plaque rupture in vulnerable plaques as well as to avoid over-treatment of stable plaques [21].

To improve plaque rupture risk assessment, it is crucial to obtain more data regarding the failure properties, i.e. ultimate stress and strain, of plaque caps. Studies on plaque failure properties are scarce and show high variability. Furthermore, most of these studies examine the ultimate tensile strength using uni-axial tensile tests [39, 40, 41, 42, 44, 45, 46]. However, extraction of failure properties based on tensile experiments is not straightforward, since the experiments are difficult to perform on small samples, are subject to local imperfections and cutting artefacts, and the results depend on the orientation of the sample with respect to the collagen fibres. In addition, the stress state may not be representative for the complex stress and strain state in real fibrous caps. Compression tests are less susceptible to cutting artefacts and geometrical imperfections, and have been performed on atherosclerotic plaque tissue. However, these studies were not designed to examine the failure behaviour of plaques.

Most studies investigating plaque failure properties focused on plaques acquired from large arteries such as the aorta [39, 40, 41] and iliac arteries [45]. To the authors'

knowledge, no studies have been conducted testing the mechanical failure properties of plaque caps in carotid arteries using indentation tests.

The present study examines human carotid plaque caps using indentation experiments to analyse the failure properties. For this purpose, a new micro-indentation test setup was designed and plaque caps were indented until failure occurred. In combination with inverse finite element analysis the ultimate stress and strain were inferred.

6.2 Materials and methods

6.2.1 Sample preparation and cap thickness measurements

The current study was approved by the Medical Ethical Committee of the Catharina Hospital in Eindhoven. From ten patients (7 male, 3 female, age 62-79), plaques were obtained after carotid endarterectomy. The plaques were snap-frozen using liquid nitrogen and stored at -80°C. At a later stage, the frozen samples were thawed in Phosphate Buffered Saline (PBS) to room temperature and subsequently dissected to isolate fibrous caps from the carotid atherosclerotic plaques. The sizes of two plaque caps were sufficient to prepare two additional samples, so that in total 12 caps were obtained for testing.

A commercially available instant adhesive (Bison Gel, Bison International B.V.) was used to glue the isolated plaque caps on a 4 mm thick stainless steel plate. The centre of the plate contained a hole with a diameter of 2 mm which was covered by the fibrous cap. Following the protocol by Topoleski et al. (1997) [67], Salunke et al. (2001) [69], and Holzapfel et al. (2004) [45], the tissue was placed in PBS for 30 min in room temperature to equilibrate. Afterwards, the thickness of the fibrous cap was measured using digital microscopy and accessory measurement software (Keyence VKX-500FE). Per sample, images were taken from four sides of the stainless steel plate. For each side, three thickness measurements were performed and the averaged values were used as fibrous cap thickness.

6.2.2 Indentation test and loading protocol

To test the failure properties of the plaque caps, an indentation test was used (Figure 6.1). The indentation was performed at room temperature in the radial direction of

the plaque cap using a screw-driven indentation device (Zwick Z010 TN2A). A stainless steel cono-spherical indenter was placed at the centre of the stainless steel plate above the hole, so that the fibrous cap was pushed through the hole during indentation. The indentation force was measured using a 20 N load-cell with a minimum force resolution of 1 mN.

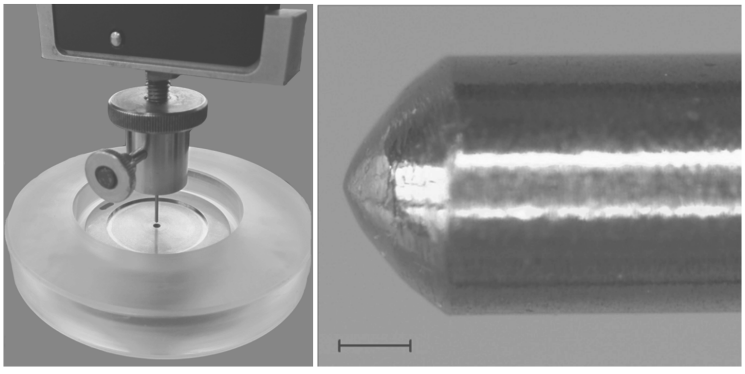

Figure 6.1: *On the left hand side, the experimental setup. Indentation tests were performed in a conventional screw-driven testing machine. The fibrous caps were glued to a stainless steel plate which contained a hole (diameter 2 mm) in the centre. The plate was placed in a water bath filled with PBS. Subsequently, the tissue was indented with a cono-spherical indenter which was centered with respect to the hole in the stainless steel plate. On the right, the indenter had a diameter of 1 mm and a cono-spherical tip. The scale bar represents 250 µm.*

Following the approach described in Maher et al. (2009, 2011) [42, 43], an indentation rate of 0.001 mm/s was used to approach the fibrous cap until a pre-load of 10 mN was reached. The position where the force was reaching the pre-load of 10 mN was set as reference position (0 mm indentation depth). Afterwards, the indentation was controlled via the indentation depth at a quasi-static indentation rate of 0.02 mm/s, similar to the indentation rates used in Holzapfel et al. (2004) [45]; Topoleski et al. (1997) [67] and Chai et al. (2013) [71].

Cyclic loading-unloading indentation tests were conducted by incrementally increasing the indentation depth by 0.25 mm, from 0.25 mm up to a maximum of 4.0 mm. During unloading the indenter was moved back to its reference position. The sample was loaded once at each indentation depth. The sample was left to recover at the start position for 5 minutes after each loading-unloading cycle. The caps were kept moisturised

in PBS and were loaded until the fibrous cap was fully punctured. After finishing the mechanical testing, the fibrous cap was visualised using the digital microscope to verify whether puncturing of the tissue had occurred.

From the indentation experiment, for each cycle, the indentation force F_z and indentation depth d_z were measured and recorded. Based on these measurements inverse Finite Element Analysis was conducted to infer the ultimate stress and ultimate strain of fibrous plaque caps.

6.2.3 Inverse Finite Element Analysis

A displacement-driven axi-symmetric finite element (FE) model was generated in MSC Marc (Version 2005r3, MSC Software Cooperation), mimicking the indentation experiment. Subsequently, the ultimate stress and strain were estimated by fitting the simulated indentation force-displacement curve to the experimental force response of all loading cycles until initial failure occurred (Figure 6.2, see section 6.2.2). To assess the fitting quality a customized Matlab (Version 2007b, MathWorks Inc.) code was used.

For each experiment (section 6.2.2), a dedicated FE model (Figure 6.3) was generated, incorporating the measured cap thickness h. Under axi-symmetry assumptions, 2D half blocks were modelled representing the plaque tissue. The radius of the tissue R was set at 4 mm. The indenter was modelled as a rigid body with the same cono-spherical geometry as in the experiment. The stainless steel plate was also modelled as a rigid body. The edge of the hole in the stainless steel plate was slightly rounded (radius = 50 µm) to avoid stress concentrations at the boundaries of the plate. The contact option "glue" (MSC.Marc, 2005) was used between the tissue and both, the part of the plate parallel to the tissue and the rounded part of the plate. The contact between the tissue and the part of the plate perpendicular to the tissue as well as between the indenter and tissue were assumed to be frictionless.

The tissue close to the indenter and hole in the stainless steel plate received a fine mesh while the surrounding tissue gradually received a coarser mesh. Depending on the tissue thickness, the generated models consisted of 4500 to 9000 elements. The tissue

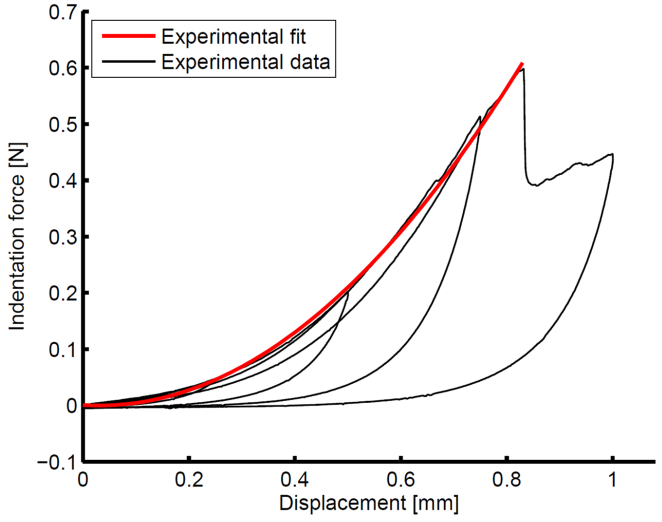

Figure 6.2: *The experimental fit. The experimental fit was defined as a non-linear fit through the loading parts of the applied indentation cycles up to the point of initial failure.*

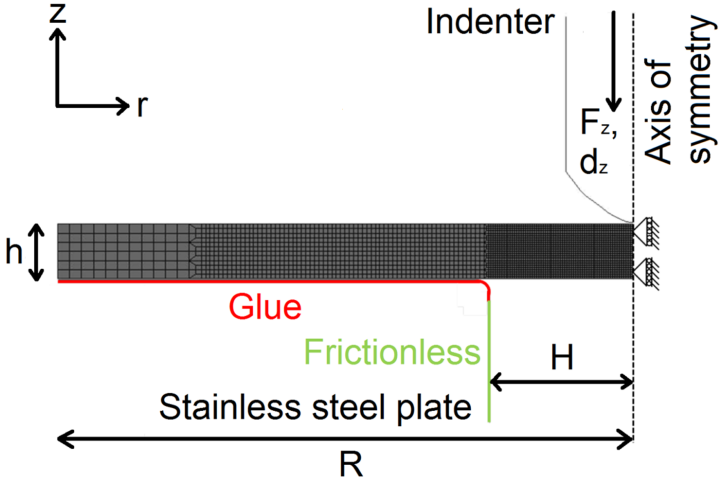

Figure 6.3: *Schematic of the axisymmetric finite element model representing the experimental setup. This model was used to extract the ultimate stress and strain values from the experiments. Cap thickness (h) was adjusted for each cap based on the initial thickness measured using digital microscopy. H = radius hole; R = radius sample; h = thickness tissue; F_z = indentation force; d_z = indentation depth.*

was modelled using four-node, bilinear, axi-symmetric elements, with full integration and Hermann formulation to deal with incompressibility. Non-linear geometry effects,

including large strains, were included. The displacement of the indenter was prescribed up to the ultimate displacement obtained from the experiments.

The fibrous cap was modelled as a hyper-elastic material using a two-term Ogden strain energy formulation [132], simulating the nonlinear stress strain characteristics of plaque components. Furthermore, tissue properties were assumed uniformly distributed, isotropic, and incompressible [105, 133, 134]. A two-term strain energy form (W)

$$W = W(\lambda_1, \lambda_2, \lambda_3) = \sum_{i=1}^{2} \frac{\mu_i}{\alpha_i}(\lambda_1^{\alpha_i} + \lambda_2^{\alpha_i} + \lambda_3^{\alpha_i} - 3) \tag{6.1}$$

was used, where λ_{1-3} are the principal stretch ratios, μ_i are moduli constants [Nm^{-2}] and α_i [-] are exponent constants. The parameters α_i and μ_i were iteratively estimated by minimising the difference between force-indentation data obtained from the computational simulations and the data measured during the experiment (Figure 6.1). For the experimental data, only measurements until the initial failure point of the plaque cap were taken into account for the parameter estimation. A drop in the measured force signal during indentation was considered to indicate initial failure of the plaque cap.

The quality of the fit between experimental and simulated data was measured by determining the mean absolute error MAE

$$MAE = \frac{\sum_{i=1}^{N} |exp_i - sim_i|}{N} \tag{6.2}$$

where N is the number of data points, exp the experimental data points and sim the simulated data points. The MAE was then normalised by the mean experimental value (exp) to provide a relative measure of fit error (mean relative error (MRE)). A $MRE < 20\%$ was considered a good fit [71].

$$MRE = \frac{MAE}{\overline{exp}} \tag{6.3}$$

6.3 Results

6.3.1 Cap thickness

The plaque cap thicknesses are summarised in Table 6.1, where the first column consists of the sample identification (ID). The second, third and fourth column show the measured mean, standard deviation, and coefficient of variance, respectively. The last

column contains remarks about the sample.

Table 6.1: *Cap thickness, P=plaque number, S=sample number, CV= coefficient of variation.*

Sample ID	mean [mm]	SD [mm]	CV [%]	Remarks
P1S1	0.72	0.22	30.6	-
P1S2	1.18	0.14	11.6	Sever calcification
P2S1	0.75	0.05	7.1	Detached from stainless steel plate
P3S1	0.79	0.14	17.9	Force oscillation and air bubble formation
P3S2	0.6	0.13	21.1	-
P4S1	0.97	0.14	14.6	Tissue was thickened at testing location
P5S1	0.51	0.23	44.8	-
P6S1	1.82	0.23	12.6	Tissue contained lipid at testing location
P7S1	1.13	0.6	52.8	Severe calcification
P8S1	1.95	0.11	5.5	Detached from stainless steel plate
P9S1	1.18	0.16	13.2	-
P10S1	1.68	0.12	7.3	-
Mean	1.11	0.46	19.9	

NF: not found

The average measured fibrous cap thickness ranged from 0.51 mm to 1.95 mm. It has to be noted that the cap thickness generally varied considerably (mean coefficient of variance of 20%). Three atherosclerotic caps (P1S1, P5S1, and P7S1) showed a substantial variation of more than 30%.

6.3.2 Indentation results

Behaviour until initial failure

All samples exhibited the following mechanical behaviour during the indentation cycles up to the initial failure point:

(a) As expected for soft collagenous tissue, the load deformation behaviour was nonlinear, with pronounced stiffening at increasing indentation depths;

(b) Differences between the loading and unloading response within one indentation cycle were demonstrated, indicating hysteresis;

(c) A softening effect was observed, characterised by a lower resulting force for the same applied indentation depth in a new loading cycle. This effect seemed to increase with increasing indentation depth. However, the effect of softening was minimal;

After the initial point of failure, three different types of typical force-displacement responses were recorded. The three representative force-displacement curves are shown in Figure 6.4, Figure 6.5, and Figure 6.6. The points of initial failure are denoted with the black arrows marked with (A).

Behaviour after initial failure

For most caps, namely six, (Figure 6.4) the force pattern prior to the point of initial failure was not characterised by a smooth increase in force like in the other samples, but by a change in steepness and smoothness of the force response. After passing the initial failure point, the next loading cycle crossed the load at the end of the previous loading cycle, while the indentation force was still increasing. After reaching the maximum load, the sample demonstrated a force response similar to the second pattern described (Figure 6.5).

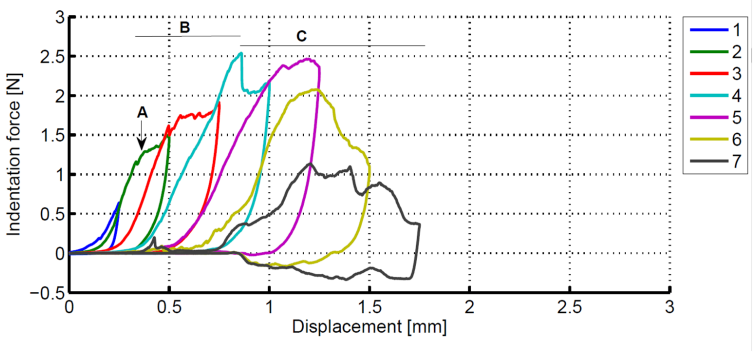

Figure 6.4: *Force-displacement curves of P1S2, which were similar to P6S1, P7S1, P8S1, P9S1 and P10S1. The force pattern prior to the point of initial failure was characterised by a change in steepness and smoothness. After passing the point of initial failure (A) the force gradually increased (B). After reaching the point of maximum force, the force gradually decreased (C). The different colours represent the subsequent indentation cycles.*

The second force-indentation curves are shown in Figure 6.5, representatively for three plaque caps. After the initial failure point, the force dropped rapidly, as described in the previous paragraph. However, it did not decrease to 0 N immediately but the samples were able to bear a lower load. This occurred either within the same loading cycle, or in the following one.

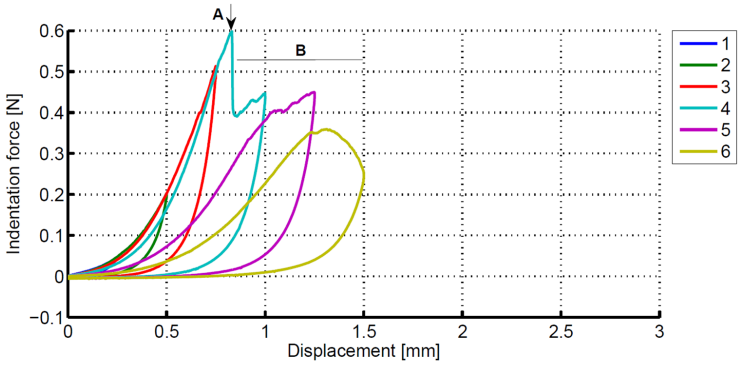

Figure 6.5: *Force-displacement curves of sample P1S1. This is a representative illustration of the failure pattern of samples P1S1, P3S2 and P5S1. The point of initial failure (A), defined by a rapid but relatively small decrease in force, was followed by a gradual decrease in indentation force (B). The different colours represent the subsequent indentation cycles.*

For one plaque cap, the force-displacement pattern exhibited a mechanical behaviour which is shown in Figure 6.6. Here, after a smooth, nonlinear force increase, a sudden drop in force occurred. During the next loading cycle, this rapid decrease reached almost 0 N.

6.3.3 Parameter identification

Ogden material constants

The combination of indentation experiments and computer modelling enabled inverse FE analysis to derive the mechanical properties of human atherosclerotic carotid plaque caps. For every sample, the Ogden material constants were identified. The results are summarised in Table 6.2. The first column shows the sample ID. For sample P2S1

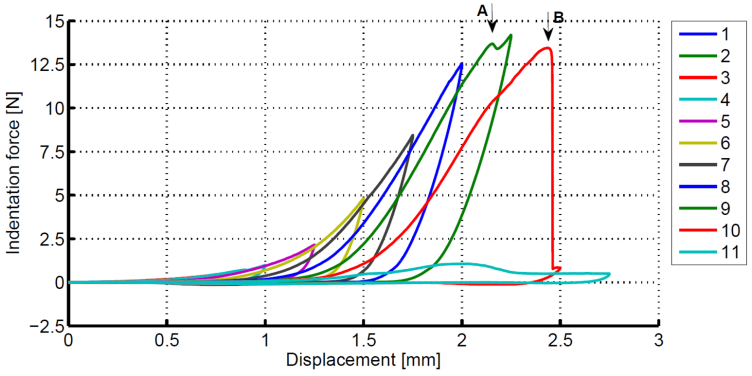

Figure 6.6: *Force-displacement curves of sample P4S1. The force response was characterized by a smooth, nonlinear increase in force prior to the point of initial failure (A), followed by a rapid decrease in force to almost 0 N (B). The different colours represent the subsequent indentation cycles.*

and P8S1 no properties are presented, because the sample detached from the stainless steel plate during the indentation experiment. In the following columns, the Ogden material constants (μ_1, α_1, μ_2, α_2) are summarised. The median (25th percentile-75th percentile) of the moduli constants μ_1 and μ_2 found for the plaque caps were 40 kPa (19.1 kPa-101.8 kPa) and 52 kPa (28.6 kPa-101.8 kPa) respectively. The median (25th percentile-75th percentile) of the exponent constants α_1 and α_2 were 11.0 (7.1-12.8) and 8.0 (6.3-15.0), respectively. The last column in Table 6.2 contains the MRE. The maximum MRE was 16.3%, indicating good quality fits and that the simulated data describe the experimental data very well.

Ultimate strength

The ultimate strength of the plaque caps was also determined. The obtained results are summarised in Table 6.3. The first column shows the sample ID. The following columns contain the ultimate strength data (maximum stress $\sigma_{max.princ.}$ Von Mises stress σ_{VM}, maximum strain $\varepsilon_{maxprinc.}$, and Von Mises strain $\varepsilon_{VM.}$). The median (25th percentile-75th percentile) of the maximum stress $\sigma_{max.princ.}$ and peak Von Mises stress σ_{VM} were 10.8 MPa (5.2 MPa-37.5 MPa) and 30.8 MPa (5.4 MPa-116.3 MPa), respectively. The median (25th percentile-75th percentile) of the maximum strain $\varepsilon_{maxprinc.}$ and the Von Mises strain $\varepsilon_{VM.}$ were 0.4 (0.3-1.0) and 0.8 (0.5-2.1), respectively. It should be noted that, for one plaque where two additional caps were obtained, the ultimate

Table 6.2: *Ogden material constants, see eq. 6.1, obtained from the last indentation cycle before initial failure occurred describing the mechanical properties of atherosclerotic plaques at large compressive strain.*

Sample ID	Material properties				
	μ_1 [kPa]	α_1[-]	μ_2[kPa]	α_2[-]	MRE [%]
P1S1	17	11	38	8	8.2
P1S2	40	25	52	25	8.4
P2S1	-				
P3S1	-				
P3S2	120	8	110	5.5	14.7
P4S1	86	7	86	6	16.3
P5S1	65	13	65	16	8.4
P6S1	5	12	5	12	9.4
P7S1	340	22	340	22	3.4
P8S1	-				
P9S1	25.5	7.5	25.5	7.5	7.8
P10S1	15	6	20.5	5.6	11
Median	40	11	52	8	8.4
25th percentile	19.1	7.1	28.6	6.3	7.9
75th percentile	101.8	12.8	101.8	15	10.6

strength data differed considerably.

6.4 Discussion

The present study aims at the characterisation of the mechanical failure behaviour of human atherosclerotic carotid fibrous caps using indentation tests and subsequent inverse Finite Element Analysis. Qualitatively, the samples demonstrated similar force responses during the initial phase of the tests. In agreement with previous studies, nonlinear behaviour, hysteresis, and softening were observed. Furthermore, in most samples after the point of initial failure, a gradual decrease in force was observed, suggesting the gradual rupturing of collagen fibres. When quantifying the ultimate strength of the carotid fibrous caps, a high variability was observed. The variability in the ultimate strain was lower than in the ultimate stress. In addition, especially the ultimate stresses obtained in this study were considerably higher than the ultimate stresses reported in literature.

Table 6.3: *Ultimate strength described as maximum stress $\sigma_{max.princ}$, peak Von Mises stress σ_{VM}, maximum strain εmax.princ, and Von Mises strain ε_{VM}.*

Sample ID	Ultimate strength			
	$\sigma_{max.princ.}$ [MPa]	σ_{VM} [MPa]	$\varepsilon_{maxprinc.}$[-]	$\varepsilon_{VM.}$[-]
P1S1	1.0	1.3	0.3	0.7
P1S2	6.7	32.9	0.2	0.5
P2S1	-			
P3S1	-			
P3S2	37.5	65.3	0.8	1.5
P4S1	79.9	177.0	1.0	2.1
P5S1	5.2	5.4	0.3	0.5
P6S1	1.0	4.0	0.5	1.0
P7S1	25.2	118.7	0.3	0.5
P8S1	-			
P9S1	60.0	116.3	1.0	2.1
P10S1	14.9	28.7	1.1	2.3
Median	10.8	30.8	0.4	0.8
25th percentile	5.2	5.4	0.3	0.5
75th percentile	37.5	116.3	1.0	2.1

Cap thickness

The carotid plaque cap thicknesses measured in this study (1.11±0.46 mm) correspond to the data found in literature for aortic fibrous caps (1.2±0.4 mm [41]; 1.1±0.2 mm [64]. The caps tested in this study appear to be thicker than the carotid plaque caps tested by Barrett et al. (2009) [70], who found an average thickness of 0.5 mm for isolated human carotid fibrous cap. For this study, some additional tissue (fatty tissue, fibrous tissue) might have stayed attached to the cap, because removal of these tissue components might have damaged the structural integrity of the tissue.

Our thickness measurements illustrated the irregular thickness distribution of carotid fibrous caps, with coefficients of variation up to 45%. Therefore, it is questioned whether it is justified to use an average thickness in the FE analysis. Using a cap specific 3D FE model reflecting the actual cap geometry allows the thickness variability to be taken into account and thus leads to a more accurate calculation of ultimate strength.

Indentation experiments

The carotid plaque caps tested in this study showed highly nonlinear behaviour, which corresponds to the behaviour found for aortic, iliac, and carotid plaque caps [39, 41, 45, 70]. Further characteristics observed in this study including hysteresis and stress softening, were also described in studies, conducting cyclic uni-axial tensile tests on porcine aorta and carotid arteries [135, 136], and human aorta [137]. Furthermore, these features were also observed when cyclic compression was applied on human carotid endarterectomy samples [43, 135].

It has been suggested that stress softening of arteries is a result of damage to the tissue [135, 138]. The damage mechanisms responsible for softening of arterial tissue are not fully understood. However, it has been speculated that softening is caused by the breaking of non-covalent cross-links resulting in slip of collagen fibres in the matrix, while failure of the fibres results in permanent deformations [135, 139].

We qualitatively analysed the force-displacement responses to describe differences in failure patterns. Most samples showed tissue softening indicating tissue damage when reaching the initial failure point. Afterwards, a gradual indentation force decrease was observed. Previous studies on plaque failure do not present the data after reaching the initial point of failure [39, 41, 42, 44, 45]. The obtained force pattern might imply gradual failure of collagen fibres. At the initial point of failure some fibres break, whereas others are able to withstand the applied load and fail later at higher indentation depths. On the other hand, earlier we showed that during indentation the main strain was perpendicular to the main collagen fibre alignment direction [100]. This suggests that the cross-links between the collagen fibres may be the first structure to mechanically fail rather than the collagen fibres themselves. The gradual failure of cross-links after initial failure may explain the gradual softening of the plaque caps.

Ultimate strength

An inverse finite element analysis was used to determine the ultimate strength of the carotid fibrous caps. Previous studies have measured the ultimate strength of aortic [39, 40, 41] and iliac [45] fibrous plaque caps by performing uni-axial ultimate tensile tests. In general, these previously reported strength values are in good agreement but show high variability, especially in the ultimate stress values (Table 6.4). Assuming isotropic Ogden material behaviour, the peak maximum principal stresses and strains

we obtained ranged from 5.2 MPa to 37.5 MPa (median 10.8 MPa) and from 0.3 to 1.0 (median 0.4), respectively. The maximum shear stresses and strains varied between 5.4 MPa-116.3 MPa ($\sigma_{VM.}$, median: 30.8 MPa) and 0.5-2.1 ($\varepsilon_{VM.}$, median: 0.8). The variability in the ultimate stress is remarkably higher than the variability in ultimate strain corresponding to previously published data. Furthermore, the ultimate stresses we obtained are considerably higher than the ultimate stress reported in literature. Possible explanations for this might be the different specimen types being measured. Since the geometry of arteries at different locations varies and arteries from various locations experience different stresses and strains, it is suggested that the mechanical properties of the arteries from different locations also vary [135, 140]. As fibrous caps develop within the arteries, this could also hold for fibrous caps. However, Mulvihill et al. (2013) [141] also tested carotid plaques obtaining in average an ultimate stress of 431 kPa.

Additionally, the different types of mechanical tests also cause differences in results. McKree et al. (2011) [142] concluded that the obtained mechanical properties for biological soft tissue depend on the used method. Previous research groups all performed ultimate uni-axial tensile tests. Using these uni-axial tensile tests, the fibrous caps were stretched in either the circumferential or axial direction with respect to the original blood vessel and the applied tensile forces were uniformly distributed along the entire sample. This way failure will always occur at the weakest location of the sample. In the current indentation setup, however, the tissue was indented locally simultaneously stretched in the circumferential and axial direction, while being compressed in the radial direction with respect to the original vessel. The stresses were applied very locally. Thus, failure of the sample will occur at the location with the highest stress, which is not necessarily the weakest location. This may explain why the ultimate stresses, obtained in the current study, were higher than the values obtained from tensile tests described in literature. The lowest stress values obtained in this study correspond to the values obtained from tensile test. Possibly in these cases the weaker locations were tested. Plaque tissue is highly heterogeneous comprising different components, such as fibrous tissue and calcification, which can behave mechanically very different. Local testing using indentation tests allow the characterisation of this heterogeneous behaviour.

Table 6.4: *Measured ultimate strength for human atherosclerotic fibrous cap tissue using ultimate tensile tests, U=ulcerated; N-U=non-ulcerated; Circum.=circumferential.*

	Vascular beds	Testing direction	Ultimate stress [MPa]	Ultimate strain [-]
Burleigh et al. (1992) [40]	Aorta	-	0-0.8	
Loree et al. (1994) [41]	Aorta	Circum.	0.5±0.2 (n=6)	0.3±0.2
Lendon et al. (1991) [39]	Aorta	Circum.	0.2±0.05 (Ulcerated, n=18)	0.5±0.1
			0.6±0.1 (Non-ulcerated, n=22)	0.3±0.04
Holzapfel et al. (2004) [45]	Iliac artery	Axial	0.5±0.1 (n=6)	1.1±0.07
		Circum.	0.3±0.0.8 (n=8)	1.2±0.1
Mulvihill et al. (2013) [141]	Carotid artery	-	0.4±0.2 (n=25)	1.8±0.3

Limitations

The samples were frozen for logistical reasons. According to Schaar et al. (2002) [96], freezing of coronary, carotid and femoral arteries at -80°C does not affect the mechanical properties. The freezing protocol applied in this study included dipping the sample in liquid nitrogen for snap freezing. This procedure is widely used to avoid ice-crystal formation. Stemper et al. (2007) [143] used uni-axial ultimate tensile tests to show that storage at -80°C for 3 months did not affect the ultimate strength of porcine aortas. Therefore, the probability of damage of the collagen fibres due to ice crystal formation, freezing and storage was minimized. Besides, the tissue was tested at room temperature rather than at 37°C, although it is unclear whether this will affect the properties of vascular tissue [96, 144].

Furthermore, in the FE analysis, the fibrous cap tissue was treated as a homogeneous, isotropic body. Clearly, plaque tissue is highly heterogeneous in composition [145] and also the fibrous cap itself is expected to be heterogeneous. Furthermore, Chai et al. (2014) [100] and Holzapfel et al. (2004) [45] showed that fibrous cap tissue is anisotropic. However, anisotropic parameters and accurate information about the cap morphology were not determined. Therefore, homogeneity and isotropic behaviour were assumed, which might have influenced the obtained values.

Chapter 7

General discussion

7.1 Overview

Atherosclerosis is a disorder of the arterial wall. One subset of atherosclerosis is the development of a so-called vulnerable plaque. Rupture of vulnerable plaques is the main cause of cardiovascular events, such as transient ischaemic attacks, ischaemic strokes, and myocardial infarctions. For diagnosis and appropriate treatment, it is crucial to predict plaque rupture reliably. Current prediction methods focus on general morphological parameters, which are not directly connected to the actual cause of plaque rupture. From a mechanical point of view, rupture occurs when mechanical stresses in the plaque exceed the strength. Therefore, stress analysis may improve current plaque rupture prediction.

A stress analysis in plaques requires computer models. The quality of these models depends strongly on the used mechanical properties, but this offers several challenges

1. Advanced atherosclerotic plaques contain a heterogeneous component distribution. This needs to be addressed by investigating the local mechanical properties of atherosclerotic plaques.
2. It is well accepted that atherosclerotic plaques behave anisotropicly, but data on anisotropic mechanical properties of plaques are very scarce.
3. Besides cap stresses, it is important to analyse the failure properties of atherosclerotic plaque caps.

The aim of this dissertation is to improve plaque modelling by providing data to fulfil the mentioned requirements. The main findings are summarised and discussed below. Future perspectives and recommendations are presented.

7.2 Main findings

7.2.1 Mechanical testing of local mechanical properties of atherosclerotic plaques

Chapter 2 presented a review on current methods to study the mechanical properties of atherosclerotic plaque tissue. In literature, different methods have been used, such as

inflation tests or tensile tests. These two methods have benefits, but they mostly focus on global mechanical properties. The small geometries of atherosclerotic plaques make it challenging to perform local measurements with inflation and tensile tests. Micro- and nano-indentation test are better suitable for local measurements. Nano-indentation, as performed by Ebenstein et al. (2009) [50], enables mechanical tests with a very high local resolution. Ebenstein et al. (2009) [50] showed that even inside single plaque components, large variations in mechanical properties occur. However, nano-indentation can only be applied at small strains. The non-linear mechanical behaviour of plaque tissue requires strains which correspond to the *in vivo* physiological situation. Micro-indentation enables the testing of different local plaque components at a physiological strain. Barrett et al. (2009) [70] conducted micro-indentation test on carotid plaques. The tests were performed in the radial direction of the blood vessel. However, Barrett et al. (2009) [70] only tested the fibrous cap. Chapter 3 describes a method, where different components of the plaque were tested. Furthermore, by combining micro-indentation with confocal imaging, it is possible to measure the anisotropic mechanical properties of plaques (chapter 4).

7.2.2 Local mechanical properties of plaques

Based on the literature review, micro-indentation was chosen as the method to investigate the local mechanical properties of atherosclerotic plaques at physiological strain (Chapter 3). The lipid-rich necrotic cores, shoulder regions as well as the middle regions of the plaque cap and remaining intima locations were indented in the axial direction. Inverse Finite Element Analysis was used to infer the mechanical properties of the plaques. Confocal imaging was used to visualise the collagen structure at each testing location.

The results (median 30 kPa, range 6 kPa and 891 kPa) corresponded to the lower range found in literature. Collagen-rich locations were stiffer than collagen poor locations. Due to the wide spread in data, no significant differences were found between middle cap locations, shoulder cap locations, and remaining intima locations. Moreover, no differences were found between the structured and unstructured collagen locations, probably because the FE model used for the inverse analysis was still based on isotropic mechanical behaviour.

7.2.3 Anisotropic mechanical properties

In chapter 4, the mechanical properties of the collagen fibres in human carotid atherosclerotic plaques were characterised by means of micro-indentation combined with inverse FE analysis and confocal imaging. Confocal imaging enabled the visualisation of collagen fibre deformation at rest and during indentation. The undeformed images were used to determine the collagen fibre main direction and the fibre distribution. The measured indentation force-response, indentation-depth and in-plane fibre displacements were used as input parameters for the inverse FE analysis to infer the collagen fibre stiffness. The values ranged from 18 kPa to 157 kPa (25th percentile and 75th percentile), which corresponds to the lower region of the range found in literature (chapter 4).

For a full characterisation of the anisotropic mechanical properties, the 3D global architecture of fibrous tissue in atherosclerotic plaques is also required. Diffusion Tensor Imaging was used to visualise the 3D structure of the fibrous tissue in human carotid plaques (Chapter 5). The obtained data were compared to data obtained from healthy carotid arteries. As shown by Ghanzanfari et al. (2012) [122], the fibres found in healthy arteries were aligned in circumferential direction. Contrary to that, all tested atherosclerotic plaques consist of at least some fibres which were aligned in the longitudinal direction. In 4 of 9 plaques, the fibres were aligned clearly in longitudinal direction forming a continuous inner layer, which was partly surrounded by a layer of fibres oriented in circumferential direction. In the other 5 plaques a partly reorganized structure was found. This indicates a major reorganisation of stresses and strains inside arteries during the progress of atherosclerosis (chapter 5).

Due to the paucity of data on anisotropic mechanical properties of atherosclerotic plaques, most of the current computer models describing plaques assume isotropic behaviour. This probable over-simplification has negative influence on the accuracy of stress results obtained from such computer models. The data provided in this dissertation enables the inclusion of anisotropic mechanical properties of atherosclerotic plaques in computer models.

7.2.4 Failure properties

Most studies on failure properties of atherosclerotic plaques use tensile tests. For such tests long slender samples need to be cut out of the plaque tissue. Next to clamping artefact, this process may damage the structural integrity of the plaque tissue, influencing the measured failure strength. Furthermore, the fibre alignment in plaques is often not taken into account during tensile tests. Indentation testing is an alternative with well-defined boundary conditions and geometry. Moreover, when using circular shaped specimen, the specifics of the fibre orientation do not influence the obtained force displacement results. In chapter 6, an indentation method was introduced to measure the failure properties of human atherosclerotic carotid plaques caps. The measured ultimate stresses (median 14.9 MPa, 25th percentile 5.6 MPa and 75th percentile 54.4 MPa) were considerably higher than the values reported in literature, possibly because of the different testing methods. The obtained ultimate strains were similar to results found in literature. A major limitation of the described indentation study is that the FE model used for the inverse analysis was still based on isotropic mechanical behaviour.

7.3 Discussion and future perspective

7.3.1 Computer modelling of plaques

One issue of plaque modelling was the assumption of isotropic mechanical behaviour of plaque tissue. The data presented in chapter 4 and 5 allow the inclusion of anisotropic mechanical properties in computer modelling of atherosclerotic plaques, which will hopefully increase the accuracy of plaque modelling. It needs to be investigated what the influence of the inclusion of anisotropic properties on stress results are. Tang et al. (2009) [52] suggested that the maximum principal stress may increase considerable if anisotropic mechanical properties are included. The inclusion of anisotropic mechanical properties of plaques may reduce the spread in data which is mostly found in literature.

The conducted literature review (chapter 2) and the studies described in this dissertation (chapter 3, 4, and 6) show that testing of mechanical properties of atherosclerotic plaque tissue generally leads to a wide spread in obtained data. The wide spread between different studies found in literature may be caused by different testing protocols (testing method, applied strain range, testing direction, storage, plaque components

classification), and testing of different vascular beds. Possible explanations for the spread within one study are patient-specific variables (age, gender, etc.) and the testing of different plaque phenotypes. Spread within one single plaque is caused by the heterogeneous components distribution. All these parameters need to be addressed and standardised measurement protocols need to be used to allow comparison between the different studies. Suggestions for appropriate tensile testing protocols are shown in Walsh et al. (2014) [38]. Furthermore, additional data characterising the mechanical properties of plaques are required for a full characterisation. Akyildiz et al. (2013) [31] suggested that an extensive database is needed covering the mechanical properties of atherosclerotic plaques with different phenotypes. The complexity indicates that plaque-specific data is required for reliable plaque rupture prediction.

However, based on the results found in literature and in this dissertation, it is clear that obtaining an extensive database characterising the mechanical properties of different plaque phenotypes will be a very laborious endeavour. Moreover, the results shown in chapter 4, where for one single plaque the Young's moduli ranged from 6 kPa to 891 kPa, suggests that this endeavour will be very challenging. This and the fact that non-invasive imaging technologies are not sufficient to visualise plaque components accurately [31, 146] indicate that computer modelling of plaque still requires more development to become a potential tool for reliable plaque rupture risk assessment.

7.3.2 Alternatives to computer modelling of plaques

A promising method for plaque-specific characterisation may be intra-vascular ultrasound (IVUS) imaging, as proposed by Baldewsing et al. [147, 148, 149, 150]. An IVUS catheter is used to acquire the spatial strain distribution of plaques. The strain is the input for inverse FE analysis to infer the local elasticity of plaques. Furthermore, if local mechanical properties and geometrical properties are not available, strain imaging may be another method to improve plaque rupture risk assessment. The results in chapter 6 suggest that the minimum ultimate strain of carotid plaque caps is 0.2 (see Figure 7.1). This may be used as threshold for strain imaging to detect stable plaques rather than trying to identify unstable plaques.

Another possibility to improve plaque rupture risk assessment may be the use of biomarkers as surrogate markers for plaque stability [151, 152]. The development

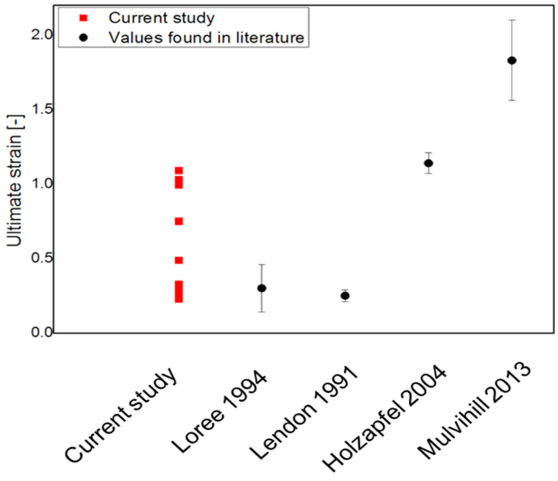

Figure 7.1: *Ultimate strain data described in chapter 6, the data correspond to data found in literature, and the minimum ultimate strain is 0.2.*

of atherosclerotic plaques and the progress into a vulnerable plaque are connected to several molecular biomarkers. The development of new molecular imaging techniques may allow the tracking of the progress of atherosclerosis. Brokopp et al. (2011) [153] showed that different plaque phenotypes are connected to different levels of Fibroblast Activation Protein. Further studies in this area may lead to the identification of biomarkers which are associated with plaque rupture and may help to improve plaque rupture risk assessment.

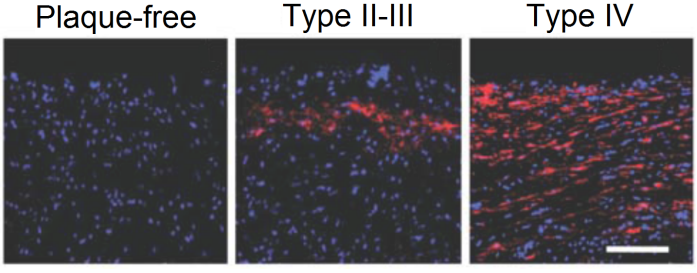

Figure 7.2: *Fibroblast activation protein expression is enhanced in plaques, scale bar = 400 µm [153]. Reprinted from Brokopp et al (2011) with permission from Oxford University Press.*

7.3.3 Plaque failure

Similar to the results on stiffness properties, determining failure properties of plaques led to a wide spread in data (chapter 6). Considerable difference was found between the data obtained from our indentation tests and the values found in literature, where mostly tensile tests were used. The different testing methods may explain the different results indicating how important the choice of testing method is. Although tensile testing and indentation both have benefits, they also have their limitations. Both techniques apply loads, not representative for the physiological situation. *In vivo* the different plaque components influence the stress distribution in an atherosclerotic plaque. The development of stress peaks may lead to plaque rupture. The lipid core size [23] and fibrous cap thickness [22] influence the plaque stress distribution. Additionally, micro-calcifications may lead to stress concentrations in a fibrous cap leading to failure of the cap [109]. Other factors, such as presence of haemorrhage [24] or the buckling of the fibrous cap [112], may also play a role. The number of parameters and their interaction influence plaque rupture risk. Thus, testing methods are required which represent the *in vivo* situation more accurately than tensile or indentation tests.

One possible approach is inflation tests combined with imaging. Boekhoven et al. (2014) [37] suggests an inflation test, where intact endarterectomy samples of carotid arteries were pressurised and imaged using ultrasound (echo-CT). Ultrasound imaging enabled the measurement of the 3D strain in the plaque, which allows the detection of calcified and lipid-rich regions. It may be possible to use inverse FE analysis to infer the mechanical properties of the plaque. This method may allow the identification of failure properties under more physiological circumstances. A potential challenge is the imaging of the rupture location to detect if failure occurred.

Another approach was proposed by Sanders et al. (2014) [154], where cap strength can be determined *ex vivo* by pressurising cross-sections of atherosclerotic plaques. Slices of plaques were placed between two plates and a viscous liquid injected into the lumen through a hole in the bottom plate pressurising the plaque.

The wide spread in failure data found in literature may be caused by the heterogeneous component distribution of atherosclerotic plaques. A method to address this is to focus on local testing. In chapter 4 a method is introduced, where the local mechanical properties of collagen fibres, the most load-bearing structures in plaques, were measured. A similar method combining mechanical testing and imaging of collagen fibres during

loading may be used to investigate the collagen fibre strength. Testing of collagen fibre strength may give a better insight into the failure mechanism of plaques.

The actual failure mechanisms of plaque rupture are unclear [155]. Studies suggest that calcium content may play a role in failure of plaques [141]. Maldonado et al. (2012, 2013) [114, 117] suggest that the presence of micro-calcifications is connected to plaque instability. Still a better understanding of plaque failure mechanism is required. A possible method may be the method used by Thambyah et al. (2012) [156], where cartilage was chemically fixed under loading condition preserving the deformed state of the tissue. The structure of the tissue was then characterised using differential interference contrast optical microscopy and scanning electron microscopy. A similar method may be used for plaque tissue and may give a better insight into plaque damage mechanisms.

7.4 Final conclusions

The aim of this dissertation was to characterise the biomechanical properties of human atherosclerotic plaques. The importance of local mechanical testing is stressed to address the heterogeneous plaque component distribution. Our results show variability in mechanical properties, which corresponds to data found in literature. It supports the idea that plaque-specific properties and modelling are required. Anisotropic mechanical properties of atherosclerotic plaques are presented which can be included in plaque modelling to potentially improve the modelling accuracy. The failure properties of plaque caps were investigated. A wide spread was found for the ultimate stresses. The ultimate strains corresponded to the values found in literature and show a smaller spread. Therefore, it is recommended to focus further research on strain imaging of plaques. Recently introduced imaging technology, such as IVUS, may improve strain imaging of plaques, which may be used as surrogate marker for plaque rupture.

Bibliography

Bibliography

[1] P. D. Richardson, "Biomechanics of plaque rupture: progress, problems, and new frontiers," *Annals of biomedical engineering* **30**(4), pp. 524–536, 2002.

[2] C. P. Bryan and G. E. Smith, *Ancient Egyptian medicine: the papyrus ebers*, Ares, 1974.

[3] A. Maton, *Human biology and health*, Prentice Hall, 1997.

[4] P. Constantinides, "Plaque fissures in human coronary thrombosis," *Journal of Atherosclerosis Research* **6**(1), pp. 1–17, 1966.

[5] W. Insull Jr, "The pathology of atherosclerosis: plaque development and plaque responses to medical treatment," *The American journal of medicine* **122**(1), pp. S3–S14, 2009.

[6] http://www.who.int/mediacentre/factsheets/fs310/en/ on 2014-09-01.

[7] P. J. Kumar and M. Clark, *Textbook of clinical medicine*, Saunders (London), 2002.

[8] T. C. Gasser, R. W. Ogden, and G. A. Holzapfel, "Hyperelastic modelling of arterial layers with distributed collagen fibre orientations," *Journal of the royal society interface* **3**(6), pp. 15–35, 2006.

[9] L. B. Goldstein, R. Adams, K. Becker, C. D. Furberg, P. B. Gorelick, G. Hademenos, M. Hill, G. Howard, V. J. Howard, B. Jacobs, *et al.*, "Primary prevention of ischemic stroke a statement for healthcare professionals from the stroke council of the american heart association," *Circulation* **103**(1), pp. 163–182, 2001.

[10] K. J. Williams and I. Tabas, "The response-to-retention hypothesis of early atherogenesis," *Arteriosclerosis, thrombosis, and vascular biology* **15**(5), pp. 551–561, 1995.

[11] J. Hulthe and B. Fagerberg, "Circulating oxidized ldl is associated with subclinical atherosclerosis development and inflammatory cytokines (air study)," *Arteriosclerosis, thrombosis, and vascular biology* **22**(7), pp. 1162–1167, 2002.

[12] D. H. Blankenhorn and H. N. Hodis, "Atherosclerosis–reversal with therapy.," *Western journal of medicine* **159**(2), p. 172, 1993.

[13] G. Sommer, *Mechanical Properties of Healthy and Diseased Human Arteries and Related Material Modeling*. PhD thesis, TU Graz, Graz, Austria, 2008.

[14] H. C. Stary, A. B. Chandler, R. E. Dinsmore, V. Fuster, S. Glagov, W. Insull, M. E. Rosenfeld, C. J. Schwartz, W. D. Wagner, and R. W. Wissler, "A definition of advanced types of atherosclerotic lesions and a histological classification of atherosclerosis a report from the committee on vascular lesions of the council on arteriosclerosis, american heart association," *Circulation* **92**(5), pp. 1355–1374, 1995.

[15] M. J. Davies and N. Woolf, "Atherosclerosis: what is it and why does it occur?," *British heart journal* **69**(1 Suppl), p. S3, 1993.

[16] J. A. Schaar, J. E. Muller, E. Falk, R. Virmani, V. Fuster, P. W. Serruys, A. Colombo, C. Stefanadis, S. W. Casscells, P. R. Moreno, *et al.*, "Terminology for high-risk and vulnerable coronary artery plaques," *European heart journal* **25**(12), pp. 1077–1082, 2004.

[17] L. H. Arroyo and R. T. Lee, "Mechanisms of plaque rupture mechanical and biologic interactions," *Cardiovascular research* **41**(2), pp. 369–375, 1999.

[18] I. J. Kullo, W. D. Edwards, and R. S. Schwartz, "Vulnerable plaque: pathobiology and clinical implications," *Annals of internal medicine* **129**(12), pp. 1050–1060, 1998.

[19] P. K. Shah, "Mechanisms of plaque vulnerability and rupture," *Journal of the American College of Cardiology* **41**(4s1), pp. S15–S22, 2003.

[20] E. Falk, P. K. Shah, and V. Fuster, "Coronary plaque disruption," *Circulation* **92**(3), pp. 657–671, 1995.

[21] P. M. Rothwell and C. P. Warlow, "Prediction of benefit from endarterectomy in individual patients: a risk-modelling study," *The Lancet* **353**, pp. 2105–2110, 1999.

[22] I. K. Jang, G. J. Tearney, B. MacNeill, M. Takano, F. Moselewski, N. Iftima, M. Shishkov, S. Houser, H. T. Aretz, E. F. Halpern, *et al.*, "In vivo characterization of coronary atherosclerotic plaque by use of optical coherence tomography," *Circulation* **111**(12), pp. 1551–1555, 2005.

[23] J. Ohayon, G. Finet, A. M. Gharib, D. A. Herzka, P. Tracqui, J. Heroux, G. Rioufol, M. S. Kotys, A. Elagha, and R. I. Pettigrew, "Necrotic core thickness and positive arterial remodeling index: emergent biomechanical factors for evaluating the risk of plaque rupture," *American journal of physiology-heart and circulatory physiology* **295**(2), pp. H717–H727, 2008.

[24] B. Chu, A. Kampschulte, M. S. Ferguson, W. S. Kerwin, V. L. Yarnykh, K. D. OBrien, N. L. Polissar, T. S. Hatsukami, and C. Yuan, "Hemorrhage in the atherosclerotic carotid plaque: a high-resolution mri study," *Stroke* **35**(5), pp. 1079–1084, 2004.

[25] F. D. Kolodgie, A. P. Burke, A. Farb, H. K. Gold, J. Yuan, J. Narula, A. V. Finn, and R. Virmani, "The thin-cap fibroatheroma: a type of vulnerable plaque: the major precursor lesion to acute coronary syndromes," *Current opinion in cardiology* **16**(5), pp. 285–292, 2001.

[26] R. Virmani, A. P. Burke, F. D. Kolodgie, and A. Farb, "Vulnerable plaque: the pathology of unstable coronary lesions," *Journal of interventional cardiology* **15**(6), pp. 439–446, 2002.

[27] R. Virmani, A. P. Burke, F. D. Kolodgie, and A. Farb, "Pathology of the thin-cap fibroatheroma," *Journal of interventional cardiology* **16**(3), pp. 267–272, 2003.

[28] R. Virmani, A. P. Burke, A. Farb, and F. D. Kolodgie, "Pathology of the vulnerable plaque," *Journal of the American College of Cardiology* **47**(8s1), pp. C13–C18, 2006.

[29] G. C. Cheng, H. M. Loree, R. D. Kamm, M. C. Fishbein, and R. T. Lee, "Distribution of circumferential stress in ruptured and stable atherosclerotic lesions a structural analysis with histopathological correlation," *Circulation* **87**, pp. 1179–1187, 1993.

[30] P. D. Richardson, M. J. Davies, and G. V. R. Born, "Influence of plaque configuration and stress distribution on fissuring of coronary atherosclerotic plaques," *The Lancet* **334**(8669), pp. 941–944, 1989.

[31] A. C. Akyildiz, *Biomechanical Modeling of Atherosclerotic plaques for risk assessment*. PhD thesis, Erasmus MC, Rotterdam, The Netherlands, 2013.

[32] V. Pazos, *Characterization of non-linear material parameters of atherosclerotic arteries using numerical and experimental models*. PhD thesis, McGill University, Montreal, Canada, 2009.

[33] L. Speelman, A. C. Akyildiz, B. Den Adel, J. J. Wentzel, A. F. W. van der Steen, R. Virmani, L. van der Weerd, J. W. Jukema, R. E. Poelmann, E. H. van Brummelen, *et al.*, "Initial stress in biomechanical models of atherosclerotic plaques," *Journal of biomechanics* **44**(13), pp. 2376–2382, 2011.

[34] J. Ohayon, P. Teppaz, G. Finet, and G. Rioufol, "In-vivo prediction of human coronary plaque rupture location using intravascular ultrasound and the finite element method," *Coronary artery disease* **12**(8), pp. 655–663, 2001.

[35] H. M. Loree, R. D. Kamm, R. G. Stringfellow, and R. T. Lee, "Effects of fibrous cap thickness on peak circumferential stress in model atherosclerotic vessels.," *Circulation Research* **71**(4), pp. 850–858, 1992.

[36] G. Finet, J. Ohayon, and G. Rioufol, "Biomechanical interaction between cap thickness, lipid core composition and blood pressure in vulnerable coronary plaque: impact on stability or instability," *Coronary Artery Disease* **15**, pp. 13–20, 2004.

[37] R. W. Boekhoven, M. Rutten, M. R. van Sambeek, F. N. van de Vosse, and R. G. P. Lopata, "Towards mechanical characterization of intact endarterectomy samples of carotid arteries during inflation using echo-ct," *Journal of biomechanics* **47**(4), pp. 805–814, 2014.

[38] M. T. Walsh, E. M. Cunnane, J. J. Mulvihill, A. C. Akyildiz, F. J. H. Gijsen, and G. A. Holzapfel, "Uniaxial tensile testing approaches for characterisation of atherosclerotic plaques," *Journal of Biomechanics* **47**, pp. 793–804, 2014.

[39] C. L. Lendon, M. J. Davies, G. V. R. Born, and P. D. Richardson, "Atherosclerotic plaque caps are locally weakened when macrophages density is increased," *Atherosclerosis* **87**(1), pp. 87–90, 1991.

[40] M. C. Burleigh, A. D. Briggs, C. L. Lendon, M. J. Davies, G. V. R. Born, and P. D. Richardson, "Collagen type i and iii, collagen content, gags and me-

chanical strength of human atherosclerotic plaque caps: span-wise variations," *Atherosclerosis* **96**, pp. 71–81, 1992.

[41] H. M. Loree, A. J. Grodzinsky, S. Y. Park, L. J. Gibson, and R. T. Lee, "Static circumferential tangential modulus of human atherosclerotic tissue," *J Biomech* **27 (2)**, pp. 195–204, 1994.

[42] E. Maher, A. Creane, S. Sultan, N. Hynes, C. Lally, and D. J. Kelly, "Tensile and compressive properties of fresh human carotid atherosclerotic plaques," *Journal of biomechanics* **42**(16), pp. 2760–2767, 2009.

[43] E. Maher, A. Creane, S. Sultan, N. Hynes, C. Lally, and D. J. Kelly, "Inelasticity of human carotid atherosclerotic plaque," *Annals of biomedical engineering* **39**(9), pp. 2445–2455, 2011.

[44] M. G. Lawlor, M. R. O'Donnell, B. M. O'Connell, and M. T. Walsh, "Experimental determination of circumferential properties of fresh carotid artery plaques," *Journal of biomechanics* **44**(9), pp. 1709–1715, 2011.

[45] G. A. Holzapfel, G. Sommer, and P. Regitnig, "Anisotropic mechanical properties of tissue components in human atherosclerotic plaques," *Transactions of the ASME-K-Journal of Biomechanical Engineering* **126**(5), pp. 657–665, 2004.

[46] Z. Teng, D. Tang, J. Zheng, P. K. Woodard, and A. H. Hoffman, "An experimental study on the ultimate strength of the adventitia and media of human atherosclerotic carotid arteries in circumferential and axial directions," *Journal of biomechanics* **42**(15), pp. 2535–2539, 2009.

[47] J. Tong, G. Sommer, P. Regitnig, and G. A. Holzapfel, "Dissection properties and mechanical strength of tissue components in human carotid bifurcations," *Annals of biomedical engineering* **39**(6), pp. 1703–1719, 2011.

[48] Y. Wang, J. A. Johnson, F. G. Spinale, M. A. Sutton, and S. M. Lessner, "Quantitative measurement of dissection resistance in intimal and medial layers of human coronary arteries," *Experimental mechanics* **54**(4), pp. 677–683, 2014.

[49] A. C. Akyildiz, L. Speelman, and F. J. H. Gijsen, "Mechanical properties of human atherosclerotic intima tissue," *Journal of Biomechanics* **47**(0), pp. 773–783, 2014.

[50] D. M. Ebenstein, D. Coughlin, J. Chapman, C. Li, and L. A. Pruitt, "Nanomechanical properties of calcification, fibrous tissue, and hematoma from atherosclerotic plaques," *Journal of Biomedical Materials Research Part A* **91**(4), pp. 1028–1037, 2009.

[51] D. M. Ebenstein, J. M. Chapman, L. Li, D. Saloner, J. Rapp, and L. A. Pruitt, "Assessing structure-property relations of diseased tissues using nanoindentation and ftir.," *In: Moss, S., (Ed.), Advanced biomaterials: Characterization, tissue engineering, and complexity* **Symposium, Boston: Mat. Res. Soc.**, pp. 47–52, 2002.

[52] D. Tang, Z. Teng, G. Canton, T. S. Hatsukami, L. Dong, X. Huang, C. Yuan, *et al.*, "Local critical stress correlates better than global maximum stress with plaque morphological features linked to atherosclerotic plaque vulnerability: an in vivo multi-patient study," *Biomed Eng Online* **8**, p. 15, 2009.

[53] H. C. Stary, D. H. Blankenhorn, A. B. Chandler, S. Glagov, W. Insull Jr, M. Richardson, M. E. Rosenfeld, S. A. Schaffer, C. J. Schwartz, and W. D. Wagner, "A definition of the intima of human arteries and of its atherosclerosis-prone regions. a report from the committee on vascular lesions of the council on arteriosclerosis, american heart association.," *Circulation* **85**(1), p. 391, 1992.

[54] K. Sakakura, M. Nakano, F. Otsuka, E. Ladich, F. D. Kolodgie, and R. Virmani, "Pathophysiology of atherosclerosis plaque progression," *Heart, Lung and Circulation* **22**, pp. 399–411, 2013.

[55] M. Naghavi, *Asymptomatic Atherosclerosis: Pathophysiology, Detection and Treatment*, Springer, 2010.

[56] U. Sadat, Z. Teng, V. E. Young, Z. Y. Li, and J. H. Gillard, "Utility of magnetic resonance imaging-based finite element analysis for the biomechanical stress analysis of hemorrhagic and non-hemorrhagic carotid plaques.," *Circulation journal: official journal of the Japanese Circulation Society* **75**(4), p. 884, 2011.

[57] N. V. Salunke and L. D. Topoleski, "Biomechanics of atherosclerotic plaque.," *Critical reviews in biomedical engineering* **25**(3), pp. 243–285, 1996.

[58] H. A. Nieuwstadt, T. R. Geraedts, M. T. B. Truijman, M. E. Kooi, A. Lugt, A. F. W. Steen, J. J. Wentzel, M. Breeuwer, and F. J. H. Gijsen, "Numerical simulations of carotid mri quantify the accuracy in measuring atherosclerotic

plaque components in vivo," *Magnetic Resonance in Medicine* **72**, pp. 188–201, 2013.

[59] H. M. Loree, B. J. Tobias, L. J. Gibson, R. D. Kamm, D. M. Small, and R. T. Lee, "Mechanical properties of model atherosclerotic lesion lipid pools," *Arterioscler Thromb Vasc Biol* **14**, pp. 230–234, 1994.

[60] A. C. Akyildiz, L. Speelman, H. van Brummelen, M. A. Gutiérrez, R. Virmani, A. van der Lugt, A. F. W. van der Steen, J. J. Wentzel, and F. J. H. Gijsen, "Effects of intima stiffness and plaque morphology on peak cap stress," *BioMedical Engineering OnLine* **10**, pp. 1–13, 2011.

[61] J. H. Gillard, "Advances in atheroma imaging in the carotid," *Cerebrovascular Diseases* **24**(Suppl. 1), pp. 40–48, 2007.

[62] D. Tang, C. Yang, J. Zheng, P. K. Woodrad, J. E. Saffiz, G. A. Sicard, T. K. Pilgram, and C. Yuan, "Quantifying effects of plaque structure and material properties on stress distributions in human atherosclerotic plaques using 3d fsi models," *J Biomech Eng* **127**(7), pp. 1185–1194, 2005.

[63] S. D. Williamson, Y. Lam, H. F. Younis, H. Huang, S. Patel, M. R. Kaazempur-Mofrad, and R. D. Kamm, "On the sensitivity of wall stresses in diseased arteries to variable material properties.," *Journal of biomechanical engineering* **125**(1), pp. 147–155, 2003.

[64] R. T. Lee, A. J. Grodzinsky, E. H. Frank, R. D. Kamm, and F. J. Schoen, "Structure-dependent dynamic mechanical behavior of fibrous caps from human atherosclerotic plaques.," *Circulation* **83 (5)**, pp. 1764–1770, 1991.

[65] R. T. Lee, S. G. Richardson, H. M. Loree, A. J. Grodzinsky, S. A. Gharib, F. J. Schoen, and N. Pandian, "Prediction of mechanical properties of human atherosclerotic tissue by high-frequency intravascular ultrasound imaging an in vitro study.," *Arterioscler Thromb Vasc Biol* **12**, pp. 1–5, 1992.

[66] J. Walraevens, B. Willaert, G. De Win, A. Ranftl, J. De Schutter, and J. V. Sloten, "Correlation between compression, tensile and tearing tests on healthy and calcified aortic tissues," *Medical engineering & physics* **30**(9), pp. 1098–1104, 2008.

[67] L. D. T. Topoleski, N. V. Salunke, J. D. Humphrey, and W. J. Mergner, "Composition-and history-dependent radial compressive behavior of human

atherosclerotic plaque," *Journal of biomedical materials research* **35**(1), pp. 117–127, 1997.

[68] L. D. T. Topoleski and N. V. Salunke, "Mechanical behavior of calcified plaques: a summary of compression and stress-relaxation experiments," *Zeitschrift für Kardiologie* **89**(2), pp. S085–S091, 2000.

[69] N. V. Salunke, L. D. T. Topoleski, J. D. Humphrey, and W. J. Mergner, "Compressive stress-relaxation of human atherosclerotic plaque," *Journal of biomedical materials research* **55**(2), pp. 236–241, 2001.

[70] S. R. H. Barrett, M. P. F. Sutcliffe, S. Howarth, Z.-Y. Li, and J. H. Gillard, "Experimental measurement of the mechanical properties of carotid atherothrombotic plaque fibrous cap," *J. Biomech.* **42**, pp. 1650–1655, 2009.

[71] C.-K. Chai, A. C. Akyildiz, L. Speelman, F. J. H. Gijsen, C. W. J. Oomens, M. R. H. M. van Sambeek, A. van der Lugt, and F. P. T. Baaijens, "Local axial compressive mechanical properties of human carotid atherosclerotic plaques-characterisation by indentation test and inverse finite element analysis," *Journal of Biomechanics* **46**, pp. 1759–1766, 2013.

[72] H. N. Hayenga, A. Trache, J. Trzeciakowski, and J. D. Humphrey, "Regional atherosclerotic plaque properties in apoe-/- mice quantified by atomic force, immunofluorescence, and light microscopy.," *J. Vasc. Res.* **48**, pp. 495–504, 2011.

[73] P. Tracqui, A. Broisat, J. Toczek, N. Mesnier, J. Ohayon, and L. Riou, "Mapping elasticity moduli of atherosclerotic plaque in situ via atomic force microscopy," *Journal of Structured Biology* **174 (1)**, pp. 115–123, 2011.

[74] V. Vaenkatesan, Z. L. Li, and W. P. Vellinga, "Adhesion and friction behaviours of polydimethylsiloxane-a fresh perspective on jkr measurements," *Polymer* **47 (25)**, pp. 8317–8325, 2006.

[75] M. A. J. Cox, N. J. B. Driessen, R. A. Boerbom, C. V. C. Bouten, and F. P. T. Baaijens, "Mechanical characterization of anisotropic planar biological soft tissues using finite indentation: experimental feasibility," *J. Biomech.* **41**, pp. 422–429, 2008.

[76] M. A. J. Cox, N. J. B. Driessen, C. V. C. Bouten, and F. P. T. Baaijens, "Mechanical characterization of anisotropic planar biological soft tissues using

large indentation: A computational feasibility study," *J. Biomech. Eng.* **128**, pp. 428–436, 2006.

[77] M. A. J. Cox, J. Kortsmit, N. J. B. Driessen, C. V. C. Bouten, and F. P. T. Baaijens, "Tissue-engineered heart valves develop native-like collagen fiber architecture," *Tissue Engineering: Part A* **16 (5)**, pp. 1527–1537, 2010.

[78] K. Nash-Krahn, C. V. C. Bouten, S. van Tuijl, M. A. M. J. van Zandvoort, and M. Merkx, "Fluorescently labeled collagen binding proteins allow specific visualization of collagen in tissues and live cell culture," *Anal Biochem* **350**, pp. 177–185, 2006.

[79] N. J. B. Driessen, M. A. J. Cox, C. V. C. Bouten, and F. P. T. Baaijens, "Remodelling of the angular collagen fiber distribution in cardiovascular tissues," *Biomechanics and modeling in mechanobiology* **7**(2), pp. 93–103, 2008.

[80] G. A. Holzapfel, T. C. Gasser, and R. W. Ogden, "A new constitutive framework for arterial wall mechanics and a comparative study of material models," *Journal of elasticity and the physical science of solids* **61**(1-3), pp. 1–48, 2000.

[81] M. H. H. Meuwissen, C. W. J. Oomens, F. P. T. Baaijens, R. Petterson, and J. D. Janssen, "Determination of the elasto-plastic properties of aluminium using a mixed numerical–experimental method," *Journal of Materials Processing Technology* **75**(1), pp. 204–211, 1998.

[82] C. A. Schulze-Bauer, C. Morth, and G. A. Holzapfel, "Passive biaxial mechanical response of aged human iliac arteries.," *Journal of biomechanical engineering* **125**(3), pp. 395–406, 2003.

[83] J. D. Humphrey, J. F. Eberth, W. W. Dye, and R. L. Gleason, "Fundamental role of axial stress in compensatory adaptations by arteries," *Journal of biomechanics* **42**(1), pp. 1–8, 2009.

[84] A. van der Horst, C. N. van den Broek, F. N. van de Vosse, and M. C. M. Rutten, "The fiber orientation in the coronary arterial wall at physiological loading evaluated with a two-fiber constitutive model," *Biomechanics and modeling in mechanobiology* **11**(3-4), pp. 533–542, 2012.

[85] N. V. Salunke and L. D. T. Topoleski, "Biomechanics of atherosclerotic plaque," *Critical Reviews in Biomedical Engineering* **25 (3)**, pp. 243–285, 1997.

[86] R. A. Boerboom, K. Nash-Krahn, R. T. A. Megens, M. A. M. J. van Zandvoort, M. Merkx, and C. V. C. Bouten, "High resolution imaging of collagen organisation and synthesis using a versatile collagen specific probe," *Journal of Structural Biology* **159**, pp. 392–399, 2007.

[87] M. A. J. Cox, N. J. B. Driessen, C. V. C. Bouten, and F. P. T. Baaijens, "Mechanical characterization of anisotropic planar biological soft tissues using large indentation: An experimental validation study," *In H. Rodrigues, M. Cerrolaza, M. Doblare, J. Ambrosio, and M. Viceconti, editors* **Proceedings of ICCB 2005, Lisbon, Portugal**, pp. 339–350, 2005.

[88] L. H. Timmins, Q. Wu, A. T. Yeh, J. E. Moore, and S. E. Greenswald, "Structural inhomogeneity and fiber orientation in the inner arterial media," *Am J Physiol Heart Circ Physiol* **298**, pp. 1537–1545, 2010.

[89] C. P. Ng and M. A. Swartz, "Mechanisms of interstitial flow-induced remodeling of fibroblast-collagen cultures," *Annals of Biomedical Engineering* **34**, pp. 446–454, 2006.

[90] D. Beattie, C. Xu, R. Vito, S. Glagov, and M. C. Whang, "Mechanical analysis of heterogeneous, atherosclerotic human aorta," *J. Biomech. Eng.* **120**, pp. 602–607, 1998.

[91] C. L. de Korte, G. Pasterkamp, A. F. W. van der Steen, H. A. Woutman, and N. Bom, "Characterization of plaque components with intravascular ultrasound elastography in human femoral and coronary arteries in vitro," *Circulation* **102**, pp. 617–623, 2000.

[92] H. Kanai, H. Hasegawa, M. Ichiki, F. Tezuka, and Y. Koiwa, "Elasticity imaging of atheroma with transcutaneous ultrasound: Preliminary study," *Circulation* **107**, pp. 3018–3021, 2003.

[93] M. T. Dirksen, A. C. van der Waal, F. M. van den Berg, C. M. van der Loos, and A. E. Becker, "Distribution of inflammatory cells in atherosclerotic plaques relates to the direction of flow," *Circulation* **98**, pp. 2000–2003, 1998.

[94] C. J. Slager, J. J. Wentzel, F. J. H. Gijsen, A. Thury, A. C. van der Wal, J. A. Schaar, and P. W. Serruys, "The role of shear stress in the stabilization of vulnerable plaques and related therapeutic implications," *Nat Clin Pract Cardiovasc Med* **2**, pp. 456–464, 2005.

[95] F. J. H. Gijsen, J. J. Wentzel, A. Thury, F. Mastik, J. A. Schaar, J. C. H. Schuursbiers, C. J. Slager, W. J. van der Giessen, P. J. de Feyter, A. F. W. van der Steen, and P. W. Serruys, "Strain distribution over plaques in human coronary arteries relates to shear stress," *Am J Physiol* **295**, pp. H1608–H1614, 2008.

[96] J. A. Schaar, C. L. de Korte, F. Mastik, and A. F. W. van der Steen, "Effect of temperature and freezing on intravascular elastography," *Ultrasonics* **40**, pp. 879–881, 2002.

[97] A. Hemmasizadeh, K. Darvish, and M. Autieri, "Characterization of changes to the mechanical properties of arteries due to cold storage using nanoindentation tests," *Annals of Biomedical Engineering* **40**, pp. 1434–1442, 2012.

[98] C. Yuan, S. Zhang, N. L. Polissar, D. Echelard, G. Ortiz, J. W. Davis, E. Ellington, M. S. Ferguson, and T. S. Hatsukami, "Identification of fibrous cap rupture with magnetic resonance imaging is highly associated with recent transient ischemic attack or stroke," *Circulation* **105**(2), pp. 181–185, 2002.

[99] F. Tavora, N. Cresswell, L. Li, D. Fowler, and A. Burke, "Frequency of acute plaque ruptures and thin cap atheromas at sites of maximal stenosis," *Arquivos Brasileiros de Cardiologia* **94**(2), pp. 153–159, 2010.

[100] C.-K. Chai, L. Speelman, C. W. J. Oomens, and F. P. T. Baaijens, "Compressive mechanical properties of atherosclerotic plaques–indentation test to characterise the local anisotropic behaviour," *Journal of Biomechanics* **47**, pp. 784–792, 2014.

[101] T. C. Gasser and G. A. Holzapfel, "Modeling the propagation of arterial dissection," *European Journal of Mechanics-A/Solids* **25**(4), pp. 617–633, 2006.

[102] M. G. D. Geers, R. De Borst, and W. A. M. Brekelmans, "Computing strain fields from discrete displacement fields in 2d-solids," *International Journal of Solids and Structures* **33**(29), pp. 4293–4307, 1996.

[103] X.-Z. Huang, Z.-Y. Wang, X.-H. Dai, M. Zhang, *et al.*, "Velocity vector imaging of longitudinal mechanical properties of upstream and downstream shoulders and fibrous cap tops of human carotid atherosclerotic plaque," *Echocardiography* **30**(2), pp. 211–218, 2013.

[104] L. Cardoso and S. Weinbaum, "Changing views of the biomechanics of vulnerable plaque rupture: A review," *Annals of biomedical engineering* **42**, pp. 1–17, 2013.

[105] A. Versluis, A. J. Bank, and W. H. Douglas, "Fatigue and plaque rupture in myocardial infarction," *Journal of biomechanics* **39**(2), pp. 339–347, 2006.

[106] M. Kaartinen, A. Penttilä, and P. T. Kovanen, "Accumulation of activated mast cells in the shoulder region of human coronary atheroma, the predilection site of atheromatous rupture.," *Circulation* **90**(4), pp. 1669–1678, 1994.

[107] G. K. Sukhova, U. Schonbeck, E. Rabkin, F. J. Schoen, A. R. Poole, R. C. Billinghurst, and P. Libby, "Evidence for increased collagenolysis by interstitial collagenases-1 and-3 in vulnerable human atheromatous plaques," *Circulation* **99**(19), pp. 2503–2509, 1999.

[108] R. K. Kumar and K. R. Balakrishnan, "Influence of lumen shape and vessel geometry on plaque stresses: possible role in the increased vulnerability of a remodelled vessel and the 'shoulder' of a plaque," *Heart* **91**(11), pp. 1459–1465, 2005.

[109] Y. Vengrenyuk, S. Carlier, S. Xanthos, L. Cardoso, P. Ganatos, R. Virmani, S. Einav, L. Gilchrist, and S. Weinbaum, "A hypothesis for vulnerable plaque rupture due to stress-induced debonding around cellular microcalcifications in thin fibrous caps," *Proceedings of the National Academy of Sciences* **103**(40), pp. 14678–14683, 2006.

[110] F. D. Kolodgie, J. Narula, A. P. Burke, N. Haider, A. Farb, Y. Hui-Liang, J. Smialek, and R. Virmani, "Localization of apoptotic macrophages at the site of plaque rupture in sudden coronary death," *The American journal of pathology* **157**(4), pp. 1259–1268, 2000.

[111] A. P. Burke, A. Farb, G. T. Malcom, Y. Liang, J. E. Smialek, and R. Virmani, "Plaque rupture and sudden death related to exertion in men with coronary artery disease," *JAMA: the journal of the American Medical Association* **281**(10), pp. 921–926, 1999.

[112] M. Abdelali, S. Reiter, R. Mongrain, M. Bertrand, P. L. LAllier, E. A. Kritikou, and J.-C. Tardif, "Cap buckling as a potential mechanism of atherosclerotic plaque vulnerability," *Journal of the Mechanical Behavior of Biomedical Materials* **32**, pp. 210–224, 2014.

[113] Y. Vengrenyuk, L. Cardoso, and S. Weinbaum, "Micro-ct based analysis of a new paradigm for vulnerable plaque rupture: cellular microcalcifications in fibrous caps," *Molecular and Cellular Biomechanics* **5**(1), p. 37, 2008.

[114] N. Maldonado, A. Kelly-Arnold, Y. Vengrenyuk, D. Laudier, J. T. Fallon, R. Virmani, L. Cardoso, and S. Weinbaum, "A mechanistic analysis of the role of microcalcifications in atherosclerotic plaque stability: potential implications for plaque rupture," *American Journal of Physiology-Heart and Circulatory Physiology* **303**(5), pp. H619–H628, 2012.

[115] S. H. Rambhia, X. Liang, M. Xenos, Y. Alemu, N. Maldonado, A. Kelly, S. Chakraborti, S. Weinbaum, L. Cardoso, S. Einav, *et al.*, "Microcalcifications increase coronary vulnerable plaque rupture potential: a patient-based micro-ct fluid–structure interaction study," *Annals of biomedical engineering* **40**(7), pp. 1443–1454, 2012.

[116] A. Kelly-Arnold, N. Maldonado, D. Laudier, E. Aikawa, L. Cardoso, and S. Weinbaum, "Revised microcalcification hypothesis for fibrous cap rupture in human coronary arteries," *Proceedings of the National Academy of Sciences* **110**(26), pp. 10741–10746, 2013.

[117] N. Maldonado, A. Kelly-Arnold, L. Cardoso, and S. Weinbaum, "The explosive growth of small voids in vulnerable cap rupture; cavitation and interfacial debonding," *Journal of biomechanics* **46**(2), pp. 396–401, 2013.

[118] P. B. Dobrin, T. H. Schwarcz, and R. Mrkvicka, "Longitudinal retractive force in pressurized dog and human arteries," *Journal of Surgical Research* **48**(2), pp. 116–120, 1990.

[119] L. Cardamone, A. Valentin, J. F. Eberth, and J. D. Humphrey, "Origin of axial prestretch and residual stress in arteries," *Biomechanics and modeling in mechanobiology* **8**(6), pp. 431–446, 2009.

[120] L. Robert, A. M. Robert, and B. Jacotot, "Elastin–elastase–atherosclerosis revisited," *Atherosclerosis* **140**(2), pp. 281–295, 1998.

[121] C. Yang, R. G. Bach, J. Zheng, I. Ei Naqa, P. K. Woodard, Z. Teng, K. Billiar, and D. Tang, "In vivo ivus-based 3-d fluid–structure interaction models with cyclic bending and anisotropic vessel properties for human atherosclerotic coronary plaque mechanical analysis," *Biomedical Engineering, IEEE Transactions on* **56**(10), pp. 2420–2428, 2009.

[122] S. Ghazanfari, A. Driessen-Mol, G. J. Strijkers, F. M. W. Kanters, F. P. T. Baaijens, and C. V. C. Bouten, "A comparative analysis of the collagen architecture in the carotid artery: Second harmonic generation versus diffusion tensor imaging," *Biochemical and biophysical research communications* **426**(1), pp. 54–58, 2012.

[123] A. Vilanova, S. Zhang, G. Kindlmann, and D. Laidlaw, "An introduction to visualization of diffusion tensor imaging and its applications," in *Visualization and Processing of Tensor Fields*, pp. 121–153, Springer, 2006.

[124] S. Mori and J. Zhang, "Principles of diffusion tensor imaging and its applications to basic neuroscience research," *Neuron* **51**(5), pp. 527–539, 2006.

[125] M. McCormick, T. Varghese, X. Wang, C. Mitchell, M. A. Kliewer, and R. J. Dempsey, "Methods for robust in vivo strain estimation in the carotid artery," *Physics in medicine and biology* **57**(22), p. 7329, 2012.

[126] M. Cinthio, Å. R. Ahlgren, J. Bergkvist, T. Jansson, H. W. Persson, and K. Lindström, "Longitudinal movements and resulting shear strain of the arterial wall," *American Journal of Physiology-Heart and Circulatory Physiology* **291**(1), pp. H394–H402, 2006.

[127] F. Baaijens, C. Bouten, and N. Driessen, "Modeling collagen remodeling," *Journal of biomechanics* **43**(1), pp. 166–175, 2010.

[128] N. J. B. Driessen, W. Wilson, C. V. C. Bouten, and F. P. T. Baaijens, "A computational model for collagen fibre remodelling in the arterial wall," *Journal of theoretical biology* **226**(1), pp. 53–64, 2004.

[129] N. J. B. Driessen, G. W. M. Peters, J. M. Huyghe, C. V. C. Bouten, and F. P. T. Baaijens, "Remodelling of continuously distributed collagen fibres in soft connective tissues," *Journal of biomechanics* **36**(8), pp. 1151–1158, 2003.

[130] J.-O. Deguchi, E. Aikawa, P. Libby, J. R. Vachon, M. Inada, S. M. Krane, P. Whittaker, and M. Aikawa, "Matrix metalloproteinase-13/collagenase-3 deletion promotes collagen accumulation and organization in mouse atherosclerotic plaques," *Circulation* **112**(17), pp. 2708–2715, 2005.

[131] A. V. Finn, M. Nakano, J. Narula, F. D. Kolodgie, and R. Virmani, "Concept of vulnerable/unstable plaque," *Arteriosclerosis, Thrombosis, and Vascular Biology* **30**(7), pp. 1282–1292, 2010.

[132] R. W. Ogden, "Large deformation isotropic elasticity-on the correlation of theory and experiment for incompressible rubberlike solids," *Proceedings of the Royal Society of London. A. Mathematical and Physical Sciences* **326**(1567), pp. 565–584, 1972.

[133] Z.-Y. Li, S. Howarth, T. Tang, M. Graves, J. H. Gillard, *et al.*, "Does calcium deposition play a role in the stability of atheroma? location may be the key," *Cerebrovascular diseases* **24**(5), pp. 452–459, 2007.

[134] Z.-Y. Li, T. Tang, J. U-King-Im, M. Graves, M. Sutcliffe, and J. H. Gillard, "Assessment of carotid plaque vulnerability using structural and geometrical determinants," *Circulation Journal* **72**(7), pp. 1092–1099, 2008.

[135] E. Maher, M. Early, A. Creane, C. Lally, and D. J. Kelly, "Site specific inelasticity of arterial tissue," *Journal of biomechanics* **45**(8), pp. 1393–1399, 2012.

[136] A. Garcia, M. Martinez, and E. Pena, "Determination and modeling of the inelasticity over the length of the porcine carotid artery," *Journal of biomechanical engineering* **135**(3), p. 031004, 2013.

[137] H. Weisbecker, D. M. Pierce, P. Regitnig, and G. A. Holzapfel, "Layer-specific damage experiments and modeling of human thoracic and abdominal aortas with non-atherosclerotic intimal thickening," *Journal of the mechanical behavior of biomedical materials* **12**, pp. 93–106, 2012.

[138] E. Pena, V. Alastrue, A. Laborda, M. A. Martinez, and M. Doblare, "A constitutive formulation of vascular tissue mechanics including viscoelasticity and softening behaviour," *Journal of biomechanics* **43**(5), pp. 984–989, 2010.

[139] T. C. Gasser and G. A. Holzapfel, "A rate-independent elastoplastic constitutive model for biological fiber-reinforced composites at finite strains: continuum basis, algorithmic formulation and finite element implementation," *Computational Mechanics* **29**(4-5), pp. 340–360, 2002.

[140] F. H. Silver, P. B. Snowhill, and D. J. Foran, "Mechanical behavior of vessel wall: a comparative study of aorta, vena cava, and carotid artery," *Annals of Biomedical Engineering* **31**(7), pp. 793–803, 2003.

[141] J. J. Mulvihill, E. M. Cunnane, S. M. McHugh, E. G. Kavanagh, S. R. Walsh, and M. T. Walsh, "Mechanical, biological and structural characterization of in vitro

ruptured human carotid plaque tissue," *Acta biomaterialia* **9**(11), pp. 9027–9035, 2013.

[142] C. T. McKee, J. A. Last, P. Russell, and C. J. Murphy, "Indentation versus tensile measurements of young's modulus for soft biological tissues," *Tissue Engineering Part B: Reviews* **17**(3), pp. 155–164, 2011.

[143] B. D. Stemper, N. Yoganandan, M. R. Stineman, T. A. Gennarelli, J. L. Baisden, and F. A. Pintar, "Mechanics of fresh, refrigerated, and frozen arterial tissue," *Journal of Surgical Research* **139**(2), pp. 236–242, 2007.

[144] G. V. Guinea, J. M. Atienza, M. Elices, P. Aragoncillo, and K. Hayashi, "Thermomechanical behavior of human carotid arteries in the passive state," *American Journal of Physiology-Heart and Circulatory Physiology* **288**(6), pp. H2940–H2945, 2005.

[145] R. Virmani, F. D. Kolodgie, A. P. Burke, A. Farb, and S. M. Schwartz, "Lessons from sudden coronary death a comprehensive morphological classification scheme for atherosclerotic lesions," *Arteriosclerosis, thrombosis, and vascular biology* **20**(5), pp. 1262–1275, 2000.

[146] H. A. Nieuwstadt, L. Speelman, M. Breeuwer, A. van der Lugt, A. F. W. van der Steen, J. J. Wentzel, and F. J. H. Gijsen, "The influence of inaccuracies in carotid mri segmentation on atherosclerotic plaque stress computations," *Journal of biomechanical engineering* **136**(2), p. 021015, 2014.

[147] R. A. Baldewsing, J. A. Schaar, C. L. de Korte, F. Mastik, P. W. Serruys, and A. F. van der Steen, "Intravascular ultrasound elastography: A clinician's tool for assessing vulnerability and material composition of plaques.," *Studies in health technology and informatics* **113**, pp. 75–96, 2004.

[148] R. A. Baldewsing, J. A. Schaar, F. Mastik, C. W. J. Oomens, and A. F. W. van der Steen, "Assessment of vulnerable plaque composition by matching the deformation of a parametric plaque model to measured plaque deformation," *Medical Imaging, IEEE Transactions on* **24**(4), pp. 514–528, 2005.

[149] R. A. Baldewsing, F. Mastik, J. A. Schaar, P. W. Serruys, and A. F. W. van der Steen, "Youngs modulus reconstruction of vulnerable atherosclerotic plaque components using deformable curves," *IEEE Ultrasonics Symposium* **32**(2), pp. 201–210, 2006.

[150] R. A. Baldewsing, M. G. Danilouchkine, F. Mastik, J. A. Schaar, P. W. Serruys, and A. F. W. van der Steen, "An inverse method for imaging the local elasticity of atherosclerotic coronary plaques," *Information Technology in Biomedicine, IEEE Transactions on* **12**(3), pp. 277–289, 2008.

[151] W. Koenig and N. Khuseyinova, "Biomarkers of atherosclerotic plaque instability and rupture," *Arteriosclerosis, thrombosis, and vascular biology* **27**(1), pp. 15–26, 2007.

[152] M. Wildgruber, F. K. Swirski, and A. Zernecke, "Molecular imaging of inflammation in atherosclerosis," *Theranostics* **3**(11), p. 865, 2013.

[153] C. E. Brokopp, R. Schoenauer, P. Richards, S. Bauer, C. Lohmann, M. Y. Emmert, B. Weber, S. Winnik, E. Aikawa, K. Graves, *et al.*, "Fibroblast activation protein is induced by inflammation and degrades type i collagen in thin-cap fibroatheromata," *European heart journal* **32**, pp. 2713–2722, 2011.

[154] S. N. Sanders, F. N. van de Vosse, and M. C. M. Rutten, "Rupture risk assessment for carotid plaques." Poster at Reseach Day, 2014. Eindhoven University of Technology.

[155] T. C. Gasser and G. A. Holzapfel, "Modeling plaque fissuring and dissection during balloon angioplasty intervention," *Annals of Biomedical Engineering* **35**(5), pp. 711–723, 2007.

[156] A. Thambyah, G. Zhang, W. Kim, and N. D. Broom, "Impact induced failure of cartilage-on-bone following creep loading: a microstructural and fracture mechanics study," *Journal of the mechanical behavior of biomedical materials* **14**, pp. 239–247, 2012.

Acknowledgements

"Coming together is a beginning; keeping together is progress; working together is success." Henry Ford
This dissertation is the result of four years of research, work and sweat. However, it would have never been successfully completed without the support of a number of people. It was a privilege for me, I feel lucky and I am grateful that I could be part of this multi-disciplinary project and that I had the opportunity to meet and work with so many talented people.

"A leader is best, when people barely know he exists, when his work is done, his aim fulfilled, they will say: we did it ourselves." Lao Tzu
I thank my copromotor and doctoral advisor Dr. Cees Oomens for always being there when needed. Cees, hartelijk bedankt voor alles. Bedankt dat je altijd er was als het nodig was, maar ook voor het feit dat je me mijn eigen weg hebt laten kiezen. My promotor Prof. Frank Baaijens, the big boss. Frank, bedankt voor jouw leiding en jouw ideeën. Jouw ideeën hebben me geholpen om uit mijn soms veel kleine stappen een grote stap te maken.

I thank the examination committee, especially the external members Prof. van der Steen and Prof. Daemen, for evaluating my dissertation.

Many thanks to the people of the Biomechanics lab of the Erasmus MC Rotterdam, it was a real pleasure collaborating and working with you. A big thanks to Dr. Ali C Akyildiz who spent long days and nights with me conducting measurements. Dr. Lambert Speelman, Harm Nieuwstadt and Dr. Frank Gijsen for discussions and support. I also thank Kim van Gaalen for technical support and histology. Thanks also to Dr. Gustav Strijkers for conducting DTI measurements and helping me to understand the world of imaging a bit better. I want to thank my project partners in work package 3, Prof. Frans van de Vosse, Prof. Marcel Breeuwer from Philips, Dr. Marcel Rutten, Dr. Peter Brands from Esaote, and Renate Boekhoven for their input during our project meetings.

I thank the entire Soft Tissue Mechanics and Engineering group at the TU/e for the good working enviroment. Special thanks to Inge van Loosdregt for helping me to improve my Dutch, and to Pim Oomen for improving the inverse analysis.

Many thanks also to Erwin Dekkers, for designing modifications for our experimental setups. Erwin bedankt voor jouw hulp. Door jou konden wij onze experimenten verbeteren. Ook bedankt aan Leo Wouters voor het helpen met ons computers in het

lab. Thanks to Dr. Martijn Cox and Tom Lavrijsen for introduction to the micro-indentation technique. Martijn, bedankt voor jouw help aan het begin van mijn PhD. Jouw hulp was een van de redenen waarom ik zo goed kon beginnen en al in mijn eerst jaar aan mijn eerste artikel kon werken. Thanks also to the surgeons at Catharina Hospital, Dr. Marc van Sambeek and Dr. Bianca Bendermacher for nice collaborations and providing us with the samples. Marc, bedankt voor het laten zien van de endarterectomy operatie. Dit en jouw discussies hebben me altijd geholpen om te zien waarom wij onderzoek in dit gebied doen en waarom het zo belangrijk is. Dr. Marc van Turnhout and Marcel Wijlaars for helping me with the fight against troublesome microscopes. Marc en Marcel, bedankt ervoor, dat jullie altijd tijd hadden om me met de Andor en ander microscopen te helpen. Dr. Moniek de Liefde, Marc van Maris and Dr. Mascha Maenhout for being there when needed and general help in the cell lab, bio and multi-scale lab.

"Take the attitude of a student, never be too big to ask questions, never know too much to learn something new." Og Mandino
During my time as a PhD student I had the opportunity to supervise a number of students. I thank Raphael Richert for conducting multi-photon imaging of plaques, Karlijn Groenen for failure tests on plaques which led to the results summarised in chapter 6. I also thank Sarah Billard and my MSc student Michiel Suijker for working on the extension tests of plaques. I appreciate the work of Caroline Balesman, Rob Driessen, Saskia van Loon, Jiri Obels, who worked on testing the influence of snap-freezing on mechanical properties of plaques. Many thanks also to Jerome Cremers, for designing a temperature control for the micro-indentation test. Another group of BSc student, Daniel den Boer, Ronald van der Meer, Britt van Rooij, and Carlo Theunisz, thanks a lot for designing new smaller indenters. I am also grateful for the work of Laura Tiemeijer, who tested the temperature control of the indentation test. Furthermore, I have to thank my Bachelor students, Rick Beenders, Luc Bakker, Joep Kamps, Frank Hoeven and Thomas Meurs for conducting the failure tests of plaques.

"All work and no play makes Jack a dull boy." James Howell
During my time at TU/e, I found lots of opportunities to have fun and enjoyment. These moments would not have been as enjoyable without the many colleagues (and friends) I had during my time at TU/e. I thank Dr. Samaneh Ghazanfari, Dr. Francesca Storti, Chiara Tamiello, Ümit Arabul, Maarten Heres Tommaso Ristori, Johanna Melke, Franz Bormann, Vanessa Zonca, Siavash Maraghechi, Arianna Mauretti, Valentina

Bonito, Tina Thakkar, Maqsood Ameen, Dr. Lambert Bergers, and Dr. Giulia Argento for the time we spend together inside and outside TU/e. I also want to thank Salman Shafqat for the "serious" discussions we had and for his support during the proof-reading process of this thesis. Furthermore, special thanks to my female buddy Emily Jane Scott, for her proof-reading efforts. Florian Eberhardt, my friend since grammar school. Lieber Flo, vielen Dank dafür, dass wir immer noch zusammen rumhängen. All die Jahre warst du immer einer meiner Konstanten im Leben, egal wo auch immer es mich hinverschlagen hat, auf dich war immer Verlass.

"In every conceivable manner, the family is link to our past, bridge to our future." Alex Haley. Meine Eltern, vielen Dank für den Rückhalt und das Vertrauen in mich. Ohne euch wäre ich heute nicht, wer ich bin. Fung-Yin, I know that you did not have a choice, but thank you for being my baby-sister. *"A sister can be seen as someone who is both ourselves and very much not ourselves- a special kind of double"* Toni Morrison.

About the author

Chen-Ket Chai was born on 4th of May 1984 in Schwerte (Germany). He attended the Martino-Katharineum Gymansium (grammar or high school) in Braunschweig (Germany) graduating in 2003. Afterwards, he enrolled in the Biomedical Engineering programme at the Faculty of Electrical Engineering at the Anhalt University of Applied Science in Köthen (Germany). During his undergraduate studies he worked for 5 months as a research assistant at the Fraunhofer Institute for Biomedical Engineering in St. Ingbert (Germany). There he designed and tested dry surface-electrodes for ECG measurements. During his final semester he worked at the Fraunhofer Institute for Mechanics of Materials in Halle (Germany) which led to his thesis about 'Analysis of chemical stability of nano-porous alumina in aqueous solutions'. He graduate from Anhalt University as a Diplom-Ingenieur (FH) and decided to enroll in the graduate programme Biomedical Engineering at the University of Hanover (Germany). During his studies he also worked as a research assistant at the Laser Centre Hanover where he helped to design experimental setups to test the mechanical and optical properties of eye lenses. In 2010, he wrote a thesis about 'Analysis of focal length changes of porcine and primate eye lenses during simulated accommodation after treatment with femto-second laser-pulses' and obtained his Master of Science degree. During the same year he applied for the Leonardo-Da-Vinci programme and obtained a grant which allowed him to work as an Academic Visitor at the University of Oxford (UK). His work in Oxford led to his first scientific publication in the peer-reviewed Journal of Experimental Eye Research. From 2010 to 2014, Chen-Ket Chai worked as a PhD candidate on the biomechanical properties of atherosclerotic plaques at the Eindhoven University of Technology (TU/e, The Netherlands).

He is member of the Verein Deutscher Ingenieure (VDI, Association of German Engineers). He was board member of Hora Est for the year 2011-12. From 2012 to 2014, he was member of the Department Council at TU/e. He is also founding-member of the first English-speaking Rotary Club in Eindhoven. His hobbies include squash, cooking, ultimate frisbee and football.

List of publications

- **C.-K. Chai**, H. J. Burd, and G. S. Wilde. Shear modulus measurements on isolated human lens nuclei. Journal of Experimental Eye Research. 103:78-81, 2012.

- **C.-K. Chai**, A. C. Akyildiz, L. Speelman, F. J. H. Gijsen, C. W. J. Oomens, M. R. H. M. van Sambeek, A. van der Lugt, and F. P. T. Baaijens. Local axial compressive mechanical properties of human carotid atherosclerotic plaques-characterisation by indentation test and inverse finite element analysis. Journal of Biomechanics, 46:1759-1766, 2013.

- **C.-K. Chai***, L. Speelman*, C. W. J. Oomens and F. P. T. Baaijens. Compressive mechanical properties of atherosclerotic plaques-indentation test to characterise the local anisotropic behaviour. Journal of biomechanics 47:784-792, 2014. *these authors contributed equally to this work.

- P. Wise, N. H. Davies, J. Kortsmit, L. Dubuis., **C.-K Chai**, F. P. T. Baaijens, M. S. Sirry, and T. Franz. Excessive volume of hydrogel injectates may compromise the efficacy for the treatment of acute myocardial infarction (*submitted*).

- **C.-K. Chai**, A. C. Akyildiz, L. Speelman, F. J. H. Gijsen, C. W. J. Oomens, M. R. H. M. van Sambeek, A. van der Lugt, and F. P. T. Baaijens. Local anisotropic mechanical properties of human carotid atherosclerotic plaques - characterisation by micro-indentation and inverse finite element analysis (*accepted*).

- **C.-K. Chai**, K. H. J. Groenen, L. Speelman, F. J. H. Gijsen, C. W. J. Oomens, M. R. H. M. van Sambeek, A. van der Lugt, and F. P. T. Baaijens. Mechanical failure properties of human atherosclerotic carotid plaque caps - characterisation using indentation test (*submitted*).

PhD portfolio

Courses	
Taking charge of your PhD (Planning, Management)	2011
Scientific integrity	2011
Art of presenting science	2011
Dutch for beginners	2011
Dutch for intermediate	2011
Dutch for advanced	2012
Dutch for advanced plus	2012
Writing articles and abstracts	2012
Supervising Master students	2012
Teaching and learning in higher education for PhD students	2012
Poster pitch	2013
Entrepreneurship for PhD candidates	2013

Seminars and workshop	
Biostatistics for Biomedical Engineering	2012
Summer school on Biomechanics (Graz University of Technology)	2012
LabVIEW Core 1	2014

Teaching activities	
Supervising 4 Bachelor students (minor project)	2011
Supervising 1 Bachelor student (major project)	2012
Supervising 1 student (4 months internship)	2012
Supervising 4 Bachelor students (minor project)	2012
Supervising 1 Master student	2012
Tutor for the course pathology imaging and analysis	2012
Supervising 1 Master student	2013
Supervising 1 Bachelor student (major project)	2013
Supervising 3 Bachelor students (minor project)	2013
Supervising 3 Bachelor students (minor project)	2013
Supervising 1 student (3 months internship)	2014

Podium presentations	
EUROMECH 534 Advanced Experimental Approaches and Inverse Problems in Tissue Biomechanics (St. Etienne, France)	2012
8th symposium on Biomechanics in Vascular Biology and Cardiovascular Disease (Rotterdam, The Netherlands)	2013
ASME 2013 Summer Bioengineering Conference (Sunriver, USA)	2013
two presentation at the 7th World Congress of Biomechanics (Boston, USA)	2014
12th international symposium on Computer Methods in Biomechanics (Amsterdam, The Netherlands)	2014

Poster presentation	
9th symposium on Biomechanics in Vascular Biology and Cardiovascular Disease (Montreal, Canada)	2014